Title: Refractory for Black Liquor Gasifiers

Type of Report: Final Technical Report

Reporting Period Start Date: October 1, 2002

Reporting Period End Date: September 30, 2005

Principal Authors: William L. Headrick Jr., Alireza Rezaie Xiaoting Liang, Musa Karakus and Jun Wei

Date Report Issued: December 2005

DOE Award Number: DE-FC26-02NT41491

Name and Address of Submitting Organization:

Curators of the University of Missouri on behalf of University of Missouri-Rolla
Sponsored Programs
1870 Miner Circle
215 ME Annex
Rolla, MO 65409-1330

DISCLAIMER

ABSTRACT

The University of Missouri-Rolla identified materials that permit the safe, reliable and economical operation of combined cycle gasifiers by the pulp and paper industry. The primary emphasis of this project was to resolve the material problems encountered during the operation of low-pressure high-temperature (LPHT) and low-pressure low-temperature (LPLT) gasifiers while simultaneously understanding the materials barriers to the successful demonstration of high-pressure high-temperature (HPHT) black liquor gasifiers. This study attempted to define the chemical, thermal and physical conditions in current and proposed gasifier designs and then modify existing materials and develop new materials to successfully meet the formidable material challenges.

Resolving the material challenges of black liquor gasification combined cycle technology will provide energy, environmental, and economic benefits that include higher thermal efficiencies, up to three times greater electrical output per unit of fuel, and lower emissions. In the near term, adoption of this technology will allow the pulp and paper industry greater capital effectiveness and flexibility, as gasifiers are added to increase mill capacity. In the long term, combined-cycle gasification will lessen the industry's environmental impact while increasing its potential for energy production, allowing the production of all the mill's heat and power needs along with surplus electricity being returned to the grid. An added benefit will be the potential elimination of the possibility of smelt-water explosions, which constitute an important safety concern wherever conventional Tomlinson recovery boilers are operated.

Developing cost-effective materials with improved performance in gasifier environments may be the best answer to the material challenges presented by black liquor gasification. Refractory materials were selected or developed that reacted with the gasifier environment to form protective surfaces in-situ; and were functionally-graded to give the best combination of thermal, mechanical and physical properties and chemical stability; and are relatively inexpensive, reliable repair materials. Material development was divided into 2 tasks:

Task 1 was development and property determinations of improved and existing refractory systems for black liquor containment. Refractory systems of interest include magnesium aluminate and barium aluminate for binder materials, both dry and hydratable, and materials with high alumina contents, 85-95 wt%, aluminum oxide, 5.0-15.0 wt%, and BaO, SrO, CaO, ZrO_2 and SiC.

Task 2 was finite element analysis of heat flow and thermal stress/strain in the refractory lining and steel shell of existing and proposed vessel designs. Stress and strain due to thermal and chemical expansion has been observed to be detrimental to the lifespan of existing black liquor gasifiers. The thermal and chemical strain as well as corrosion rates must be accounted for in order to predict the lifetime of the gasifier containment materials.

TABLE OF CONTENTS

LIST OF GRAPHICAL MATERIALS

INTRODUCTION

Papermaking by the kraft process involves treatment of wood chips in a digester vessel with a steam-sodium sulfide-sodium hydroxide mixture to separate the cellulose fibers from the lignin that binds them together. The streams exiting the digester vessel include a fiber-rich stream that is further treated to provide the fibers that are used to form paper or other cellulose-based products. The other stream is identified as black liquor which is an aqueous solution containing the waste organic material including the lignin as well as the spent pulping chemicals that are primarily sodium carbonate and sodium sulfate. Black liquor (BL), a by-product of the papermaking process, is an important liquid fuel in the pulp and paper industry[1]. A diagram highlighting the steps in papermaking and chemical recovery is shown in Figure 1.

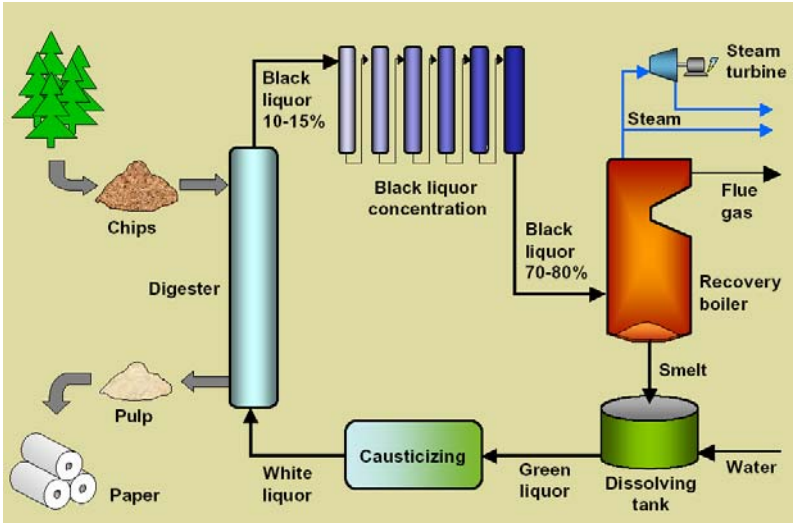

Figure 1 Schematic description of the pulping process

The weak black liquor has a solids content of approximately 15% by weight but the strong black liquor resulting from the concentrator has a solids content of around 75%[2].

Black liquor represents a readily available renewable energy source which is expected to become an increasingly important resource for power generation in the pulp and paper industry in the future[3].

As is seen in Figure 2, the worldwide black liquor production is increasing. Moreover, the contribution of the United States to this rate is disproportionately high which shows the huge amount of energy and electricity power which can be obtained from black liquor by 2025[4]. Therefore development of a refractory lining material resistant to harsh condition of black liquor gasifier is necessary to provide a stable operating condition. The most readily apparent feature of gasification based power plants compared to existing power plants is the much higher levels of electricity production resulting from the high efficiencies of gas turbine cycles compared to those of steam turbines[5]. The following electrical power yields are rough

estimates; 500-800 kWh/ADMT[1] for recovery boiler technology and 1200-1800 kWh/ADMT for pressurized black liquor gasification with combined cycle technology[6].

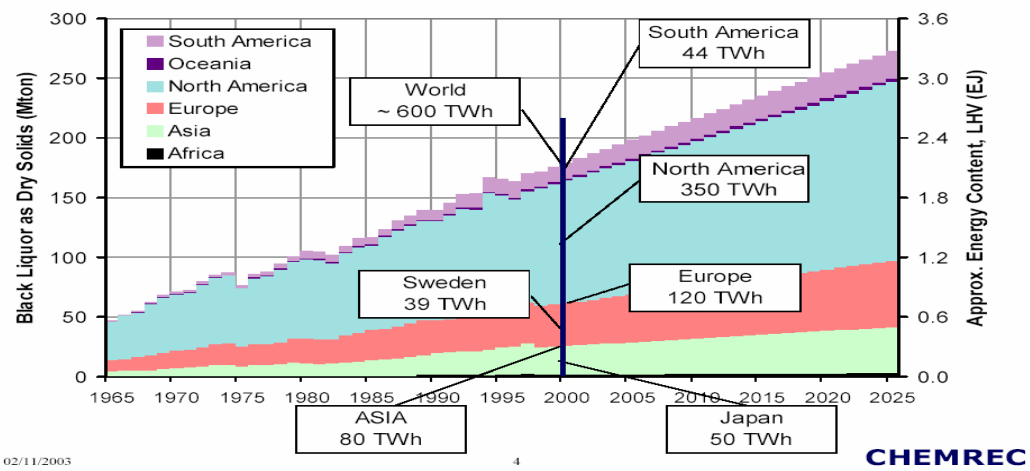

Figure 2 Estimated black liquor production (World)

Figure 3 shows the potential for electricity production from Black Liquor in Sweden. Of course the same trend should exist in the other countries of the world such as the United States. Again the importance of the role of Black Liquor Gasification as a future source of energy is obvious in this figure so attempts to further develop this process are warranted[4].

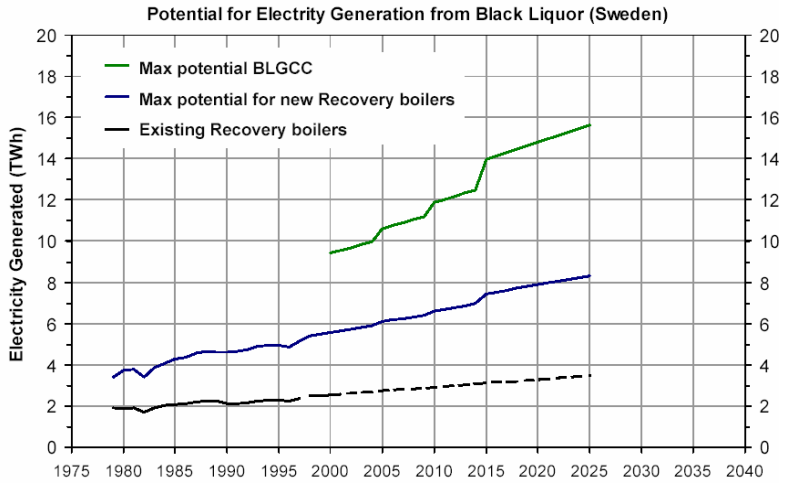

Figure 3 Maximum electric power Potential from black liquor

In a very simple way in gasification process, the carbon in the dry solids reacts with steam which is formed when the black liquor is heated in the reactor[6].

$$C + H_2O \longrightarrow CO + H_2 \qquad (1)$$

[1] ADMT=Air Dried per Metric Ton

This is an endothermic reaction, which requires a temperature of $1650-1830^{\circ}F(900-1000^{\circ}C)$ in order to proceed rapidly. In the gasification process, an exothermal reaction is used to raise the temperature to the required level and generate the heat needed to support the reaction shown above. This exothermal reaction is combustion (oxidation) of carbon to carbon dioxide[6].

$$C + O_2 \longrightarrow CO_2 \qquad (2)$$

Adding the above two reaction gives:

$$2C + H_2O + O_2 \longrightarrow CO + CO_2 + H_2 \qquad (3)$$

Very simplified, the black liquor is partially burned and partially gasified.

Black liquor gasification (BLG) is a process wherein black liquor is partially burned with a substoichiometric amount of air or oxygen to recover process chemicals and convert the organic portion of the liquor into a usable fuel gas[7]. Boilers and gasifiers are the two main equipment types used to convert some of the chemical energy of black liquor by combustion of the liquor which yields an inorganic smelt and gases. The old method to regenerate the pulping chemicals as well as recover some of the heating value contained in the organic components was the black liquor recovery boiler. Concentrated black liquor is injected into this boiler where the water is evaporated, organic materials are burned to produce heat and steam, and inorganic components are recovered in the bottom of the boiler in a partially reduced state, primarily as sodium carbonate and sodium sulfate[8].

Recovery boilers have been used successfully for many years but they have a number of shortcomings. First, the boiler is the most expensive piece of capital equipment in a typical kraft pulp mill. Second, the boiler is not efficient for recovering energy from black liquor and producing electric power. Besides, there is a safety issue because of the potential for recovery boiler explosions if the pressurized water contained in the tubes leaks and contacts the bed of molten smelt. Contact of this hot water with the molten smelt can result in violent explosions [7, 8]. The pulp and paper industry is interested in increasing the chemical recovery process efficiency, either by improving recovery boiler performance or by implementing alternative technologies. The development and selection of recovery equipment during the next two decades will be affected by[7]:

- Aging recovery equipment
- Need for incremental pulp production capacity
- Changes in mill energy demand, i.e. more electricity and less stream
- More stringent emissions regulations

It is reported that the net power output per ton of pulp is 40.7 MW in recovery boiler and 78.4 MW in CHEMREC BL gasifier. Also it is reported that the overall thermal efficiency is 67.5% in recovery boiler and 77.5% in CHEMREC BL gasifier[9].

Black liquor gasification (BLG) is widely viewed as the technology most likely to replace the recovery boiler. Gasification is the conversion of low-cost solids (like biomass) or liquids (like black liquor) into clean-burning gases (usually for replacement of fossil fuels)[10]. Combined cycle denotes the use of a gaseous fuel in a gas turbine followed by the production of steam, which is subsequently used in a steam turbine such that both turbines produce electric power. Splitting sulfur and sodium present in the recovered pulping chemicals into

separate process streams is the other advantage of the BLG process. This opens up the opportunity to produce a wide range of pulping liquor compositions [6, 7, 11].

The temperature level defines whether the technology operates below or above the melting point of the smelt produced[9, 10]. Among different gasification processes, only two of them have had satisfactory results and are still in operation. The first one is the low temperature process (600-800 $^{\circ}C$) represented by which developed the process and the other one is high temperature process (900-1000 $^{\circ}C$) invented by Chemrec[7, 10]. Chemrec and Noell are two companies developing pressurized, high temperature gasifiers [5].

Low Temperature Black Liquor Gasification is based on indirect heating of a fluid bed with tube bundles comprised of pulsed heater tailpipes [11]. The process involves steam reforming of the black liquor. In this process, the temperature is kept low enough such that the smelt doesn't become molten or even reach the point where it becomes sticky[7]. The liquor is gasified at a temperature of 600-800 $^{\circ}C$ under reducing conditions[12]. A schematic of a typical reformer/gasifier system is shown in Figure 4. This system utilizes a fluidized bed of sodium carbonate particles. Steam introduced through the bottom of the vessel serves as the fluidizing gas as well as the source of water for the reforming operation. The black liquor is introduced through a nozzle system also located on the bottom of the vessel. Heat is transferred to the bed through several tube modules that carry hot combustion gas. Heat from the combustion gases is transferred through the walls of the bed tubes to the bed material where the reforming operation occurs[7, 8]. The composition of product gas is mainly hydrogen (≈80%) in addition to carbon dioxide (≈10%) and methane, ethane and propane (≈10%) [11].

In this system, the alkali salts are kept below their melting point. Consequently, no component is exposed to molten salts and most are utilized at temperatures below those encountered in the higher temperature process. The outer surface of the bed tubes will be exposed to a gas mixture that includes hydrogen, hydrogen sulfide, steam, and carbon monoxide and the tubes will also be subjected to the movement of the particles in the fluidized bed. The gases exiting the bed tubes are directed into another chamber that is connected to a heat recovery system. The reformer/gasifier vessel is lined with refractory. The erosive action of the bed particles is a concern in the bed area, while above the bed, degradation of the refractory by the aggressive gases as well as mechanical damage from material condensing on the refractory lining are concerns [8].

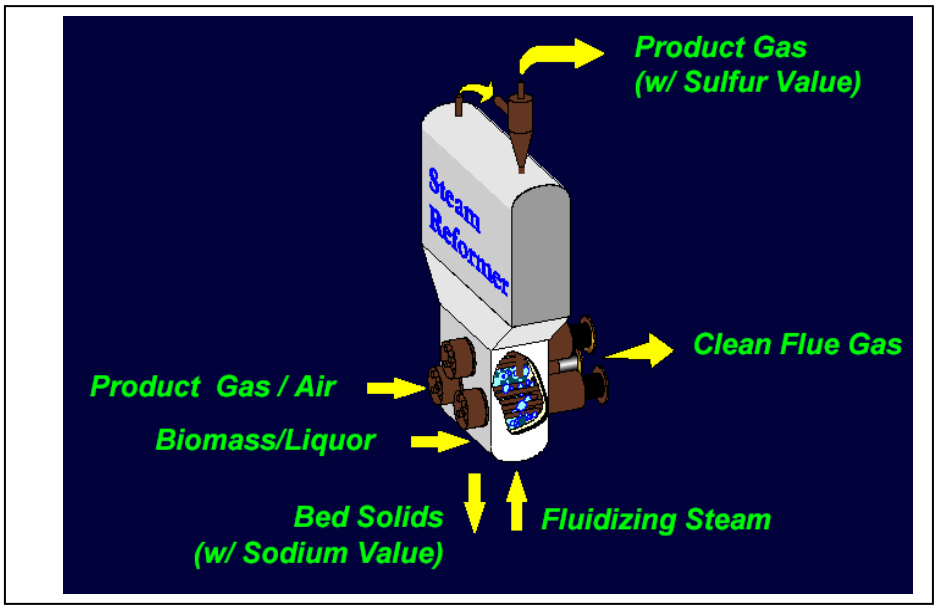

Figure 4 Schematic of steam reformer/gasifier vessel[13]

The high temperature gasification process can be operated near atmospheric pressure or at significantly elevated pressures [7, 8, 14]. A schematic of a high-temperature, low-pressure (HTLP) gasifier is shown in Figure 5. In this refractory lined vessel, the black liquor fuel and the air for partial combustion are injected at the top of the vessel. The organic material contained in the black liquor is gasified and the inorganic salts are left in the liquid state, primarily on the gasifier wall. The liquid and gaseous products are carried out the bottom of the gasifier vessel. The product gas is routed through a gas clean-up system to remove residual particulates and H_2S and the inorganic salts are directed to the green liquor tank[8].

There is some limited experience with high-temperature, high-pressure (HTHP) gasification. A 10 tons/day pilot scale unit has been operated in Sweden. A total of only about 1000 hours operating time was accumulated on black liquor feed[8].

There are two competing designs being considered for the HTHP gasifier. One design utilizes a thick refractory lining within a metal pressure vessel. This design has a refractory lining similar to that shown in Figure 5 for the HTLP. The alternative design, called a cooling screen (Figure 6), utilizes a helically coiled metal tube that has a refractory surface coating and contains pressurized cooling water. Currently, a high-temperature, high-pressure demonstration scale unit is under construction in Sweden. Operation is expected to begin in mid to late 2003 and both the thick refractory lining and the cooling screen design will be tested[8].

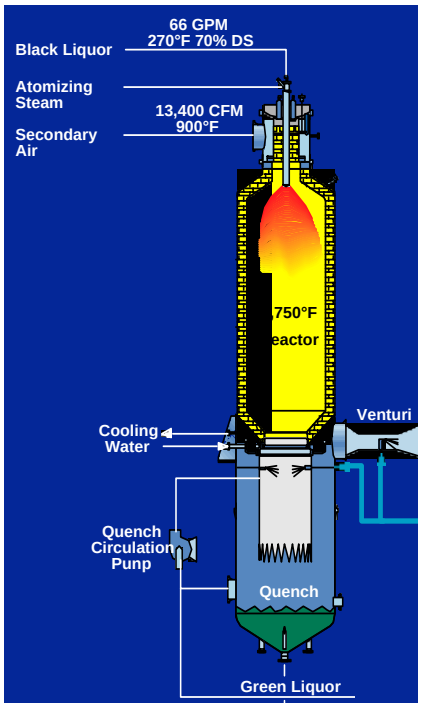

Figure 5 Schematic of high temperature, low pressure gasifier

In the high temperature systems, the units operate at temperatures above the melting point of the inorganic salts, between 900-1000 $^{\circ}C$, and at pressures ranging from 2 to 4 MPa, depending on the desired pressure level for gas turbine operation. The synthesis gas is a high value product composed of chemicals such as hydrogen, methanol or ammonia[10].

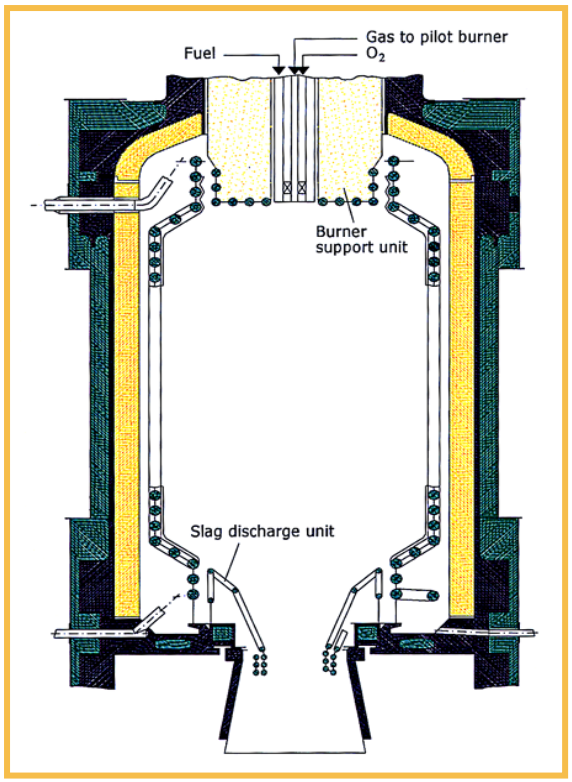

Figure 6 Schematic of high temperature, high pressure gasifier[8]

The core component of the Chemrec system is the gasifier, a refractory lined entrained flow reactor where the black liquor is decomposed under strongly reducing conditions. Preheated air is used as oxidant and reducing atmosphere turns to oxidizing in the starting up or shutting down the furnace. Injection of steam also provides some oxidizing conditions intermittently. The black liquor droplets are dried and partially combusted, producing combustible gas and smelt drops. The dry solids are loaded with alkaline catalyst containing volatiles and a high content of oxygen. Under gasification conditions, black liquor pyrolyses very rapidly. The black liquor is a unique material because of the extremely fine dispersion of sodium (or potassium) throughout the carbon matrix. The high catalyst loading and fine distribution of catalyst is believed to be responsible for the very high gasification rates experienced[3].

It is reported that, during black liquor gasification, sodium and potassium vapors are released in relatively large quantities. Preliminary data indicates that alkali volatilization can be in excess of 20% of the total sodium entering with the black liquor[3]. But equilibrium calculations of black liquor composition at $950^{\circ}C$ under atmospheric pressure, by FactSage database, show that the amount of sodium and potassium vapors in the gasifier atmosphere doesn't exceed 2%. It is also reported that gaseous alkali compounds are formed above $900^{\circ}C$, in the form of diatomic sodium and sodium hydroxide[3]. Furthermore, the total pressure affects the equilibrium amount of alkali in the gas. Higher pressure results in considerably lower alkali release. Lowering the air/fuel ratio results in significantly increased alkali volatilization. In the HTHP process, the reactor pressure increases to 20-40 atm compared to atmospheric pressure which is normally used in HTLP process. As was

mentioned, the reactor temperature in the high temperature process is between 900-1000$^{\circ}C$, normally kept in the 950-975$^{\circ}C$ range[3, 10].

The gaseous atmosphere in the gasifier includes hydrogen, hydrogen sulfide, carbon monoxide, carbon dioxide, nitrogen, methane and steam. In addition, most of the interior surface of the gasifier vessel is exposed to molten salt (Na_2CO_3 and Na_2S) flowing to the outlet of the reactor in a reducing environment. The use of oxygen in place of air provides the possibility of substantially higher gasification temperature, up to 1400$^{\circ}C$ [15].

In Alumino-silicate refractories, the alkali penetrates into the brick structure, reacts with the brick components and results in the formation of expansive phases containing varied combinations of alkali, alumina, and silica. Cracking and spalling occur from the resulting mechanical stresses associated with the formation of these expansive phases. Below approximately 1260$^{\circ}C$, the phases such as nepheline (soda + alumina + silica), leucite and kalsilite (potash + alumina + silica) are formed with a large volume change. Above 1260$^{\circ}C$, the fireclay group typically reacts with the volatile alkali to form a viscous glass. The viscous glassy layer may protect the refractory and stabilize the wear, however, exposure to increased temperature can greatly accelerate the pace of fluxing and wear. Alkali also causes free alumina phases $(\alpha - alumina)$ to recrystallize into $\beta - alumina$ which associates with a large volume expansion. In the experiment accomplished at 1204$^{\circ}C$ for 5 hours on 60% alumina samples mixed with sodium carbonate in different proportions, it was found that the 5% soda pellet appeared relatively unaffected. The 10% soda pellet also appeared relatively unaffected; however, XRD analysis showed the formation of nepheline in some quantity. The 20% sample was weakened and friable, the 30% soda sample showed signs of the initial expansive phase formation followed by the formation of liquid phases and 40% soda sample showed significant shrinkage associated with liquid formation. It means that greater soda levels result in the formation of greater quantities of expansive and/or liquid phases. In the case of 90% alumina mullite bonded samples; soda reacted with both the free alumina and the mullite bond, to form nepheline and $\beta - alumina$. The proposed reactions for the mentioned interaction are as follows[16]:

$$Na_2O + 3Al_2O_3.2SiO_2 \longrightarrow Na_2O.Al_2O_3.2SiO_2 + 2Al_2O_3 \quad (4)$$

$$Na_2O + 3Al_2O_3.2SiO_2 + 2SiO_2 \longrightarrow 3Na_2O.2Al_2O_3.4SiO_2 + Al_2O_3 \quad (5)$$

$$Na_2O + Al_2O_3 \longrightarrow Na_2O.Al_2O_3 \quad (6)$$

$$Na_2O + 11Al_2O_3 \longrightarrow Na_2O.11Al_2O_3 \quad (7)$$

$$Na_2O + SiO_2 \longrightarrow Na - Si(Glass) \quad (8)$$

Yamaguchi, A. has reported that the exposure of $\beta - alumina$ powder to K_2CO_3 vapor at 1200$^{\circ}C$ changes the composition from $Na_2O.11Al_2O_3$ to $0.977K_2O.0.023Na_2O).7.5Al_2O_3$ as a result of substitution of K for Na. The lattice constant of c of $\beta - alumina$ changed from 22.54$^{\circ}A$ to 22.73$^{\circ}A$ in addition to formation of a great number of cleavages vertical to the c axis of the crystal [17]. More over it is reported that when fireclay refractories composed of mullite and silica is exposed to Na_2CO_3 vapor, the main product is nepheline

(NAS_2), but in the case of high alumina refractories composed of corundum and mullite the main reaction product is carnegieite s.s $(NAS_2 - NAs.s)^*$. Interaction of corundum with K_2CO_3 vapor, results in the formation of potassium aluminate and interaction of mullite with K_2CO_3, results in the formation of $KAS - KAs.s^*$ [2]. When $Al_2O_3 - ZrO_2 - SiO_2$ system refractories composed of corundum, baddeleyite and a glassy phase approaching the composition of albite $(NAS_6)^*$, is exposed to sodium carbonate, nepheline and carnegieite s.s $(NAS_2 - NAs.s)^*$ are formed as a result of interaction of alumina and albite with sodium carbonate and sodium zirconate is formed as a result of interaction of baddeleyite with sodium carbonate. In the case of exposure to K_2CO_3 vapor, $(K, Na)AS_2^*$ (kalsilite) and $KAS - KAs.s^*$ are formed as the result of interaction of alumina and albite with $\mathrm{K_2CO_3}$ vapor and K_2O-rich glass is formed as a result of interaction of baddeleyite with K_2CO_3 vapor[17].

Silica refractories exposed to sodium and potassium carbonate vapor at $1370^\circ C$ shows excessive corrosion and depth of reaction. The reaction of potash appears to be more aggressive. Cracking and spalling were observed in mullite bricks in potash environment as a result of formation of potassium aluminate and potassium aluminum silicate. The porosity of the sample has a considerable effect on the degree of corrosion. A high degree of inter-joint reaction with silica especially in the potash test was observed. Bonded AZS^* composition shows substantial improvement over zircon with respect to degree of reaction with alkali vapors but is still vulnerable to spalling. A decrease in alumina content and lower apparent porosity tend to improve resistance to potash vapor. Fused alumina shows negligible interface reaction but tends to demonstrate a high degree of inter-joint reaction with silica[18].

N. R. Brown has reported that Na_2O reacts rapidly with high silica refractories, %10 Na_2O will form 50% liquid at temperatures as low as $1100^\circ C$. In the case of mullite refractories, formation of expansive phases such as $NaAlO_2$, $\beta - Al_2O_3$ and carnegieite at low temperatures, and formation of liquid phases at $T \geq 1000^\circ C$ is proposed to be the failure mechanism [4]. In the case of exposure to K_2O, high silica refractories form leucite $(KAS_4)^*$. Kaliophilite $(KAS_2)^*$ appears in the fireclay refractories and at about 60% Al_2O_3, $K - \beta - Al_2O_3$ is formed. In the case of high alumina refractories $K_2O.Al_2O_3$ (potassium aluminate) is formed as well as $K - \beta - Al_2O_3$[19].

C. R. Kennedy who studied alkali attack on mullite refractories in coal gasifier, detected $NaOH$ in the samples in the case of existence of water vapor. The proposed corrosion reaction he proposed is as follows:

$$11(Al_6Si_2O_{13}) + 26(NaOH) \longrightarrow 22(NaAlSiO_4) + 4(NaAl_{11}O_{17} + 13H_2O) \qquad (9)$$

In $\mathrm{Na_2O\text{-}SiO_2\text{-}Al_2O_3}$ phase diagram and according to the lever rule, a reaction between a Na compound and mullite should produce $\sim$ 40wt% $\beta - \mathrm{Al_2O_3}$ and $\sim$ %60 nepheline with $\sim$ %30 volume expansion which easily explains the failure cause. It is also reported that at 900-1400$^\circ C$, the corrosion by alkali compounds slows down by the increase in the alumina

content of aluminous refractories. Formation of β - alumina was observed only at temperatures in excess of $1100^{\circ}C$. At $950^{\circ}C$, high silica (~%60) refractories performed better because of the ability of high silica refractories to react more rapidly with the alkali and contain its attack at the surface[20].

Sodium sulfate condensation as a result of reaction between sodium vapor and sulfur oxides and formation of nepheline $(754 - 954^{\circ}C)$ and noselite $(1150^{\circ}C)$ is reported to be the cause of bloating in fireclay refractories. Noselite is a nepheline sulfate mineral: $6(NaAlSiO_4).Na_2SO_4$, resulting from the conversion of nepheline by sodium sulfate. Reducing conditions enhances the formation nepheline[21].

Barrie H. Bieler found that among Na_2CO_3, Na_2SO_4 and $NaCl$, the most corrosive material on Alumina-Zirconia-Silica refractories is Na_2CO_3 and the least with $NaCl$. He suspended **Error! Objects cannot be created from editing field codes.** refractories over molten Na_2CO_3 at $1371^{\circ}C$. He tested other types of refractories over different types of salts as well. If water vapor present, formation of $NaOH$ is probable because of interaction of sodium carbonate and water. It is reported that at higher temperatures up to $1470^{\circ}C$, the chemical species are not only liquid Na_2CO_3 but also some liquid $NaOH$ and gaseous CO_2, H_2O and Na_2O. The major crystalline species in AZS refractories is monoclinic ZrO_2; the minor one is alpha alumina. SiO_2 is present only as an aluminosilicate glass. In the samples exposed to alkali vapors, different zones appeared. The gray central core grades into a more bleached zone, which is more pronounced in the case of exposure to Na_2CO_3 vapor. This then grades into a zone one millimeter wide which is slightly yellow composed of smaller crystals of monoclinic ZrO_2 with a wicker pattern of $\alpha - Al_2O_3$. In this yellow band, the original dendritic texture of ZrO_2 is broken up into smaller aggregates of ZrO_2 crystalline masses. The outermost layer, mottled white and light gray, is locally very porous and has a "warty" outer surface. This zone appears to be composed of porous aggregates of poorly crystalline material composed of mixed hydrated carbonates and hydroxides of sodium in both the $NaOH$ and Na_2CO_3 vapor corroded samples. Sodium aluminate, $NaAlO_2$ may be present in minor amounts[22].

R. A. Peascoe et al, reported the behavior of mullite, $MgAl_2O_4$ spinel, MgO, alumina, alumina-chromia based and Si_3N_4 refractories exposed to black liquor at $1000^{\circ}C$. In the case of mullite based refractories, molten smelt attacks mullite and forms sodium aluminum silicates accompanied by a dramatic volume change. $MgAl_2O_4$ refractories in in the case of polycrystalline spinel in MgO matrix showed minimal penetration and reaction due to minimal porosity or lack of α-alumina in the matrix. Fused spinel containing large spinel crystals was altered from the surface due to low porosity and slow diffusion of smelt. Samples containing $\alpha - alu\,\min a$ or components such as $CaAl_4O_7$ in the matrix are not resistant. Minimal reaction was observed in MgO based refractories but $\beta - Si_3N_4$ sample dissolved in the molten smelt. Molten smelt were found in the interior of the chromia/alumina sample with the primary reaction products of sodium aluminate and chromate[23].

Tadaoki Fukui et al reported that the reactivity of each sodium compound would be in the following descending order[24]:

$$Na_2CO_3 > Na_2SO_4 > NaCl \qquad (10)$$

This can be expected from the dissociation constants of these compounds:

$$K_{Na_2CO_3} = 1 \times 10^{-3} \qquad \text{at } 1400^\circ C \qquad (11)$$

$$K_{Na_2SO_4} = 1 \times 10^{-9} \qquad \text{at } 1400^\circ C \qquad (12)$$

$$K_{NaCl} = 1 \times 10^{-13} \qquad \text{at } 1450^\circ C \qquad (13)$$

They reported that a high reactivity vapor, sodium carbonate, is caught at the surface of refractory but the lower reactivity vapors, sodium sulfate and sodium chloride, infiltrated into the specimens through the pores and interstices around the grains[24].

Commercial high temperature black liquor gasifiers are generally cylindrical in shape as shown in Figure 7. The height ranges from 1.5 m to 25 m and diameter ranges from 0.5 m to 5 m. In the gasifier reactor vessels, there are usually 2-6 coaxial layers of component lining[25]. Refractory lining is used to protect the exterior metallic part of the gasifier vessel. A dense refractory material layer is designed to be exposed to the highest temperature environment. The second “safety” layer is usually made of a similar material. Subsequent layers are used to provide insulation and allow for expansion. The steel shell is used to provide reaction space and confinement. The gasifier generally operates at temperature ranging from 950 to 1000 ^oC.

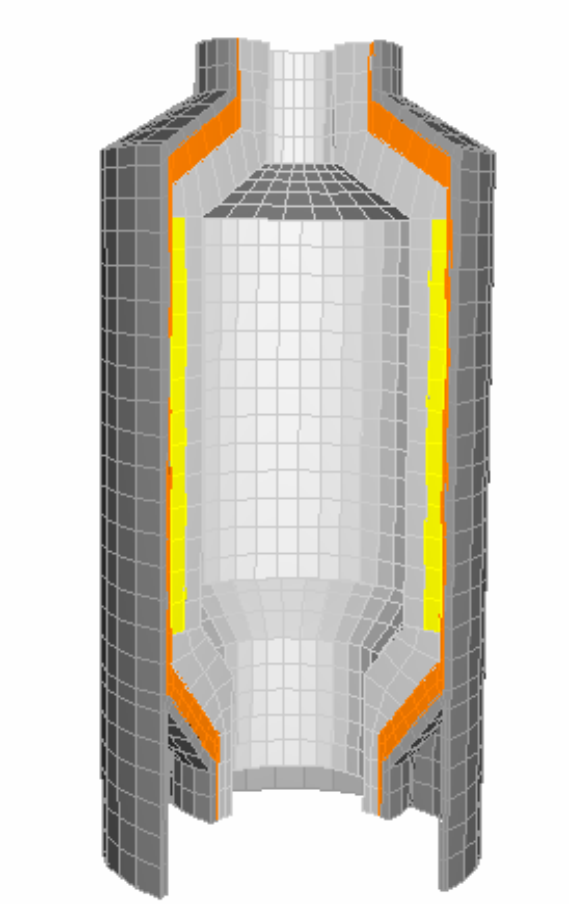

Figure 7 Schematic construction of a typical high temperature gasifier

The commercial high temperature black liquor gasifier was developed by Kvaerner Chemrec. A pilot plant first started running in 1994 at a pulp mill near Karlstad, Sweden[26]. The first commercial size Chemrec system (75-100 tons of dry solids/day) was built at the AssiDomän mill in Frövifors in 1991. This air blown gasifier has performed well and been proven to be easy to operate and maintain. The first commercial Chemrec system in North America started operation in 1996 at Weyerhaeuser's New Bern, SC, USA[27]. It was an atmospheric, air-blown, entrained bed gasifier operating between 950-1000 ^{o}C with a capacity of 350 ton black liquor solids per day. However, this system was shutdown in January 2000 due to failure of the stainless steel shell[28].

The current refractory materials for the BLG reactor vessel lining are not deemed adequate. The combination of high temperature and alkalinity produces an aggressive environment for the reactor lining. Chemrec has used several refractory materials in the pilot units and the commercial atmospheric units. The refractories last from 1 to 18 months, with a replacement cost of up to 1 million dollars and several weeks of downtime. Severe refractory thinning occurred and several bricks were found lost from the upper part of the gasifier vessel during operation. The refractory lining is subjected to the penetration of sodium and subsequent reactions with alkali-rich molten smelt, such that the refractory undergoes significant volume change and strength degradation. Several refractory samples have been studied after immersion in molten smelt[29]. The results of their study are summarized below. For mullite

based refractories, molten smelt first attacks mullite and forms sodium aluminum silicates. This reaction is accompanied by a volume change. A significant surface expansion occurs during immersion testing in smelt. Furthermore, a liquid phase can develop in the mullite refractory as Na_2O concentration increases. Surface expansion coupled with the loss of structural integrity lead to the spalling of the lining. $MgAl_2O_4$ spinel based refractories react with the smelt to form $NaAlO_2$ and MgO, with an associated expansion of 2.1% to 13%. For α/β-alumina refractories, expansion was accommodated partly through spalling and a significant radial expansion of the gasifier's lining. The alumina refractories show the least corrosion, the chemical expansion of alumina samples is from 0 to 0.7%. Due to this reason, fused cast alumina which is expansive and sensitive to thermal shock is being used in the most recent commercial high temperature black liquor gasifier at New Burn, SC, USA[30].

Computer simulation of existing materials will accelerate the development of these new materials. Compared to experimental characterization, computer simulation is much faster and more economical.

EXECUTIVE SUMMARY

The University of Missouri-Rolla identified materials that permit the safe, reliable and economical operation of combined cycle gasifiers by the pulp and paper industry. The primary emphasis of this project was to resolve the material problems encountered during the operation of low-pressure high-temperature (LPHT) and low-pressure low-temperature (LPLT) gasifiers while simultaneously understanding the materials barriers to the successful demonstration of high-pressure high-temperature (HPHT) black liquor gasifiers. This study used the chemical, thermal and physical conditions in current and proposed gasifier designs and then modified existing materials and developed new materials to successfully meet the formidable material challenges.

Resolving the material challenges of black liquor gasification combined cycle technology will provide energy, environmental, and economic benefits that include higher thermal efficiencies, up to three times greater electrical output per unit of fuel, and lower emissions. In the near term, adoption of this technology will allow the pulp and paper industry greater capital effectiveness and flexibility, as gasifiers are added to increase mill capacity. In the long term, combined-cycle gasification will lessen the industry's environmental impact while increasing its potential for energy production, allowing the production of all the mill's heat and power needs along with surplus electricity being returned to the grid. An added benefit will be the potential elimination of the possibility of smelt-water explosions, which constitute an important safety concern wherever conventional Tomlinson recovery boilers are operated.

Developing cost-effective materials with improved performance in gasifier environments may be the best answer to the material challenges presented by black liquor gasification. Refractory materials were selected or developed that reacted with the gasifier environment to form protective surfaces in-situ; and were functionally-graded to give the best combination of thermal, mechanical and physical properties and chemical stability; and are relatively inexpensive, reliable repair materials.

Today one of the main obstacles in the development of this technology is the development of refractory materials for protective lining of the gasifier. So far the materials used for this application have been based on alumino-silicate refractories but, thermodynamics and experience showed that these materials are not sufficiently resistant to black liquor under the harsh working conditions of Black liquor gasifiers. Consequently development of cost-effective materials with improved performance in gasifier environments to answer the material challenges presented by black liquor gasification (HTHP, HTLP) was the objective of this project. Refractories provided by in-kind sponsors were tested by cup testing, density/porosity determinations, chemical analysis and microscopy. Magnesia and spinel based gunnable refractories and mortars were developed in this project. They show great promise and should improve the current status of high temperature gasification. Fused cast magnesia rich spinel refractories were also proposed as the best available hot face material. Computer simulation of existing and proposed materials accelerated materials research in developing these new materials, and it is less costly and time consuming.

The results of thermodynamics and experiment for the reaction of black liquor smelt with various ceramics were in agreement for some candidate materials but not for others. Reactions were correctly predicted for Al_2O_3, CeO_2, MgO, $MgAl_2O_4$, but not for $3Al_2O_3.2SiO_2$, ZrO_2, Y_2O_3, $LiAlO_2$, $BaAl_2O_4$. Failure of the thermodynamic predictions was

attributed to lack of data for the reaction products produced by reaction of molten black liquor smelt with candidate materials. Sessile drop experiments were used to verify thermodynamic predictions and to determine contact angles of the molten Na_2CO_3 and K_2CO_3 on candidate materials. $MgAl_2O_4$ showed the highest contact angle with Na_2CO_3 (13.3 ± 1.2 degrees) while, the highest contact angle for K_2CO_3 (9.9 ± 1.5 degrees) was obtained with MgO. Although CeO_2 and MgO were wet by Na_2CO_3 and K_2CO_3, they did not react with either. Consequently, either CeO_2 or MgO could be used for refractories for applications requiring contact with black liquor smelt. The best choice for this application may be $MgAl_2O_4$. Although $MgAl_2O_4$ reacts with both Na_2CO_3 and K_2CO_3, a dense layer of MgO forms quickly and prevents further attack. Based on these considerations, MgO and $MgAl_2O_4$ are suggested for further investigation in the form of rotary finger corrosion tests, sessile drop studies with actual black liquor smelt, or trials in test gasifiers.

Samples provided by in-kind sponsors were tested using cup testing. The best performing materials in the cup testing were fused cast materials. Magnesia brick and castables performed well and should be further developed and moved into industrial trials. A spinel based mortar, MORCOCOAT SP-P, has been commercially prepared and is to be used in future gasifier installations.

A coupled thermal-mechanical model accounting for the chemical reaction was developed for refractory linings in a high temperature black liquor gasifier. This model was implemented into a commercial finite element code. The stress and strain distributions, time dependent thermomechanical behavior of the refractory lining under thermal loading and chemical attack are evaluated. The chemical reaction of the black liquor smelt and the refractory dominates the stress and strain development in the refractory lining. Four possible failure modes of the refractory lining are surmised by the stress and strain analysis. The model helps understand the failure behavior of the refractory lining in a high temperature black liquor gasifier system.

Chemical reaction and thermal expansion with improper constraints caused the most compressive damage in the refractory structure. Layered damage occurred in the refractory structure due to the tensile damage. Expansion allowance affected the damage of the refractory structure. Tensile damage could be reduced by allowing for larger expansion.

Continuum damage mechanics based analytical model was appropriate for predicting the failure behavior of the vessel refractories and refractory cup under thermal loading and chemical attack. The predicted damage patterns predicted by the model were in qualitative agreement with those observed in practice in the cup test. The maximum compressive damage occurs on the surface of the cup where is in contact with the black liquor smelt. The maximum tensile damage was found to occur at the end of the reaction zone. Chemical corrosion is the dominate factor of the damage of the refractory brick.

Gasifier end-users are still experiencing major refractory problems. Refractories are one of many issues still slowing use of this energy saving technology. Without continued assistance from DOE black liquor gasifiers currently in use may be shut down and future work abandoned.

EXPERIMENTAL

Both computer modeling and experimental verification were used in this study to develop and test new refractory materials suitable for black liquor gasification. FactSage 5.1 is a thermodynamic database which was used to do thermodynamic equilibrium calculations. This database can used to find the main refractory compounds formed due to reactions with black liquor smelt.

As sodium carbonate is the main corrosive component of black liquor smelt in contact with refractories, the interaction of refractory components with Na_2CO_3 was measured using sessile drop testing in conjunction with grazing x-ray diffraction and scanning electron microscopy to determine the depth of reaction and contact angle between the smelt and refractory substrate. Materials which performed best against Na_2CO_3 were additional exposed to K_2CO_3 by sessile drop testing as with Na_2CO_3.

The contact angle for molten Na_2CO_3 was measured on candidate refractory materials using standard sessile drop testing in accordance with a previously described set-up[31,32]. Several of the candidates investigated by thermodynamic modeling were not selected for sessile drop testing. Specifically, BaO and Li_2O were eliminated due to environmental issues and La_2O_3 and CaO were not examined due to their very high susceptibility to hydration. Other candidate ceramics were fabricated as cylindrical pellets ~2 cm in diameter. Al_2O_3, CeO_2, and MgO pellets were fabricated through uniaxial pressing (~65 MPa) of a high purity powder (>99.5%) and sintering at 1600°C. Mullite, Y_2O_3, $MgAl_2O_4$, $BaAl_2O_4$, and $LiAlO_2$ pellets were purchased from Custom Technical Ceramics, Inc and ZrO_2 pellet were purchased from Vesuvius McDanel Inc. The density and percent of open porosity of each of the substrates were measured using Archimedes' technique (Table IV). Pellets were mounted, ground, and polished using successively finer abrasives with a minimum abrasive size of 1 μm. A resistance heated horizontal tube furnace equipped with a high purity mullite tube was used for the reactions. A small quantity (0.2 to 0.3 g) of Na_2CO_3 was pressed into a cylindrical pellet ~0.6 cm in diameter and ~0.6 cm high, which was placed on the polished specimen. The specimen and Na_2CO_3 pellet were then placed in a crucible on a D-tube, inserted into the center of the furnace, and leveled. The ends of the furnace were sealed with gas-tight end caps, which had optical quality fused quartz windows to allow for viewing throughout the experiment. An atmosphere of flowing argon (~200 cm^3/min) was maintained. The specimen was heated at ~6°C/min to 1000°C and held for ten hours. Specimen temperature was monitored with a type K thermocouple sheathed in an alumina tube that was inserted into the furnace just above the crucible. Once the Na_2CO_3 was melted, a video camera was used to record images of the molten drop. Contact angles were measured using images extracted from the video footage. The reported contact angles are the average of five to seven values recorded after the droplet reached a steady state contact angle.

After sessile drop testing, specimens were examined using grazing incidence x-ray diffraction (GXRD; X'Pert MRD, Panalytical, Almelo, Netherlands) to determine the reaction products. In addition to the sessile drop specimens, some of the reaction chemistries were repeated by mixing Na_2CO_3 with the appropriate ceramic powder and then reacting under identical conditions (1000°C for 10 hours). Powder x-ray diffraction analysis (XRD; XDS 2000, Scintag, Cupertino, CA) was used to determine the phases present after reaction. After examination by GXRD, sessile drop specimens were mounted in epoxy, sectioned

perpendicular to the reaction interface, and polished to 1 μm. Polished cross sections were examined using scanning electron microscopy (SEM; S-570, Hitachi, Tokyo) and energy dispersive spectroscopy (EDS; AAT, X-ray Optics, Gainsville, FL). X-ray mapping was used to measure the depth of penetration into the substrate.

Results from thermodynamic modeling and sessile drop testing were presented to refractory manufacturers. Refractory manufacturers supplied commercially available materials for cup testing with smelt provided by Weyerhaeuser from their commercial high temperature black liquor gasifier. The cups were evaluated by standard ASTM procedures for chemical composition, density, porosity and smelt reactions and penetration. The best commercially available refractories were recommended for industrial trail and used as a starting point for the development of novel refractories for improved resistance to smelt attack. Improved and novel materials were then tested as the commercial materials by cup testing and compared to the commercially available materials.

Cup test processing was performed at UMR. Cups were prepared from monolithic materials according to the manufacturers directions as a 9" long by 4.5" wide by 3" deep sample with 2 of 1.5" diameter by 1.5" deep holes formed during casting. Brick samples were cut from a 9 inch straight into 2 of 4.5 inch by 4.5 inch by 2.5 inch specimens. A diamond core drill cored a 1.5" diameter by 1.5" deep core. The core was removed with a chisel.

The removed cores were used to determine density by ASTM C-820 and sectioned for chemical analysis by ICP and microscopy. The cups are processed by drying at 110°C for 24 hours. The cup was charged with 50 grams of raw black liquor smelt. Heated at 1°C/minute to 1000 °C, held 240 hours at 1000°C and cooled at 2°C/minute to 25 °C, in an argon flooded furnace.

The existing gasifier was modeled with a simplified model using the current state of the art materials. A damage and crack opening model was used to predict maximum safe heating and cooling rates, expansion allowance needs and damage to the refractories due to constraint and chemical reaction. Tests were performed by ASTM standards to measure porosity, density, thermal conductivity, strength, creep rate and young's modulus of existing and new materials. All components replaced in industry were to be modeled by the finite element method to predict failure mode, stresses and eventually lifetime.

During the operation of a high temperature black liquor gasifier refractory, the thermal behavior, chemical reaction and mechanical behavior are coupled together. In order to simulate the realistic operational environment accurately, the heat transfer, chemical reaction and thermomechanical performance should be modeled simultaneously.

(1) Heat Transfer Model

Heat is generated inside the chamber, and transfers through the refractory tubesheet and the steel base, and then dissipates to the surrounding environment by radiation and convection. The transient heat conduction equation for an axisymmetry problem described in the cylindrical coordinate system is given as fellows [18]:

$$\rho C \frac{\partial T}{\partial t} = \frac{1}{r}\frac{\partial}{\partial r}\left(r k_r \frac{\partial T}{\partial r} \right) + \frac{\partial}{\partial z}\left(k_z \frac{\partial T}{\partial z} \right) \quad (1)$$

where ρ is the density, C is the specific heat, T is the temperature, t is the time, k_r and k_z are the conductivities in r and z directions of the material, respectively.

Both the convection and the radiation are involved in the heat transfer boundary conditions. Heat flux on a surface due to convection is governed by [19]

$$q = h\left(T - T^A\right) \tag{2}$$

where h is a reference film coefficient, and T^A is an ambient temperature.

Heat flux on a surface due to radiation to the environment is governed by [19]

$$q = e\sigma\left[\left(T - T^0\right)^4 - \left(T^A - T^0\right)^4\right] \tag{3}$$

where e is the emissivity of the surface, and σ is the Stefan-Boltzmann constant (5.67 x 10^{-8} W/m^2K^4), and T^0 is the absolute zero on the temperature scale being used.

(2) Thermoelastic Model

The relationship between strain $\{\varepsilon\}$ and displacements for axisymmetry problems is [18]

$$\{\varepsilon\} = \begin{Bmatrix} \varepsilon_r \\ \varepsilon_\theta \\ \varepsilon_z \\ \gamma_{rz} \end{Bmatrix} = \begin{Bmatrix} \partial u/\partial r \\ u/r \\ \partial w/\partial z \\ \partial u/\partial z + \partial w/\partial r \end{Bmatrix} \tag{4}$$

For the pulse combustor tubesheet, the total strain of the refractory material includes the mechanical strain and the thermal strain. The linear constitutive equation for the combustor tubesheet material can be written as [18]

$$\varepsilon_{ij} = \frac{(1+\nu)}{E}\left(\sigma_{ij} - \frac{\nu}{1+\nu} S_{kk}\delta_{ij}\right) + \alpha\Delta T\delta_{ij} \tag{5}$$

where σ_{ij} and ε_{ij} are the standard stress and strain tensors, ν is the Poisson's ratio, α is the coefficient of thermal expansion, T is the temperature, and δ_{ij} is the Kronecker delta.

For the refractory in the cup test, the total strain of the refractory material includes the mechanical, thermal strain and the chemically reactive strain. After including the chemical expansion in the stress-strain relations for the refractory, the elastic constitutive relations for the refractory material become

$$\varepsilon_{ij} = \frac{(1+\nu)}{\widetilde{E}}\left(\sigma_{ij} - \frac{\nu}{1+\nu} S_{kk}\delta_{ij}\right) + \alpha\Delta T\delta_{ij} + \varepsilon^r\delta_{ij} \tag{6}$$

where ε^r is the chemical expansion strain.

The chemical reaction of refractory material is controlled by temperature, time and the depth of penetration. Reactive strain is used to describe the chemical reaction as a function of the temperature, T, time, t, and penetration depth, d.

$$\varepsilon^r = F\left(T, t, d\right) \tag{7}$$

The equilibrium equation of the thermoelastic problem can be written as

$$\sigma_{ij,j} + f_i = 0 \tag{8}$$

where σ_{ij} are the stress components and f_i are the body forces.

(3) Damage Model

Since the failure behavior of a refractory material under tension and compression is different, two damage variables, D_t and D_c, are used to describe the tensile and compressive damages of the refractory. The damage components due to normal principal stresses are assumed to follow a simple linear damage evolution law in which damage is linearly related to the corresponding tensile and compressive principal stress components (σ_i) in a certain stress range:

$$\begin{aligned} D_i &= 0, && \text{if } \sigma_i \le \sigma_{threshold} \\ D_i &= \frac{\sigma_i - \sigma_{threshold}}{\sigma_{crit} - \sigma_{threshold}}, && \text{if } \sigma_{threshold} < \sigma_i < \sigma_{crit} \\ D_i &= 1, && \text{if } \sigma_i \ge \sigma_{crit} \end{aligned} \tag{9}$$

where i = 1, 2 which represent tensile and compressive, respectively.

The material degradation is modeled by loss of stiffness as

$$\widetilde{E} = (1 - D)E \tag{10}$$

where the total damage, *D,* is the combination of the tensile and compressive damages.

$$D = 1 - (1 - D_t) \cdot (1 - D_c) \tag{11}$$

The finite element formulation of the transient heat transfer equation (1) can be written by using Galerkin's approach in the following matrix form as [20]

$$[C]\{\dot{T}\} + [K]\{T\} = \{R\} \tag{7}$$

where $[C]$ is the heat capacity matrix, $[K]$ is the conductivity matrix, $\{T\}$ is the nodal temperature vector and $\{R\}$ is the heat source vector.

The finite element formulation of the thermoelastic problem can be obtained by deriving the equilibrium equation and applying the variational principle in the following matrix form as [20]

$$[K]\{U\} = \{F\} \tag{8}$$

where $[K]$ is the stiffness matrix, $\{U\} = \{U, W\}^T$ is the nodal displacement vector and $\{F\}$ is the summation of the body force, surface traction and thermal load vectors.

The thermal behavior and mechanical behavior are coupled together. For this reason, coupled temperature-displacement analysis is conducted by using commercial software ABAQUS [21] in the following matrix:

$$\begin{bmatrix} K_{UU} & K_{UT} \\ K_{TU} & K_{TT} \end{bmatrix} \begin{bmatrix} \Delta U \\ \Delta T \end{bmatrix} = \begin{Bmatrix} R_U \\ R_T \end{Bmatrix} \tag{9}$$

where ΔU is the respective corrections to incremental displacement due to thermal expansion, ΔT is the respective corrections to incremental temperature, K_{ij} are submatrices of the fully coupled Jacobian matrix, and R_U and R_T are the mechanical and thermal residual vectors, respectively.

RESULTS AND DISCUSSION

Black liquor is the material used in gasifiers as a raw material to produce energy. Therefore the composition of black liquor is of high importance, because of its huge effect on corrosion behavior of refractory material as a lining of gasifier vessel. The typical composition of virgin black liquor from North American wood is mentioned in Table 1.

Table 1 Typical composition of virgin black liquor from North American wood (wt. %)

	Softwood		Hardwood	
	Typical	Range	Typical	Range
Carbon, %	35.0	32-37.5	34.0	31-36.5
Hydrogen, %	3.5	3.4-4.3	3.4	2.9-3.8
Nitrogen, %	0.1	0.06-0.12	0.2	0.14-0.2
Oxygen, %	35.4	32-38	35.0	33-39
Sodium, %	19.4	17.3-22.4	20.0	18-23
Potassium, %	1.6	0.3-3.7	2.0	1-4.7
Sulfur, %	4.2	2.9-5.2	4.3	3.2-5.2
Chlorine, %	0.6	0.1-3.3	0.6	0.1-3.3
Inert, %	0.2	0.1-2.0	0.5	0.1-2.0
Total, %	100.0		100.0	

The composition of black liquor listed in Table 1 is in the form of elemental analysis but by the use of FactSage as a tool of thermodynamic modeling one can convert elemental analysis compositions to compound compositions as is observed in Table 2 which represents a typical composition of black liquor at $950^{\circ}C$ and P_t=1atm fed to the gasifier.

Table 2 Composition of Black Liquor (wt. %)

Constituents	Na_2CO_3	Na_2S	K_2CO_3	C
%	50-55	25-30	1-3	15-20

If it is assumed that all the carbon is burned by the air introduced to the gasifier, the composition of the smelt in contact of refractory lining will be approximately the composition shown in Table 3.

Table 3 Composition of Black Liquor and melting point of each component (wt. %)

Constituent	**Na_2CO_3**	**Na_2S**	K_2CO_3
%	**70-75**	**20-25**	2-5
Melting Point (^{0}C)	858	1172	901

Therefore, it is observed that about three quarters of the black liquor smelt is composed of sodium carbonate which is liquid in the operating conditions of black liquor gasifiers. Obviously the selection of refractory materials for this application should be based upon resistance to molten sodium carbonate although Na_2S and K_2CO_3 should not be ignored. The melting temperatures of the main components of black liquor are listed in Table 3. It is obvious that Na_2S is not as corrosive as two other components from the point of chemical attack because it is in solid state at the operating conditions of the BLG gasifier while sodium and potassium carbonate are in the liquid state. Obviously this statement is true only when there is no solution between Na_2CO_3 and Na_2S which based on FactSage, no solution was observed.

If refractory compounds in Al-Si-O system, are in contact with Black Liquor at $950^\circ C$ and P_t=1atm, the reaction products based on FactSage data base Gibbs free energy minimization are tabulated in Table 5. The gas phase reaction products include mostly CO and H_2 with minor amounts of H_2O, CO_2, CH_4, NaCl, KCl, N_2, $(NaCl)_2$, H_2S, Na, $(KCl)_2$ and K.

Table 4 Interaction of alumino-silicate compound refractories with black liquor at 950$^{\circ}C$

Refractory Compound / Reaction Product	Corundum	Aluminum Silicate	Mullite
Corundum	-	×	×
β"-alumina	×	-	-
β-alumina	×	-	-
k-β"-alumina	×	-	-
Nepheline	-	×	×
Albite	-	×	×
Leucite	-	×	×
Na_2S	×	-	-
Graphite	×	×	×

(×): the phase is formed, (-): the phase is not formed

It is obvious from the information in Table 4 that none of the alumino-silicate refractories, even α-alumina, are resistant to either sodium carbonate or Black Liquor at $950^{\circ}C$ which is the temperature of gasification in both HTHP and HTLP processes. It is observed that all α-alumina is converted to $\beta-$alumina in contact with Na_2CO_3 and to β"-alumina, $\beta-$alumina and $K-\beta-$alumina in contact with Black Liquor. All formed phases are in the solid state in black liquor gasification conditions. Therefore, large volume changes due to formed phases should impose large stresses in refractory structure. In this condition it is predicted that crack formation and spallation of refractory may be the main wear mechanism.

In the case of mullite; nepheline, albite, leucite and corundum are formed just based on thermodynamic equilibrium calculations. All of these phases are in the solid state and have large volume changes which are enough to produce large cracks in the structure and decrease the lining life considerably due to spallation. In this case, α-alumina formed as a reaction product of mullite with black liquor can be attacked again with black liquor and corroded by the same mechanism.

The same occurs for aluminum silicate compounds with some differences in the amount of new phases formed as a result of interaction of these compounds with Black Liquor at $950^{\circ}C$. The vaporization of refractory constituents is negligible in these conditions.

Historically the refractory materials used as the lining of high temperature black liquor gasifiers to protect the vessel have been based on alumino-silicates refractories which predictably cannot survive for a long time. The interaction between these refractories and sodium carbonate is proposed to be as follows:

$$Na_2CO_3 + SiO_2 \longrightarrow Na_2O.SiO_2(glass) + CO_2 \quad (1)$$

$$Na_2CO_3 + Al_2O_3 \longrightarrow Na_2O.Al_2O_3 + CO_2 \quad (2)$$

$$Na_2CO_3 + 11Al_2O_3 \longrightarrow Na_2O.11Al_2O_3(\beta - Alu\min a) + CO_2 \quad (3)$$

$$Na_2CO_3 + 3Al_2O_3.2SiO_2 \longrightarrow Na_2O.Al_2O_3.2SiO_2 + 2Al_2O_3 + CO_2 \quad (4)$$

$$Na_2CO_3 + 3Al_2O_3.2SiO_2 + 2SiO_2 \longrightarrow 3Na_2O.2Al_2O_3.4SiO_2 + Al_2O_3 + CO_2 \quad (5)$$

The information obtained from use of the FactSage thermodynamic data base regarding alumino-silicate refractories in contact with Black Liquor only relates to thermodynamics if equilibrium is achieved and the kinetics are not considered. Experimental verification is necessary to discover the corrosion mechanism.

Some thermodynamic studies (FactSage) were performed to predict the behavior of some simple refractory oxides and complex oxides, as well as non-oxides as new refractory material candidates, against Na_2O, Na_2CO_3, K_2O, K_2CO_3, the main components of black liquor.

Simple oxides selected as candidates for use in high temperature black liquor gasifier are Al_2O_3, SiO_2, ZrO_2, CeO_2, La_2O_3, Y_2O_3, MgO and CaO. In first step an effort was made to plot an Ellingham Diagram for these oxides against sodium oxide (and also potassium oxide) to see the potential of sodium or potassium metal vapor to reduce the candidate refractory oxides because the existence of alkaline metal vapor in the gasifier atmosphere is probable. Obviously if the free energy of formation of each candidate is less than that for sodium or potassium oxide, it means that that oxide is more stable than sodium (potassium) oxide or sodium (potassium) metal vapor is not able to reduce it. Therefore that oxide is stable and can be still be a candidate for use in our application conditions. It should be mentioned that the total pressure (P_t) selected to plot the diagram is 1 atmosphere. The plotted diagram is presented in Figure 8.

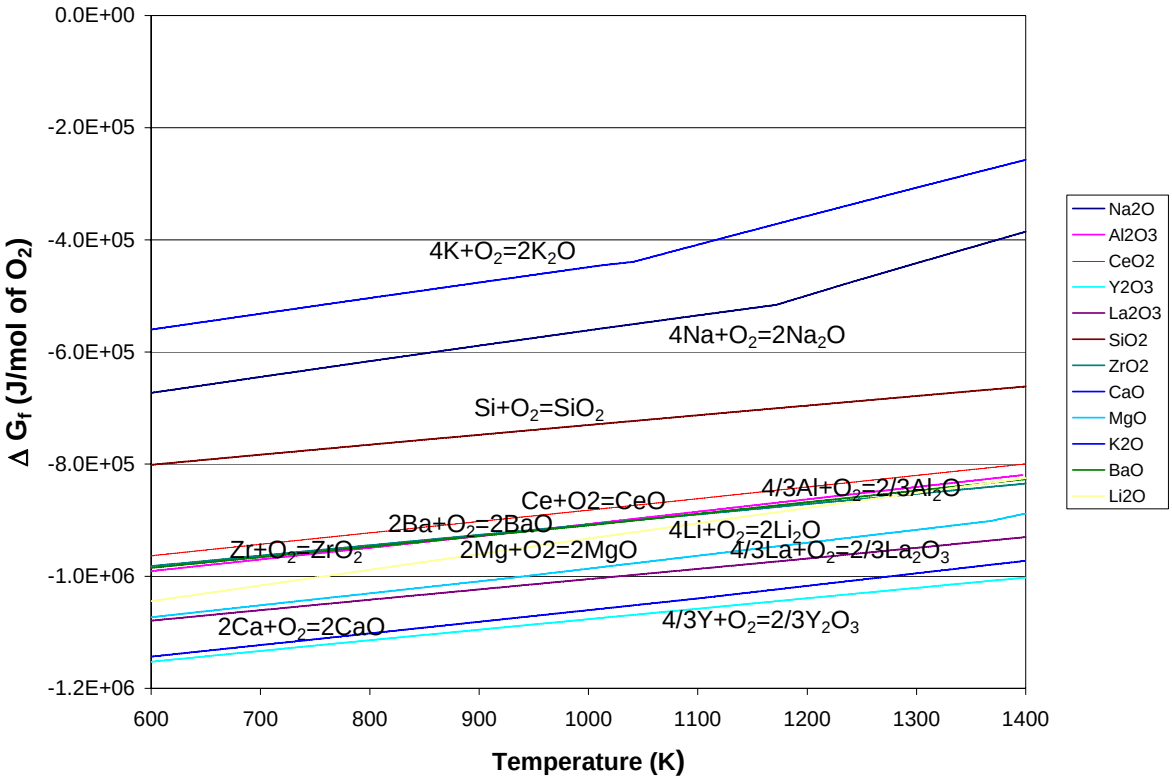

Figure 8 Ellingham Diagram of candidate simple oxides against sodium oxide

As is seen from the diagram, all of candidate refractory simple oxides are resistant to sodium metal vapor or potassium as well at P_t=1atm and $T = 600 - 1400K$ because they all have free Gibbs Energy of formation, less than that of sodium or potassium oxide. But also it should be mentioned that Ellingham Diagram can not be the only tool to evaluate the material because it doesn't show any data in the case that new compounds are formed. For example, alumina or silica is not reduced by sodium oxide but they form new compounds which are the cause of wear.

FactSage was also used to predict the behavior of candidate refractory simple oxides against the main components of black liquor at T=900-1000$^\circ C$ which is the working temperature range of high temperature BLG gasifier. The results are listed in Table 5. It shows that all our simple oxide refractories except Al_2O_3 and SiO_2 are resistant against sodium and potassium oxide and sodium and potassium carbonate.

More over, it is observed that based on the FactSage thermodynamic data base, SiC and Si_3N_4, two non-oxide refractory candidates for BLG gasifier applications, are not resistant to black liquor constituents. SiC is converted to compounds such as $(Na_2O)(SiO_2)$, $Na_6Si_2O_7$, K_2SiO_3 and $K_2Si_2O_5$ which some of them are in liquid state in operating temperature on BLG gasifier and dissolved into the smelt.

Table 5 Interaction of refractory simple oxides and non-oxide with BLG components at T=900-1000ºC

Refractory	Na_2O	Na_2CO_3	K_2O	**K_2CO_3**
Al_2O_3	×	×	×	×
SiO_2	×	×	×	×
MgO	-	-	-	-
CaO	-	-	-	-
ZrO_2	-	-	-	-
Y_2O_3	-	-	-	-
La_2O_3	-	-	-	-
CeO_2	-	-	-	-
Li_2O	-	-	-	-
BaO	×	×	×	×
SiC	×	×	×	×
Si_3N_4	×	×	×	×

(×): reaction, (-): no reaction

There is some concern regarding the hydration of two of the oxides, MgO and CaO especially when the operating condition of the gasifier includes water vapor. Therefore an effort was made to predict the hydration behavior of these oxides as a function of temperature at P_{H_2O} = 1, 20 and 100atm. The FactSage data base was used and the results of this study are listed in Figures 9 and 10.

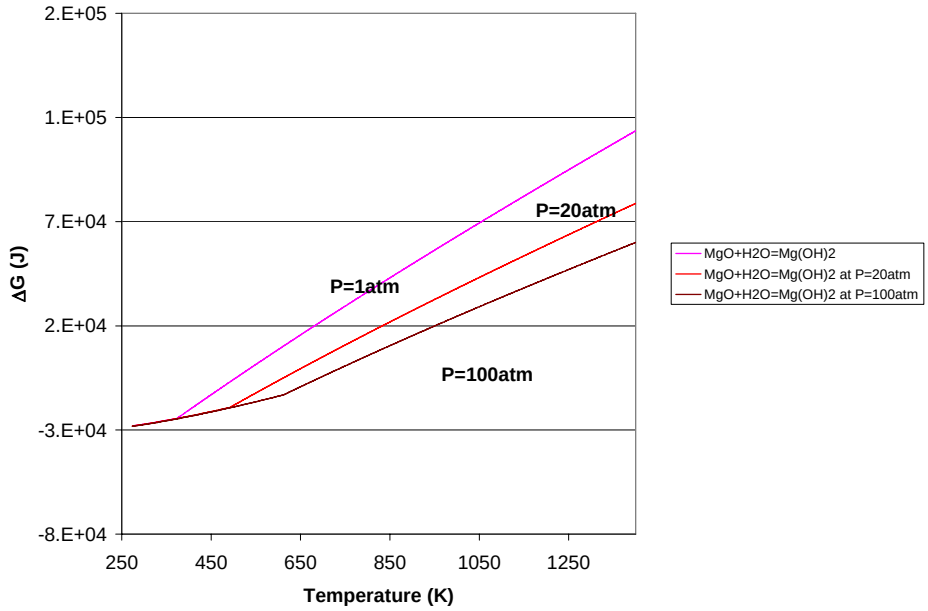

Figure 9 Hydration behavior of Magnesia

There is a temperature gradient across the refractory lining, the hydration depends on penetration of water vapor into the depth of refractory lining through porosity, cracks or joints. As it is observed from Figure 8 even at P_{H_2O} = 100atm, hydration doesn't occur for magnesia until temperatures less than $500^\circ C$ but under the same conditions, calcia hydrates easily at about T=$950^\circ C$. Therefore, it can be concluded that perhaps magnesia can be used in BLG gasifiers but calcia would have the problem of hydration because diffusion of water vapor into the refractory lining to reach the limiting hydration temperature is much more probable for calcia compared to magnesia.

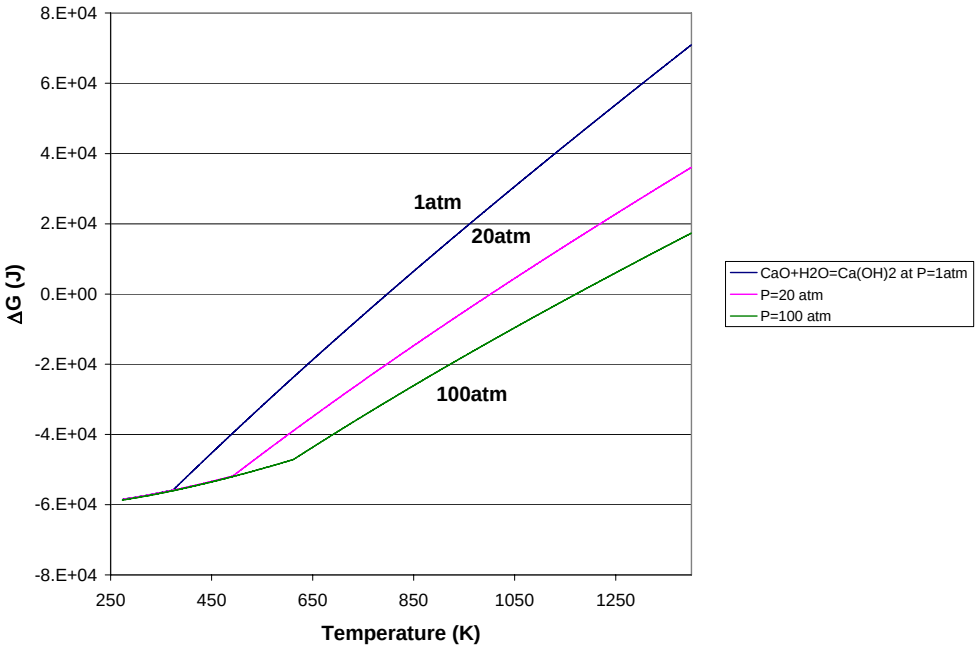

Figure 10 Hydration behavior of Calcia

The next step is to study the behavior of aluminates with alkaline atmospheres. The candidate aluminates are $MgAl_2O_4$, $BaAl_2O_4$, $LiAlO_2$ and the equation for the main corrosion reaction of these oxides with sodium oxide are as follows:

$$MgAl_2O_4 + Na_2O \longrightarrow MgO + 2NaAlO_2 \qquad (6)$$

$$BaAl_2O_4 + Na_2O \longrightarrow BaO + 2NaAlO_2 \qquad (7)$$

$$2LiAlO_2 + Na_2O \longrightarrow Li_2O + 2NaAlO_2 \qquad (8)$$

The change in the free Gibbs Energy (ΔG) because of reaction is plotted versus temperature in Figure 11. The data to plot this diagram was provided from the FactSage data base.

From this diagram it is understood that none of the aluminates are resistant to sodium oxide in the range of temperature 600-1400K because ΔG for reaction for all of them with sodium oxide is negative although it can be concluded that barium aluminate is the most resistant one and magnesium aluminate is the least resistant one against sodium oxide.

As sodium is in the form of sodium carbonate and not sodium oxide in black liquor and in the working conditions of high temperature gasifiers therefore it is worth while to try to predict the behavior of these aluminates to sodium carbonate as well.

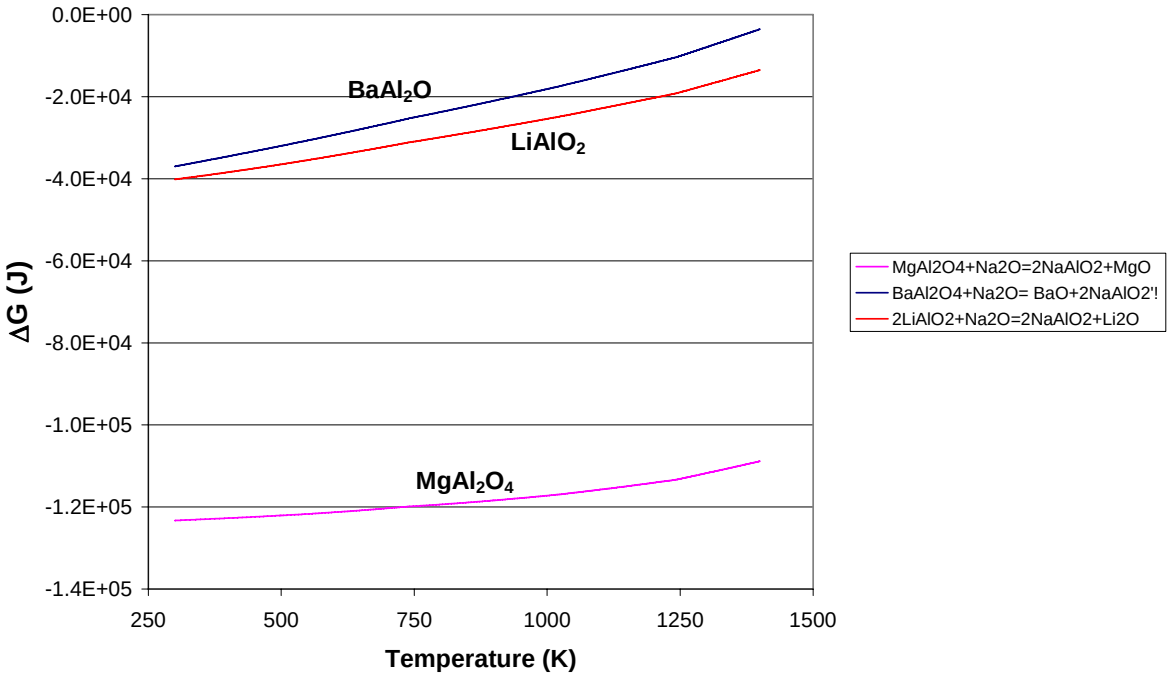

Figure 11 ΔG for the reaction between three candidate aluminates with sodium oxide

The reaction equations of candidate aluminates with sodium carbonate are as follows:

$$MgAl_2O_4 + Na_2CO_3 \longrightarrow MgCO_3 + 2NaAlO_2 \qquad (9)$$

$$BaAl_2O_4 + Na_2CO_3 \longrightarrow BaCO_3 + 2NaAlO_2 \qquad (10)$$

$$2LiAlO_2 + Na_2CO_3 \longrightarrow Li_2CO_3 + 2NaAlO_2 \qquad (11)$$

First we should know the ranges of temperatures over the carbonate products are stable. The reaction equations for stability of the three above listed reactions (the diagram for K_2CO_3 and $CaCO_3$ is plotted as well) are as follows:

$$MgCO_3 \longrightarrow MgO + CO_2 \qquad (12)$$

$$BaCO_3 \longrightarrow BaO + CO_2 \qquad (13)$$

$$Li_2CO_3 \longrightarrow Li_2O + CO_2 \qquad (14)$$

$$Na_2CO_3 \longrightarrow Na_2O + CO_2 \qquad (15)$$

ΔG for dissociation of carbonates as a function of temperature in the range of 600-1400K based on FactSage thermodynamic data base is shown in Figure 12.

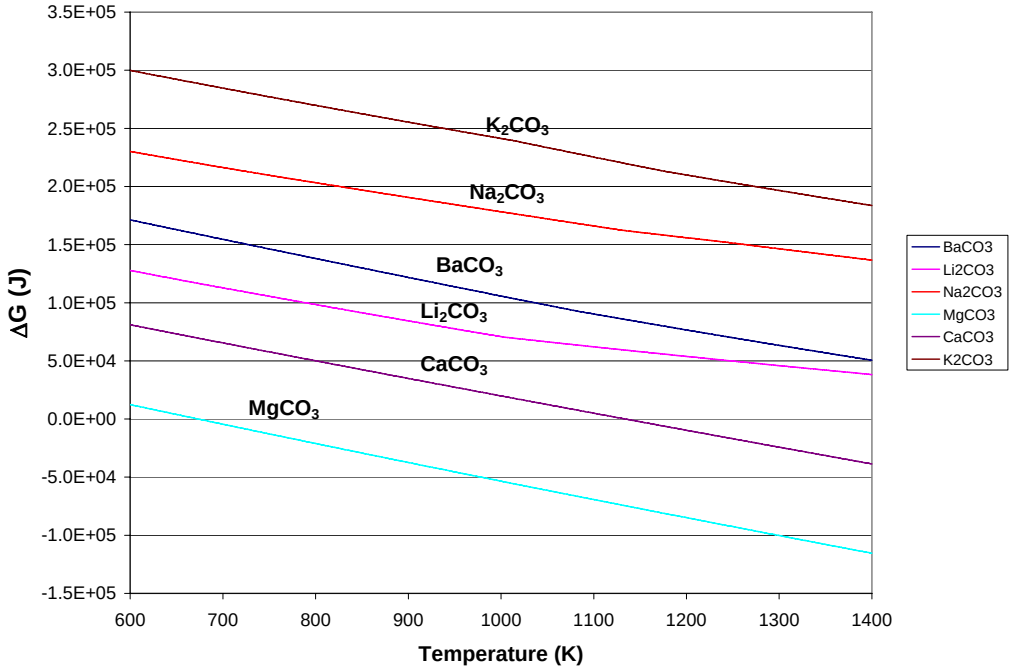

Figure 12 ΔG of dissociation of carbonates versus temperature

From Figure 11 it is recognized that all considered carbonates as reaction products of aluminates with sodium carbonate are stable except magnesium carbonate which dissociates at 673K and P_t = 1atm. The same happens to calcium carbonate but at higher temperature. Therefore from T=637K, the equation for the reaction of magnesium aluminate with sodium carbonate should change to the reaction as follows:

$$MgAl_2O_4 + Na_2CO_3 \longrightarrow 2NaAlO_2 + MgO + CO_2 \qquad (16)$$

Also it can be seen that sodium and potassium oxide are not in the form of an oxide in the range of working temperatures of BLG gasifiers but they are in carbonate form.

Now following the reactions mentioned above, thermodynamic stability of aluminates against sodium carbonate can be evaluated based on FactSage data base. Figure 13 is the result of this thermodynamic modeling in the form of ΔG of reaction versus temperature.

It is observed that all candidate aluminates are stable against sodium carbonate and among them magnesium aluminate spinel is the most resistant because it has the highest change of Free Gibbs Energy as a result of reaction with sodium carbonate.

It is hard to decide whether to candidate these aluminates for the lining of high temperature gasifiers because, although they are resistant to sodium carbonate, they are corroded by sodium oxide. Thermodynamic modeling shows that sodium is stable in the form of sodium carbonate and sodium sulfide in the operating conditions of high temperature black liquor gasifier and not in the form of sodium oxide, but it seems to be risky to use these refractory materials in these conditions because existence of sodium oxide due to introduction of water vapor to the gasifier and unstable operating condition is probable.

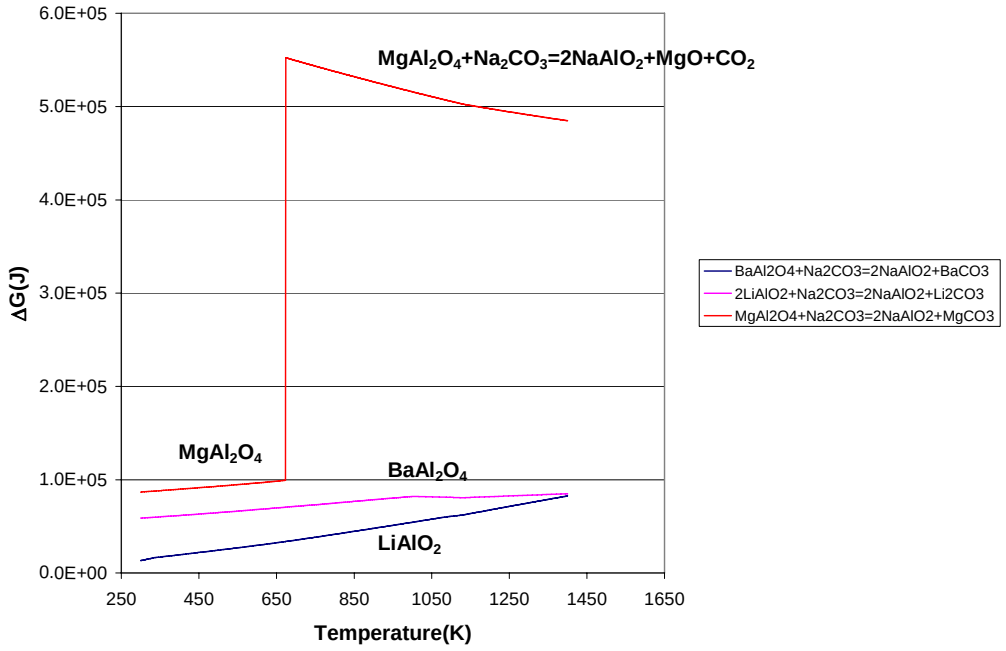

Figure 13 ΔG of reactions between aluminates and sodium carbonate

Thermodynamic modeling of reaction of aluminates with black liquor composition shows that they are not resistant to potassium containing compounds of black liquor; therefore, it was decided to study the reaction behavior of aluminates with K_2O and K_2CO_3 as well.

The main reaction of three aluminates with potassium oxide is as follows:

$$MgAl_2O_4 + K_2O \longrightarrow MgO + 2KAlO_2 \qquad (17)$$

$$BaAl_2O_4 + K_2O \longrightarrow BaO + 2KAlO_2 \qquad (18)$$

$$2LiAlO_2 + K_2O \longrightarrow Li_2O + 2KAlO_2 \qquad (19)$$

Free Gibbs energy change of the reaction as a function of temperature is plotted in Figure 14.

It is observed that none of our candidate aluminates resist potassium oxide and, among them, barium aluminate is the most resistant one and magnesium aluminate is the least. Reaction equations of aluminates with potassium carbonate are as follows:

$$MgAl_2O_4 + K_2CO_3 \longrightarrow MgCO_3 + 2KAlO_2 \qquad (20)$$

$$BaAl_2O_4 + K_2CO_3 \longrightarrow BaCO_3 + 2KAlO_2 \qquad (21)$$

$$2LiAlO_2 + K_2CO_3 \longrightarrow Li_2CO_3 + 2KAlO_2 \qquad (22)$$

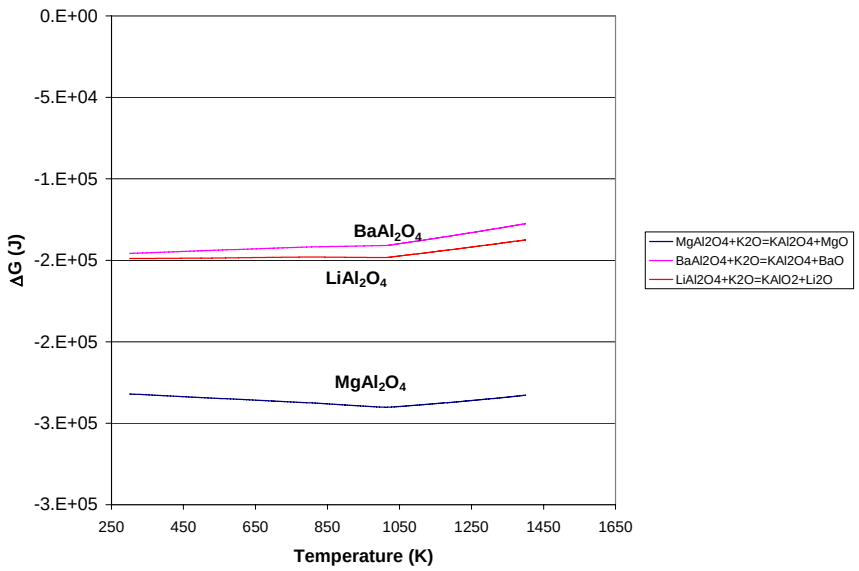

Figure 14 ΔG of reactions between aluminates and potassium oxide

ΔG of reactions between aluminates and potassium carbonate versus temperature are plotted in Figure 15. It can be concluded from this figure that among the three aluminates, only lithium aluminate is resistant to potassium carbonate and the usage of barium and magnesium aluminates in exposure to potassium carbonate is not advisable.

It can be summarized that all three aluminates are resistant to sodium carbonate, but not sodium oxide. Also it was observed that none of the aluminates are resistant to potassium oxide, but, regarding potassium carbonate, lithium aluminate is resistant.

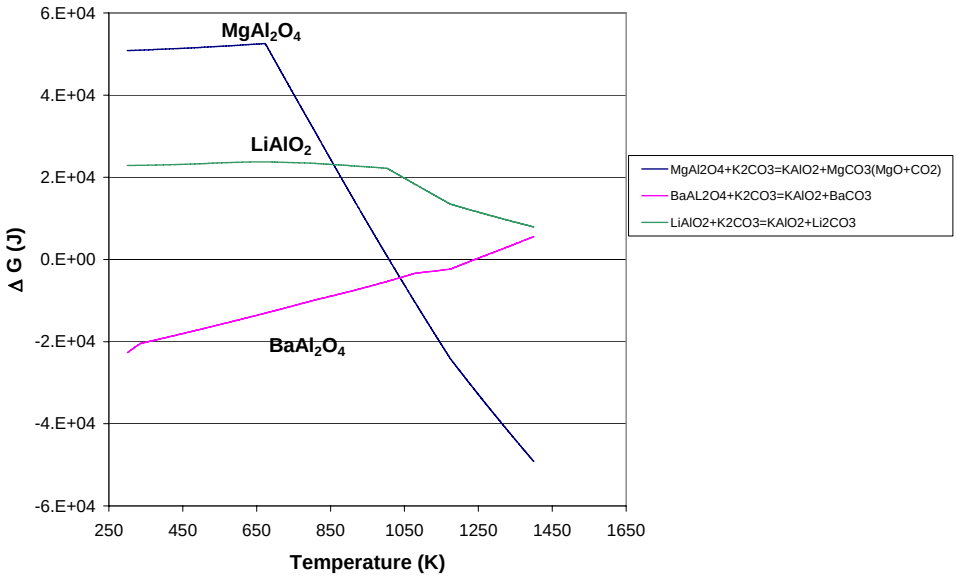

Figure 15 ΔG of reactions between aluminates and potassium carbonate

Contact angles measured for molten Na_2CO_3 on the candidate materials are shown in Figure 16. All of the candidate oxides were wet by Na_2CO_3 at 1000°C. The highest contact angle was observed on $MgAl_2O_4$ (13.3 ± 1.2 degrees) and the lowest on $BaAl_2O_4$ (~0 degree). The molten smelt was expected to wet all of the oxide refractories since the compounds in the smelt including Na_2CO_3 are highly ionic.[33] Contact angles measured for molten K_2CO_3 on the candidate materials are shown in Figure 17. For K_2CO_3, MgO showed the highest contact angle of about 9.9 ± 1.5 degrees. The lowest contact angle was observed for $BaAl_2O_4$, which was completely wet by K_2CO_3 with a contact angle of about zero.

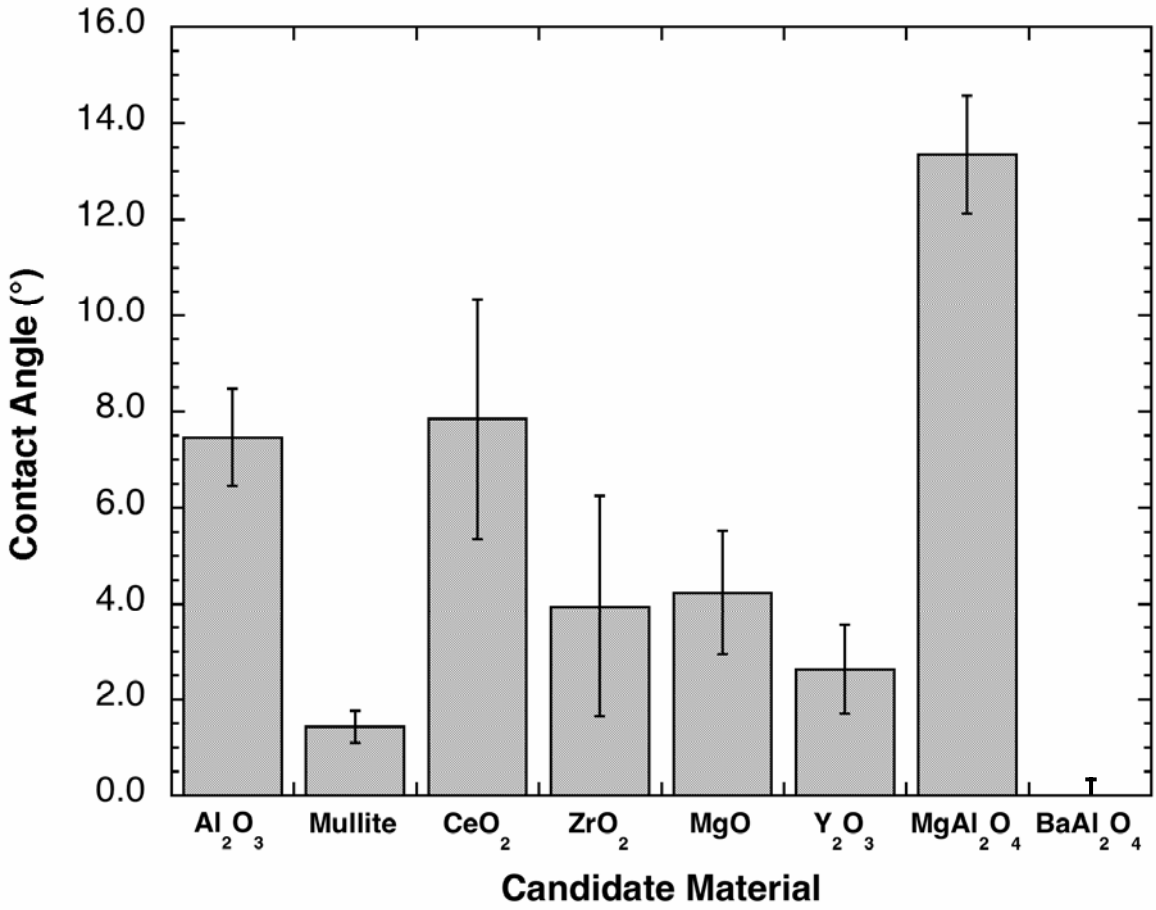

Figure 16. Contact angles for molten Na_2CO_3 on candidate refractories. Note: the contact angle was ~zero with a deviation of + 0.3 for $BaAl_2O_4$.

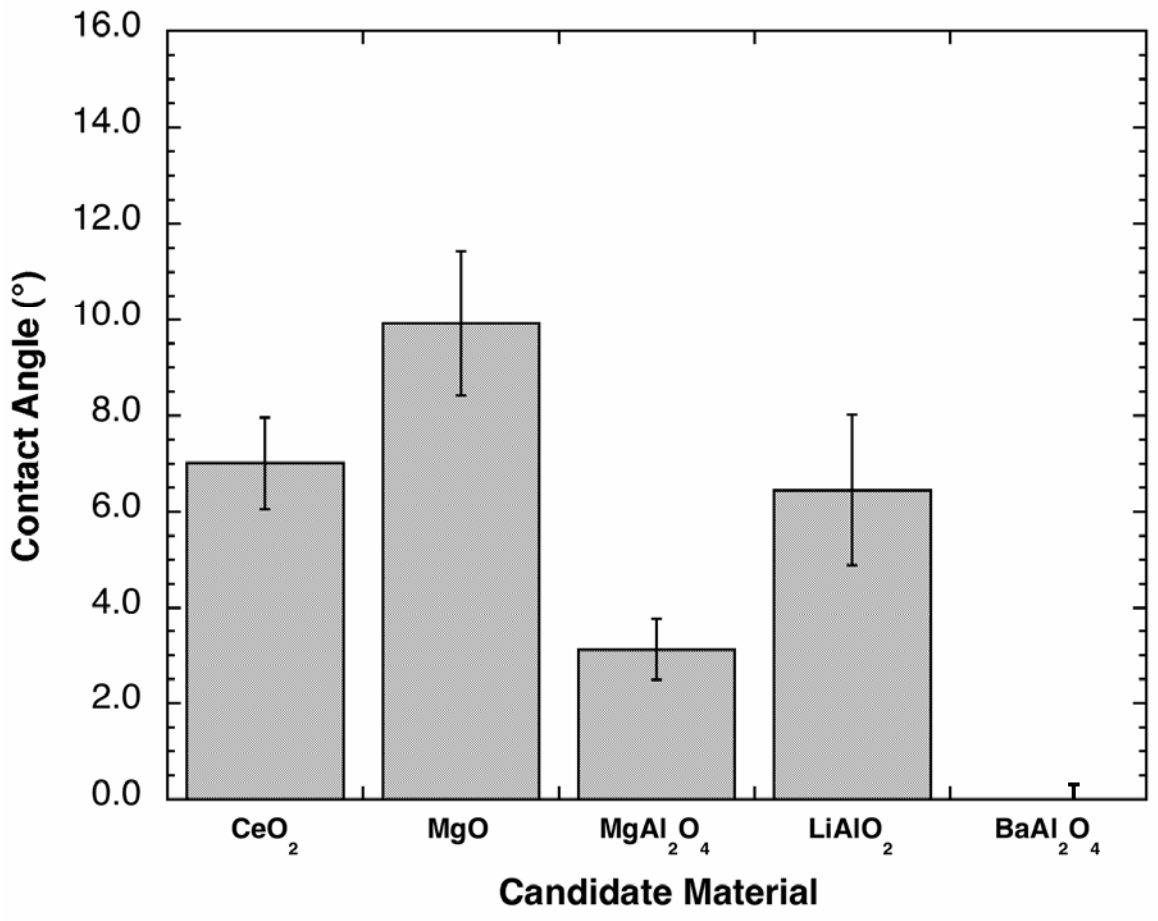

Figure 17. Contact angles for molten K_2CO_3 on candidate refractories. Note: the contact angle was ~zero with a deviation of + 0.2 for $BaAl_2O_4$.

The candidate materials could be divided into three main groups based on x-ray diffraction analysis: 1) materials that did not react; 2) those that reacted to form expansive phases that exposed the underlying material to further attack; and 3) those that quickly formed a dense, protective reaction layer that limited further reaction. The diffraction results are summarized in Table 6.

Table 6. Products formed by reaction of candidate refractories with Na_2CO_3 and K_2CO_3 at 1000°C as determined by sessile drop testing followed by XRD analysis.

Candidate Material	Na_2CO_3	K_2CO_3
Al_2O_3	$NaAlO_2$	-
$3Al_2O_3•2SiO_2$	$NaAlSiO_4$	-
CeO_2	NR	NR
ZrO_2	Na_2ZrO_3	-
MgO	NR	NR
Y_2O_3	$NaYO_2$	-
$MgAl_2O_4$	$MgO,NaAlO_2$	$MgO,KAlO_2$
$LiAlO_2$	$NaAlO_2$	$K_6Al_{44}O_{69}$
$BaAl_2O_4$	$NaAlO_2$	$Ba_3Al_2O_6$

(NR): No Reaction, (-): No Experiment

The first group, materials that did not react with either Na_2CO_3 or K_2CO_3, consisted of only MgO and CeO_2. This is in agreement with the thermodynamic analysis (Table 6), which did not predict reaction for either of these oxides. Based on relative cost and the commercial availability of MgO bricks, CeO_2, while resistant to attack, is not currently a viable candidate for high volume industrial production.

The second group that reacted with Na_2CO_3 to form expansive phases included α-Al_2O_3, $3Al_2O_3•2SiO_2$, ZrO_2, Y_2O_3, $LiAlO_2$ and $BaAl_2O_4$. After α-Al_2O_3 was exposed to molten Na_2CO_3, $NaAlO_2$ was found by XRD as had been proposed previously by C. R. Hubbard et al.[34] A volume expansion of 46% was expected for this reaction based on theoretical density as compared to 30% volume expansion measured by R. A. Peascoe et al[29]. Mullite reacted with Na_2CO_3 to form $Na_2Al_2SiO_6$. The expected volume expansion for this reaction would be 12% based on theoretical density as compared to 13% volume expansion measured by R. A. Peascoe et al.[29] Similarly, $Na_{1.75}Al_{1.75}Si_{0.25}O_4$ was formed when mullite contacted with a smelt composed of Na_2S, Na_2SO_4, and Na_2CO_3.[29] For contact of Na_2CO_3 with ZrO_2, Na_2ZrO_3 was identified by x-ray diffraction. Thermodynamic analysis in the current work had predicted no reaction. Earlier work by Yamaguchi[35] did correctly predict the reaction, and his work was verified by x-ray diffraction analysis in this study. The incorrect prediction of ZrO_2 reactivity in this study, as well as those for Y_2O_3, $LiAlO_2$, and $BaAl_2O_4$, clearly illustrate the problems that occur when databases contain inaccurate data, or as in this case, no data for certain compounds. In this case, the database employed did not contain data for Na_2ZrO_3. For Y_2O_3, $NaYO_2$, which also did not appear in the database, formed during contact with molten Na_2CO_3. The $LiAlO_2$ specimen cracked during sessile drop testing, probably due to reaction with Na_2CO_3. Analysis using GXRD showed that the $LiAlO_2$ substrate reacted with Na_2CO_3 to form $NaAlO_2$. X-ray diffraction analysis of the $LiAlO_2$ substrate exposed to K_2CO_3 showed some peaks that could be attributed to the formation of $K_6Al_{44}O_{69}$ or $KAlO_2$, but the peaks could not be assigned unambiguously due to the

similarity of the patterns and the signal to noise ratio of the data. $BaAl_2O_4$ also reacted with Na_2CO_3 and, like the other aluminates that were tested, reacted to form $NaAlO_2$. For the reaction of $BaAl_2O_4$ with K_2CO_3, one of the reaction products was $Ba_3Al_2O_6$, unlike the other aluminates that all reacted to form sodium-containing compounds.

It is interesting to note that the formation of a lithium rich layer on aluminosilicate refractories has been reported as a method to increase resistance to alkali attack.[36,37] In this method, a lithium containing material such as LiOH or Li_2CO_3 is applied to the refractory surface, which is then heated to a sufficient temperature so that the lithium containing material forms an alkali resistant surface layer. The composition of the surface layer has not been reported in detail. It generally comprises crystalline and/or glassy phases that may include lithium aluminate, lithium silicate, or lithium aluminosilicate depending on the composition of the starting refractory material.[38] Apparently, the different composition of the surface layer as compared to the pure $LiAlO_2$ investigated in this study, changes the behavior of refractory material against alkali attack. Other refractory materials such as alumina, mixed α-β alumina, and $MgAl_2O_4$ based refractories have shown improved resistance to molten alkali salts after a lithium treatment though not to the extent observed for mullite based refractories.[37] This may indicate that a surface layer containing glassy or crystalline silica could be resistant to alkali attack.

The only oxide that fell into the final group of materials that reacted, but formed protective phases was $MgAl_2O_4$. Upon reaction with Na_2CO_3, $MgAl_2O_4$ was converted to MgO and $NaAlO_2$,(Table 6) similar to the results reported by C. R. Hubbard et al.[34] The penetration of the reaction layer into the substrate was minimal (<10 μm) relative to reactions that formed expansive phases, due to the formation of a protective layer of MgO (Figure 18.). Likewise, $MgAl_2O_4$ reacted with K_2CO_3 to form MgO and $KAlO_2$ (Table 6). As with the reaction with Na_2CO_3, MgO is also presumed to form a protective layer in this system. One possible reaction path that would be consistent with the observed behavior would have $MgAl_2O_4$ dissociate to MgO and Al_2O_3 first and then the Al_2O_3 would react with the carbonates to form alkali aluminates. Once a sufficient quantity of MgO forms, it could protect the underlying $MgAl_2O_4$ from further reaction. Unlike using MgO refractories that would be susceptible to hydration, $MgAl_2O_4$ is stable against hydration and would react with the smelt to form the protective MgO layer. If the MgO layer was damaged in service or by hydration during shut down, the underlying $MgAl_2O_4$ would react with the smelt and repair itself in-situ.

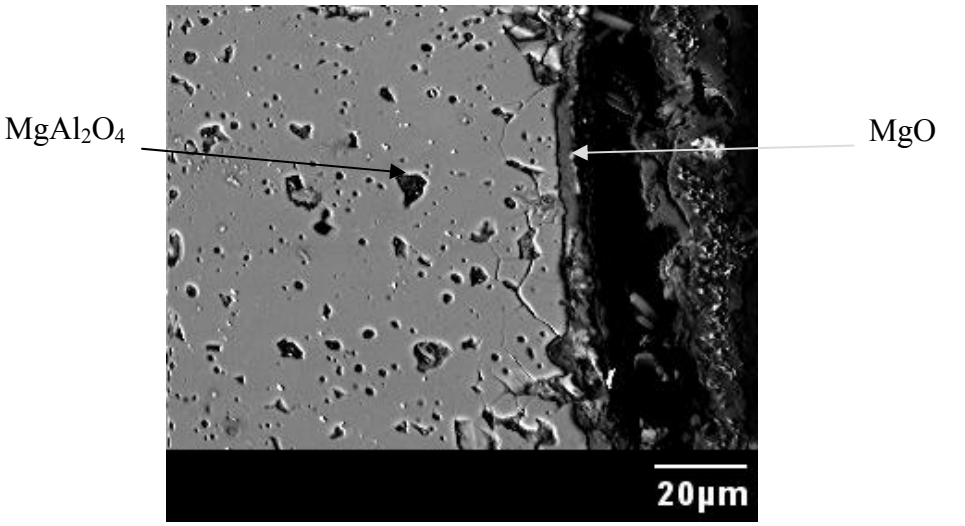

(a)

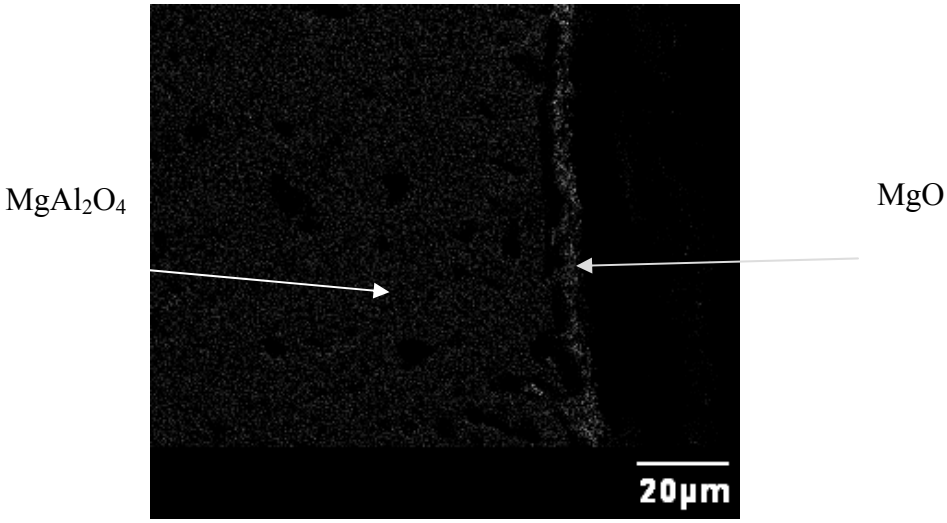

(b)

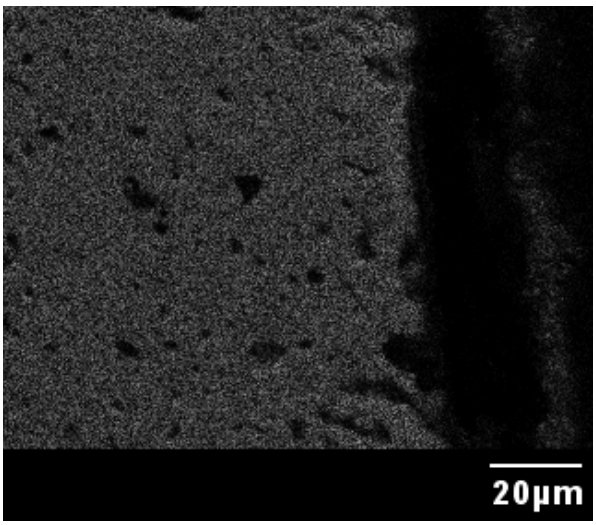

(c)

Figure 18. a) SEM micrograph showing dense MgO layer on $MgAl_2O_4$ and EDS mapping showing, (b) Mg enrichment (c) Al depletion from the reaction layer

By comparing the results of thermodynamics (Table 5) with the results of x-ray diffraction from sessile drop testing (Table 6), it was found that the thermodynamics and experiment were not in agreement for ZrO_2, Y_2O_3, $LiAlO_2$ and $BaAl_2O_4$. For α-Al_2O_3, thermodynamics predicts the formation of $Na_2Al_{12}O_{19}$ (β"-alumina). However the amount of this phase compared to the amount of $NaAlO_2$ was very small ($Na_2Al_{12}O_{19}$ / $NaAlO_2 \approx 1.4 \times 10^{-5}$) to the extent that is not detectable by grazing incidence x-ray diffraction technique. For mullite, thermodynamics predicted the instability of the candidate in contact with the smelt; but the reaction products predicted by thermodynamics were not completely in agreement with the results of XRD analysis. In contrast to the prediction by thermodynamics, α-Al_2O_3 was not identified by x-ray but $NaAlSiO_4$ which was also predicted by thermodynamics was identified. Some unidentified peaks were present in the pattern, which could belong to complex compounds in Na-Al-Si-O system. These XRD peaks could be caused by non-equilibrium phases that may disappear if longer reaction times were employed. The other reason for the discrepancy could be the lack of thermodynamic data in the database for one of the compounds, as discussed above. For $MgAl_2O_4$, the correct reaction was predicted by thermodynamics, but the reaction was impeded by the formation of a diffusion barrier (MgO) that inhibited further reaction.

The penetration of Na compounds into candidate refractories was investigated using x-ray mapping of polished cross sections of sessile drop specimens. As expected based on thermodynamics and the large volume change associated with the reaction, Na penetrated into mullite forming a distinct reaction layer at the surface of the substrate (Figure 19). Mapping showed that the reaction layer was about 50 µm thick after sessile drop test. In this geometry, it is likely that the depth of penetration was limited by the quantity of the reactant (Na_2CO_3) during the reaction as all of the smelt was consumed. For alumina, the thickness of the reaction layer was about 100 µm. Based on the volume change associated with the reaction, deeper Na penetration would be expected for alumina than mullite.

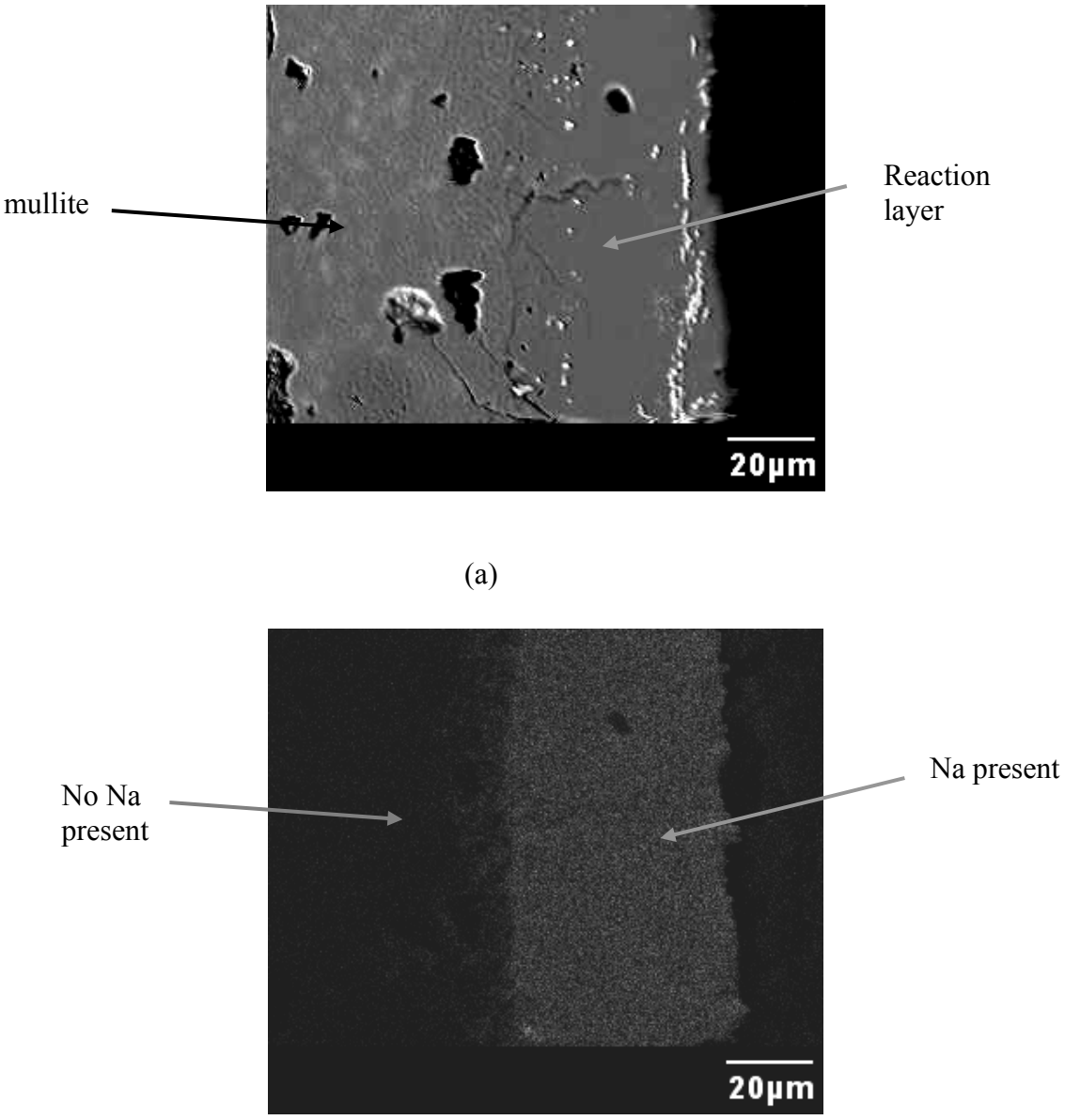

Figure 19. (a) SEM micrograph showing the reaction layer that resulted from molten Na_2CO_3 in contact with mullite, and (b) An EDS map of Na (Note that the image and EDS map have different magnifications).

The reaction layer for the ZrO_2 substrate was thin compared to alumina and mullite, ~5µm. Analysis by GXRD verified the formation of Na_2ZrO_3 as predicted by Yamaguchi[36]. Based on the reported densities, a volume expansion of 46% is predicted for conversion of ZrO_2 to Na_2ZrO_3, comparable to the expansions predicted for the reactions of alumina and mullite.

Although ZrO_2 reacted with Na_2CO_3 and formed an expansive phase, the rate of penetration was slow compared to alumina and mullite. The reaction layer for Y_2O_3 was also relatively thin, ~5-10μm. Analysis by GXRD confirmed the formation of $NaYO_2$, which should result in a volume expansion of ~15%. Based on sessile drop tests, ZrO_2 and Y_2O_3 could be candidates for black liquor smelt contact applications due to significantly slower penetration rates compared to alumina and aluminosilicates. However, neither showed the chemical resistance demonstrated by MgO or $MgAl_2O_4$.

Among the aluminates, both the $LiAlO_2$ and $BaAl_2O_4$ substrates contained open porosity. Thus, separation of the effects of penetration due to flow through pores from penetration due to formation of a reaction layer was difficult. As reported in the previous section, Na_2CO_3 reacted readily with both of these aluminates and significant penetration (on the order of the penetration observed for alumina and mullite) would be expected. As discussed previously, widespread cracking was observed upon reaction of $LiAlO_2$ with Na_2CO_3 (Figure 20). The cracking appeared to follow the grain boundaries suggesting them as the primary route of attack in this material.

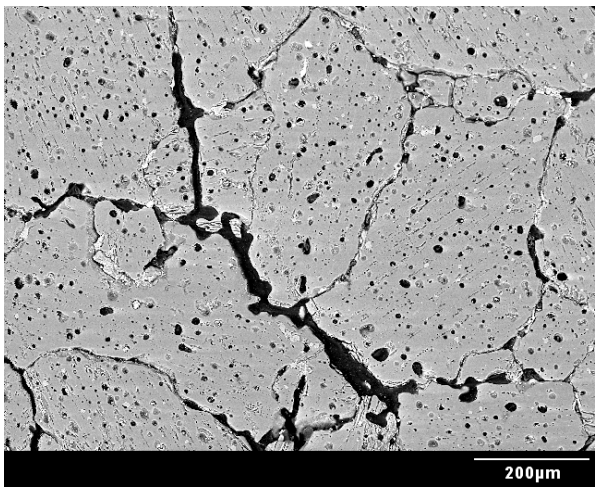

Figure 20. Crack formation in the $LiAlO_2$ substrate after contact with molten Na_2CO_3.

Although Na_2CO_3 did not react with CeO_2, some penetration of the smelt through the pores was detected. This penetration is attributed to flow of the smelt through the small volume fraction of open pores, not reaction. Archimedes' density measurements found ~2 vol% open porosity in the CeO_2 substrate. Neither thermodynamic analysis nor XRD indicate that CeO_2 should react with Na_2CO_3. Thus, CeO_2 should be considered among the candidates for black liquor contact applications, if the price and availability issues are overcome.

Based on thermodynamic analysis and sessile drop studies, dense MgO is resistant to penetration and is a candidate for applications requiring contact with molten black liquor smelt. Although the smelt was found to react with $MgAl_2O_4$, a dense MgO layer was formed *in-situ* (Figure 18), preventing further attack. The layer was approximately 3-4 μm thick and it appeared to protect the underlying $MgAl_2O_4$ substrate from further attack. Based on these results, further testing with MgO or $MgAl_2O_4$ as monolithic materials or as coatings on other substrates is warranted.

Samples of currently used, in-house, and refractories developed based on the results provided previously were provided by in-kind sponsors. These samples were tested according to the experimental procedure given in the experimental section. Table 7 is an overview of the results.

Table 7 Cup testing results

Sample Number	Al2O3 %	SiO2 %	ZrO2 %	MgO %	CaO %	Fe2O3 %	Na2O %	TiO2 %	P2O5 %	impurities %	Density (g/cc)	Theoretical Density (g/cc)	% Theoretical Density	Performance
5	93.29		5.07							1.64	3.43	4.06	84.37	Good
10	72.29	26.24								1.47	2.56	3.47	73.85	Good
16	59.46	34.06				1.51		2.33		2.64	2.46	3.35	73.35	Good
18	80.14	16.45			1.27					2.14	2.91	3.64	80.04	Good
20	97.23	1.17								1.6		3.94		Good
21	95.3	0.25		2.34						2.11	3.60	3.95	91.24	Good
25	78.2	18.1		0.1	0.1	1.4		1.9		0.2	2.69	3.17	85.02	Good
26	84	7.5		8	0.2	0.1				0.2	3.02	3.55	85.09	Good
27	0.7	0.5		96.5	1.1	0.7				0.5	2.98	3.52	84.59	Good
4	95.61		2.67							1.71	3.07	4.01	76.60	Small Cracks
8	88.72	0.8	7.76							2.72	3.29	4.10	80.19	Small Cracks
9	89.62	0.82	7.97							1.58	3.39	4.10	82.79	Small Cracks
11	89.43	0.78	7.78							2.01	3.33	4.10	81.24	Small Cracks
12	80.21	17.31								2.48	2.54	3.64	69.75	Small Cracks
13	89.74	0.81	8.11							1.34	3.24	4.10	78.99	Small Cracks
15	2.52	36.74	57.84							2.9	3.78	4.42	85.62	Small Cracks
17	95.95	0.21			0.89					2.95	3.00	3.94	76.23	Small Cracks
19	89.37	0.17		2.35			2.32		4.47	1.3	2.79	3.84	72.75	Small Cracks
24	87.1	11.36								1.54	2.82	3.69	76.41	Small Cracks
1	79.3	18.75								1.95	2.64	3.61	73.20	Failed
2	84.84	1.17	12.27							1.72	3.31	4.15	79.85	Failed
3	73.7	24.18								2.72	2.42	3.53	68.67	Failed
6	74.74	14.72	8.91							1.63	2.91	3.86	75.40	Failed
7	73.81	9.51	15.18							1.5	3.05	4.08	74.79	Failed
14	80.34	17.48								2.18	2.52	3.63	69.54	Failed

The best performing materials in the cup testing were fused cast materials. New castables appear to be outperforming any of the previously tested materials. Magnesia and spinel based castables and mortars also performed well. The materials that performed well are shown in more detail in the following discussion.

Sample number: 27

Type: Magnesia Brick

Chemistry: MgO: 96.5/98.5; CaO: Max. 1.1; Fe2O3: Max. 0.7; Al2O3: Max. 0.7; SiO2: Max. 0.5.

Density: 2.98 g/cc

Porosity: 15.4 %

Notes:

Sample 27 performed very well in the cup tests.

No reaction interface is visible on the surface of this sample. The RL and CL images illustrate the microstructure of a MgO brick (>96 % MgO) subjected to black liquor (Na_2SO_4 + Na_2CO_3) corrosion test at 1000^oC for 240 hours. Samples are taken from “left”, “right” and “bottom” sides of the test cup to determine smelt penetration and degree of refractory alteration in all three dimensions. Microstructures are identical or similar in all side and smelt penetration and the degree of alteration were indistinguishable in polished samples.

Most important feature observed was the intense delineation of grain boundaries of sintered MgO clinkers due to smelt vapor penetration. The matrix (not well polished) does not appear

to be smelt but rather fine MgO bond but may contain smelt component. An XRD run has been performed to confirm this. Although, no direct intense reaction is observed between smelt and MgO, the silicate impurities in the matrix and in grain boundaries would react readily resulting in refractory deterioration or mechanical disintegration.

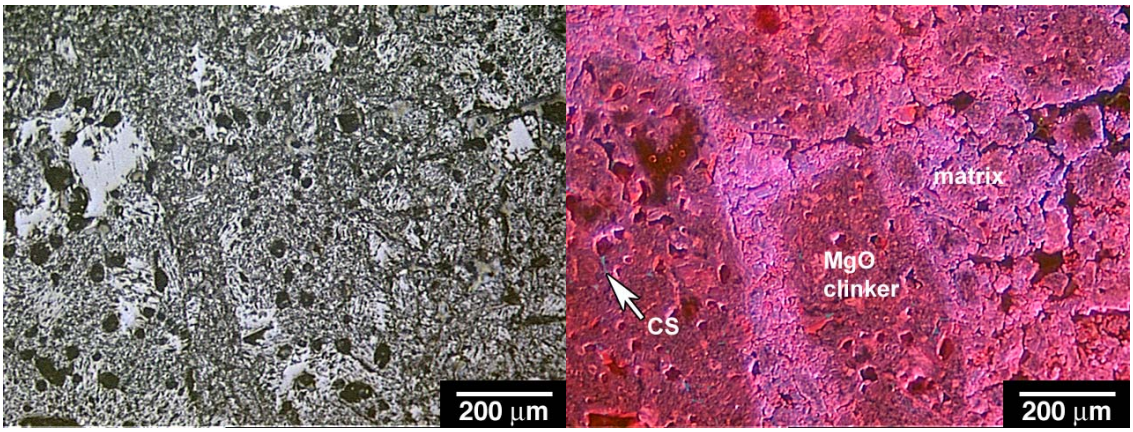

Figure 21 RL and CL pair of micrographs taken from an unused sample 27.

The unused brick is made from silicate bonded MgO (>96 % MgO). The silicate bond in MgO clinker is calcium silicate (CS) bond. Forsterite (Mg_2SiO_4) and monticellite ($CaMgSiO_4$) are not recognized under RL/CL microscopy. Calcium silicate bond makes the brick more refractory, CaO/SiO_2 ratio is larger than 1. As shown in RL/CL micrographs of tested samples, strong grain boundary delineation is observed in MgO clinker suggesting reaction between silicate bond and black liquor, although no intense reaction or reaction product is observed between black liquor and MgO brick. We suggest that before MgO brick is recommended for BLG, an in-situ test must be performed.

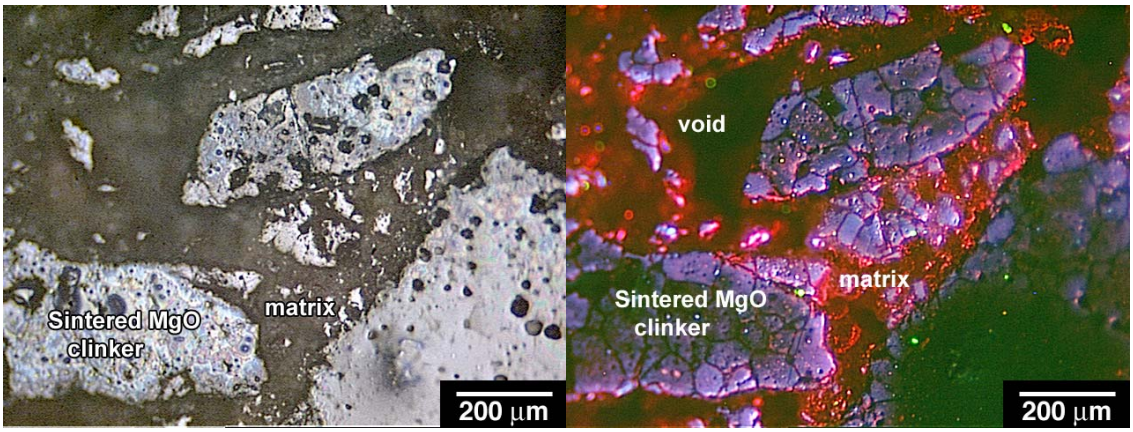

Figure 22 RL and CL microstructure of sample 27 subjected to black liquor cup test. These samples are made from the "Left" side of the test cup.

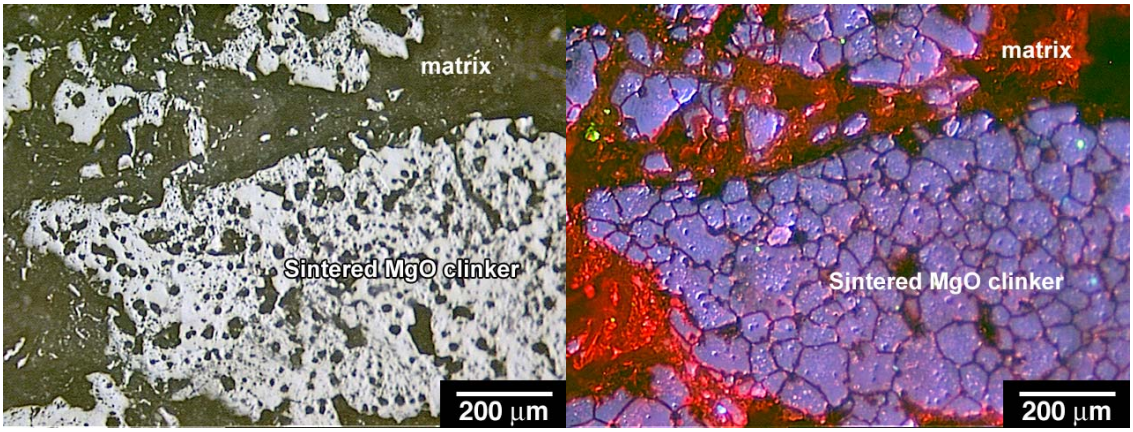

Figure 23 RL and CL microstructure of sample 27 subjected to black liquor cup test. This sample is made from the "Right" side of the test cup.

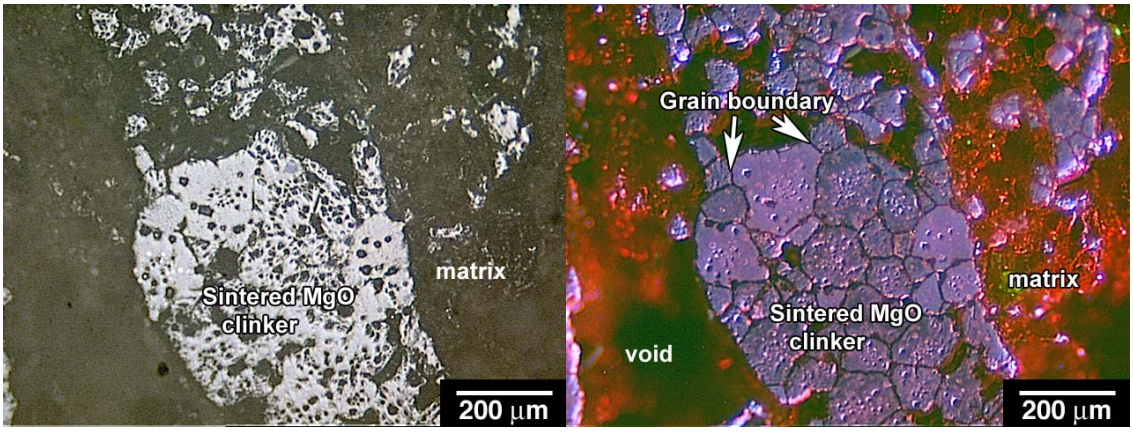

Figure 24 RL and CL microstructures of sample 27 subjected to black liquor cup test. Sample is taken from the "Bottom" side of the test cup.

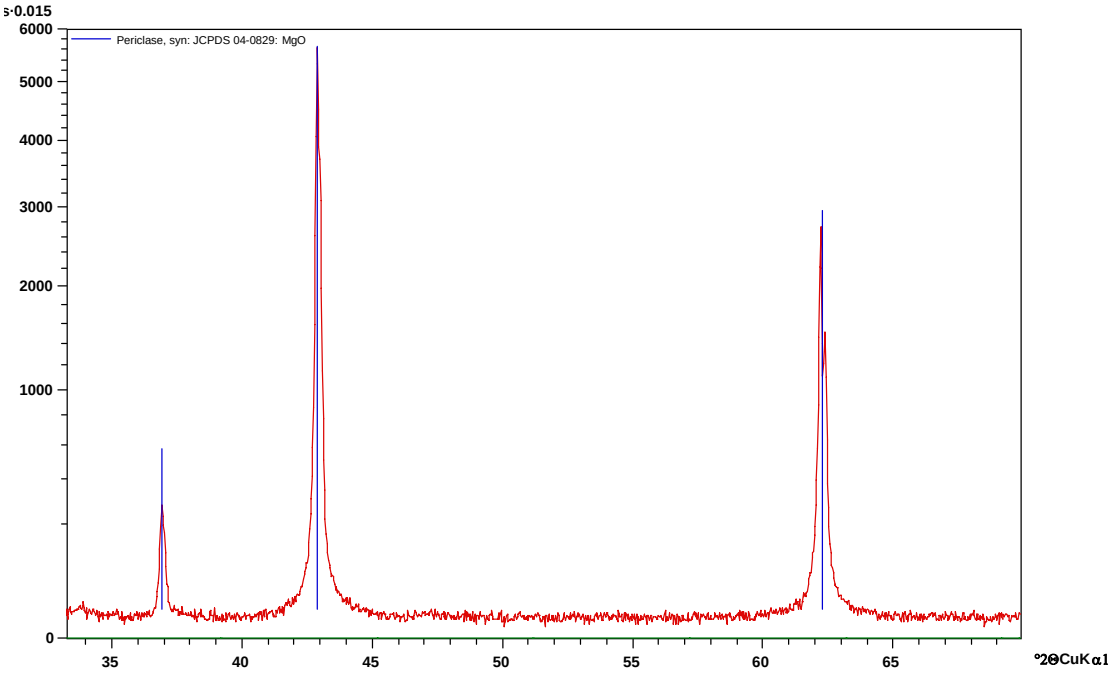

Figure 25 XRD pattern of sample 27 subjected to black liquor cup test, showing diffraction lines of only Periclase (MgO). The black liquor has a very poor crystallinity and strong MgO diffraction lines obscure the Na-carbonate and sulfate diffraction lines.

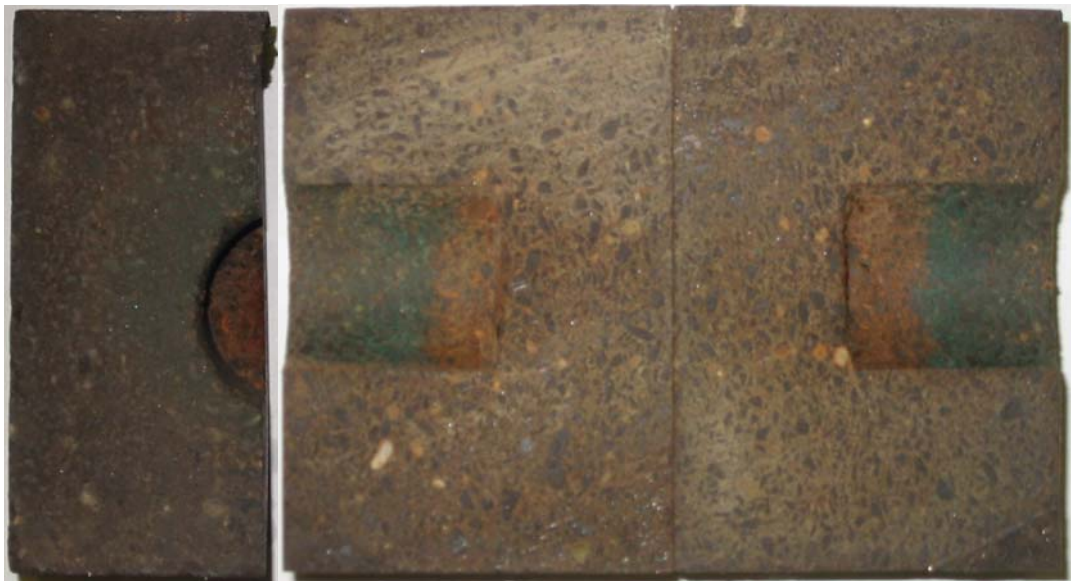

Figure 26 Cup Sample after smelt test.

A company provided two castable refractories materials, 25 and 26 to UMR for cup testing with black liquor smelts (high alkali content).

Sample: 25

Type: Castable

Chemistry: Al_2O_3 78.2%, SiO_2 18.1%, Fe_2O_3 1.4%, TiO_2 1.9%, CaO 0.1%, MgO 0.1%, Alk. 0.2%, P_2O_5, SiC, ZrO_2, Other.

Density: 2.69 g/cc

Porosity: 14.98%

Sample: 26

Type: Castable

Chemistry: Al_2O_3 84.0%, SiO_2 7.5%, Fe_2O_3 0.1%, TiO_2 0.0%, CaO 0.2%, MgO 8.0%, Alk. 0.2%, P_2O_5, SiC, ZrO_2, Other.

Density: 3.02 g/cc

Porosity: 14.91%

Cup Preparation:

Casting

25: 5.8% water was used, and the mixture is easy to cast.

26: 4.6% water was used, and the mixture is easy to cast.

Firing

All two cups were fired at 1050 °C for 5 hr. The heat rate was 1 °C/min. The cooling rate was also 1 °C/min.

Charge smelt

50 g smelt was charged to each cup.

Two cups were set in the box furnace. The furnace was flooded with Argon gas. The test temperature was 1000 °C. The test time was 240 hr. the heat and cooling rate were 1 °C/min.

Both cups have good resistance against smelts attack. Figure 27 shows the top view of sample 25 after cup test with 50 g smelts at 1000 °C for 240 hr. Figure 28 shows the cross-section in which there is an average thickness of 2.3 mm corrosion ply formed.

Figure 29 shows the top view of sample 26 after cup test with 50 g smelts at 1000 °C for 240 hr. Figure 30 shows the cross-section in which there is no corrosion ply observed.

Figure 27 Top view of sample 25 after cup test.

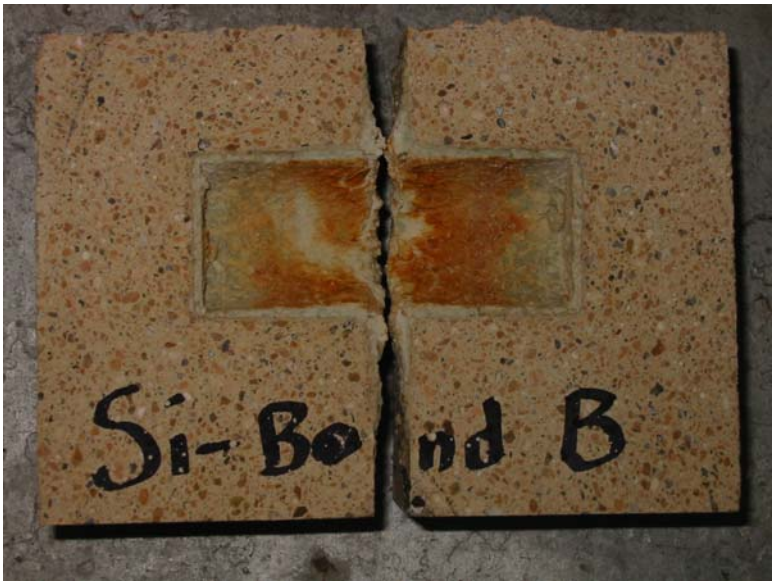

Figure 28 Cross-section of sample 25 after cup test.

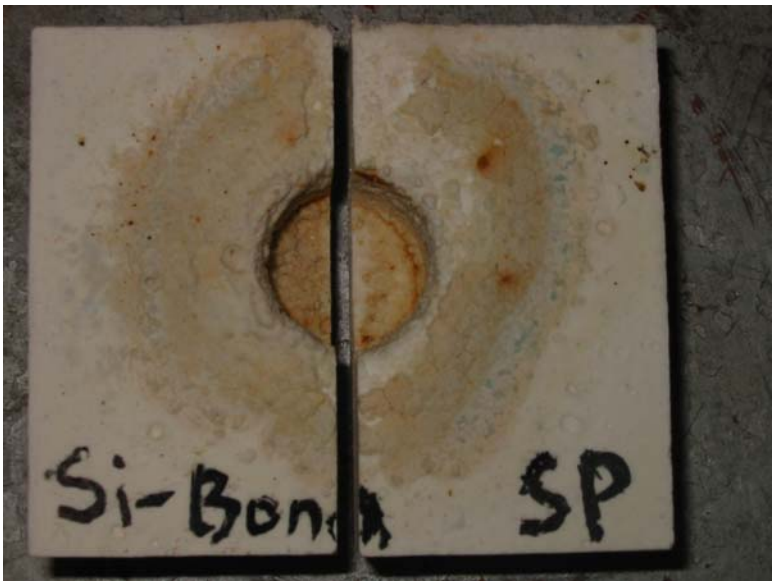

Figure 29 Top view of sample 26 after cup test.

Figure 30 Cross-section of sample 26 after cup test.

Figure 31 shows RL and CL microstructures of virgin sample 25 before firing. This sample is identified as cement-free high alumina castable refractory, which is made up of large alumina aggregates (AA), medium-sized fused mullite (FM) grains blended with most likely microsilica matrix. No calcium aluminate cement particle is identified. Alumina aggregates are highly impure containing Fe-Ti oxides as well as alkali matrix suggesting they are derived from clay-balls or bauxitic raw materials.

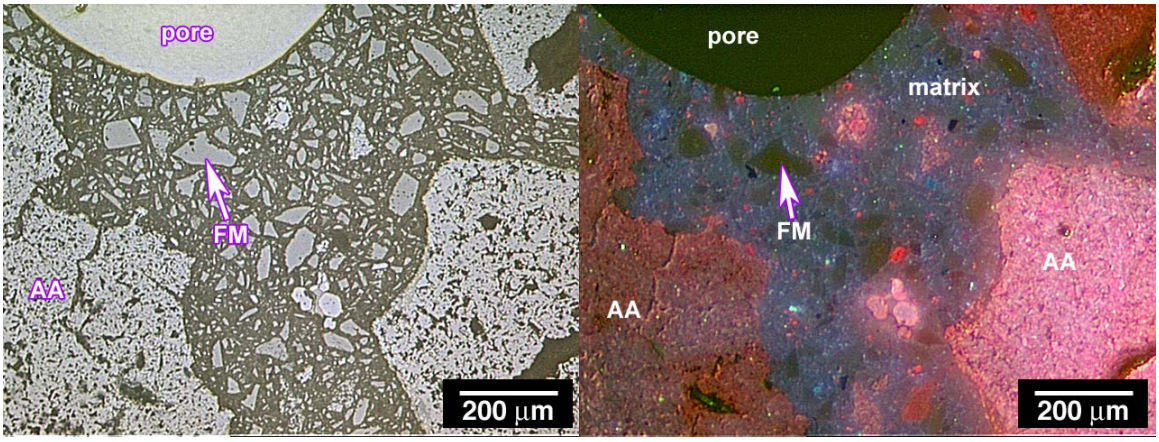

Figure 31 Pre-test microstructure for sample 25.

In Figure 32, RL/CL microstructures of sample 25 after BL smelt cup test showing reaction front. About 2 mm thick reaction interface is visible on the surface of this sample. BL smelt has reacted with refractory material to form mullite and alkali rich silicate glass.

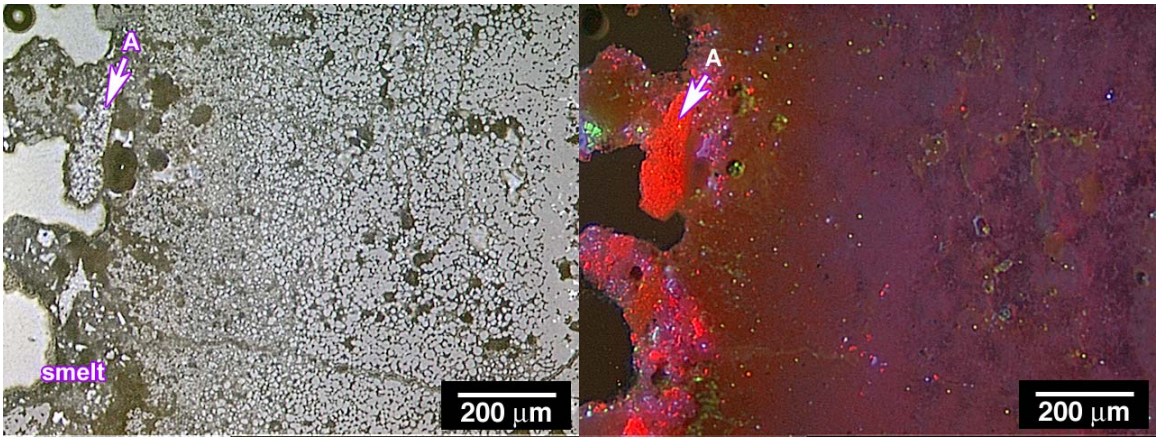

Figure 32 Post-test microstructure for sample 25.

In Figure 33, these micrographs are also taken from sample 25 (adjacent to above micrographs) showing refractory-smelt interface. A dense layer is formed at the interface, which blocked further penetration of smelt. Although, this refractory altered relatively more intense compared to sample 26, the alteration is still not too intense or strong.

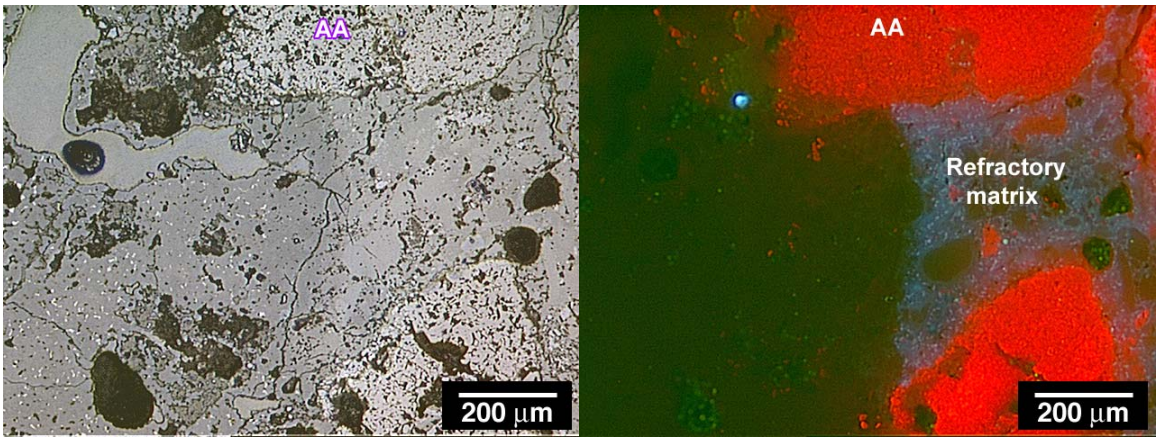

Figure 33 Post-test microstructure for sample 25.

Figure 34 shows RL/CL microstructure of sample 25 after cup test, showing interface between refractory and smelt. The thickness of alteration is negligible.

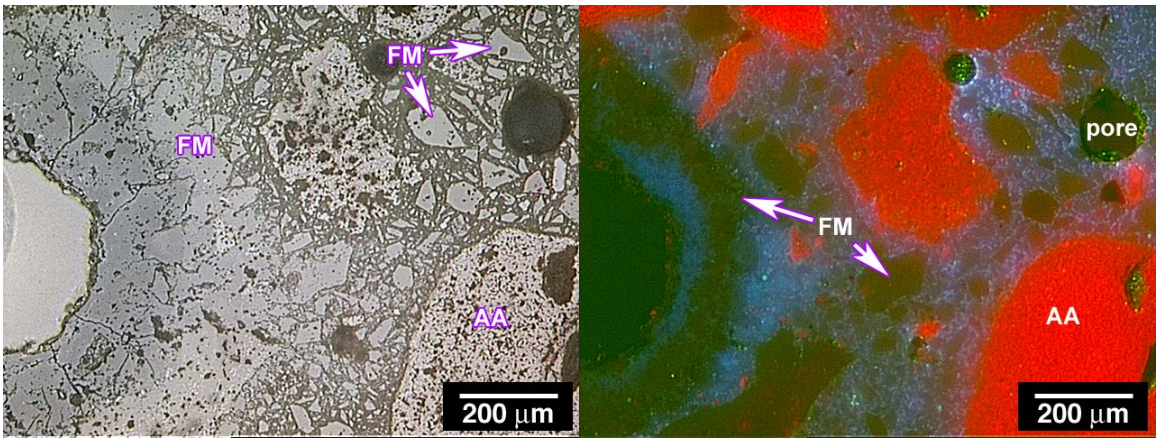

Figure 34 Post-test microstructure for sample 25.

Figure 35 shows RL and CL microstructure of virgin sample 26 before firing, which is identified as cement-free, spinel reinforced high alumina castable refractory, which contains large tabular alumina aggregates (TA), medium sized fused spinel (FS) grains, blended with most-likely microsilica (?). No calcium aluminate cement particles are identified.

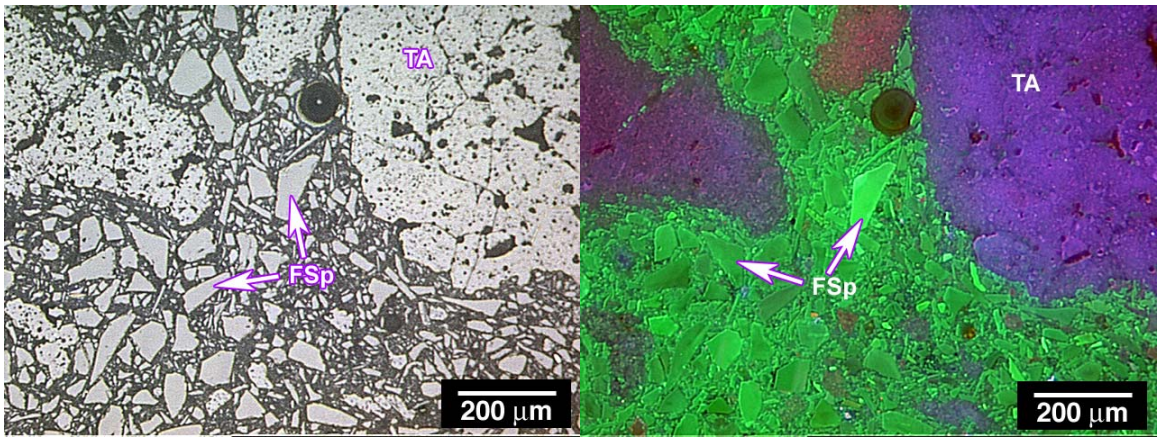

Figure 35 Pre-test microstructure for sample 26.

Figure 36 shows the same sample under low magnification showing general structure of the refractory.

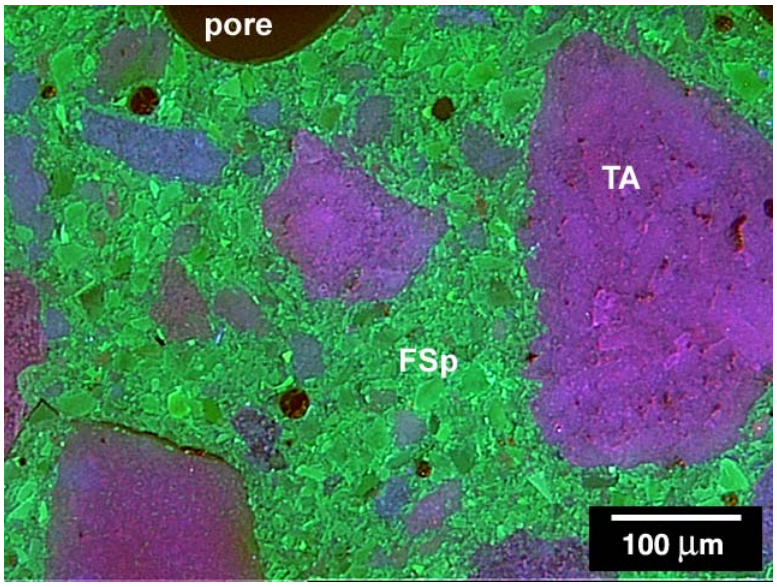

Figure 36 Pre-test microstructure for sample 26.

Figure 37 shows RL and CL micrographs taken from sample 26 after cup test, illustrating microstructure of smelt-refractory interface. Note that there is almost no smelt penetration and reaction at the interface.

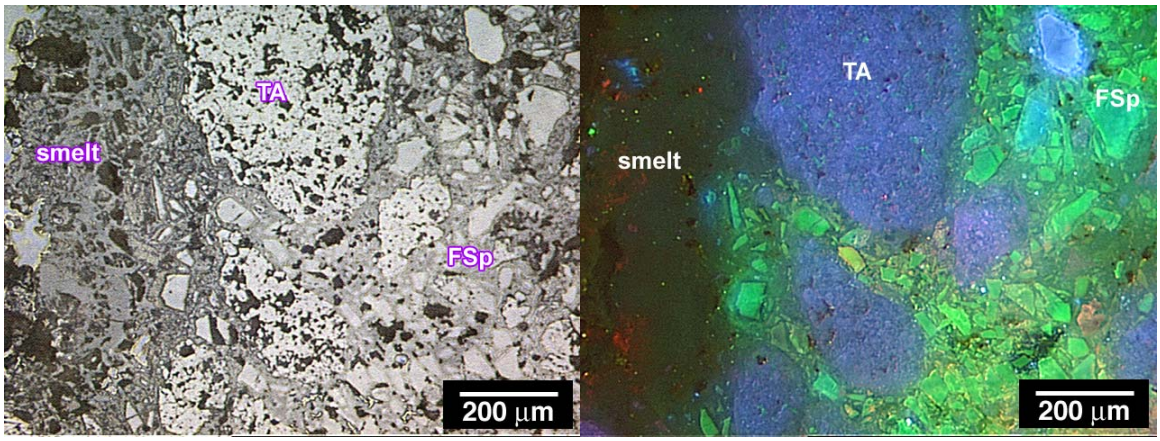

Figure 37 Post-test microstructure for sample 26.

Figure 38 shows RL and CL microstructures of sample 26 taken from refractory-smelt contact surface. Micrographs show that there is no sign of refractory degradation, for example reaction of refractory grains with smelt to form intermediate phases, in this given experimental conditions.

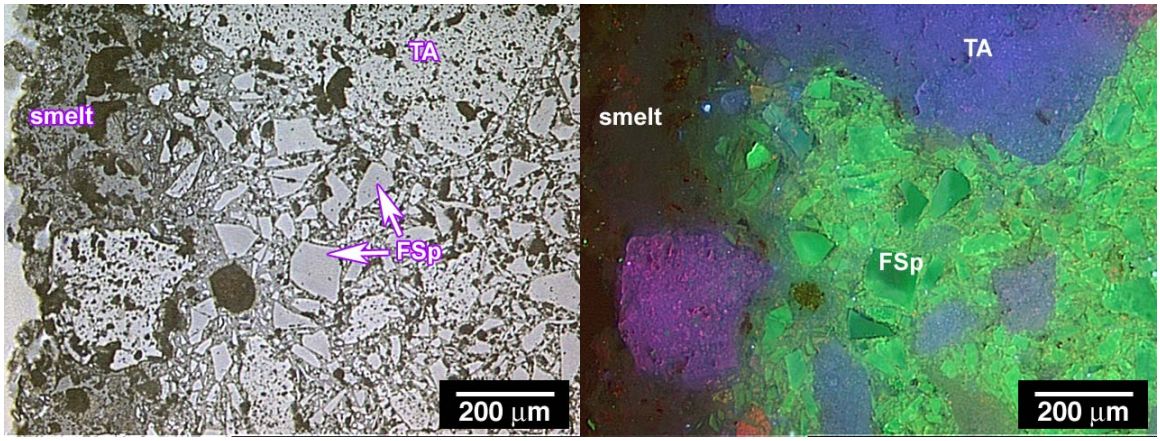

Figure 38 Post-test microstructure for sample 26.

Both 25 and 26 refractory have good corrosion resistance against smelts attack. Results indicate the 26 material is better to against smelts attack than 25.

Sample: 18

Type: Castable

Chemistry: 80% Al2O3, 16% SiO2, 1.3%CaO

Density: 2.91 g/cc

Porosity: 20%

Notes: Sample 18 performed well in the cup tests.

Compositions similar to this have been panel tested in black liquor smelt gasifiers and have performed as well as 60% alumina brick and almost as well as fused cast alumina. Sample 18 does not exhibit chemical expansion which damages most high alumina containing products

and does not seem to corrode as fast as 60% alumina brick, spinel based brick and other castable systems.

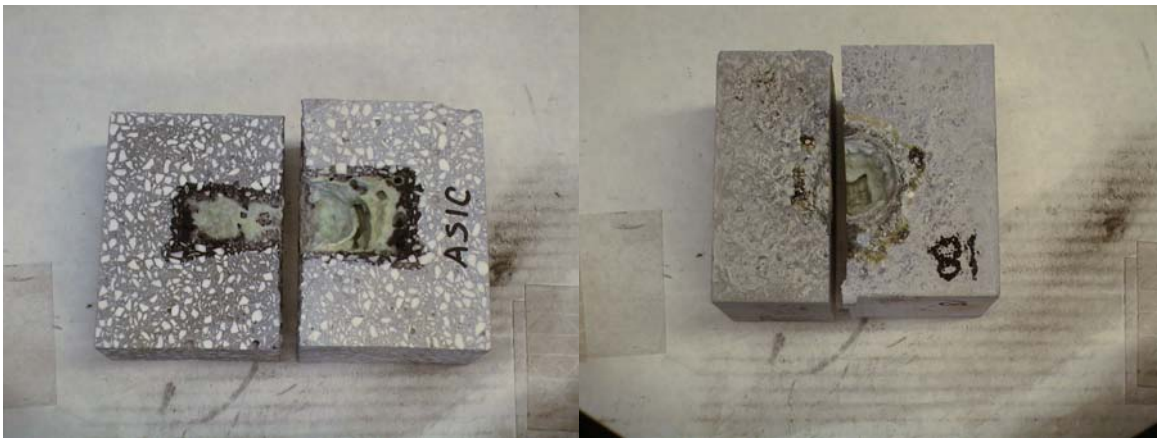

Figure 39 Sample 18 cup

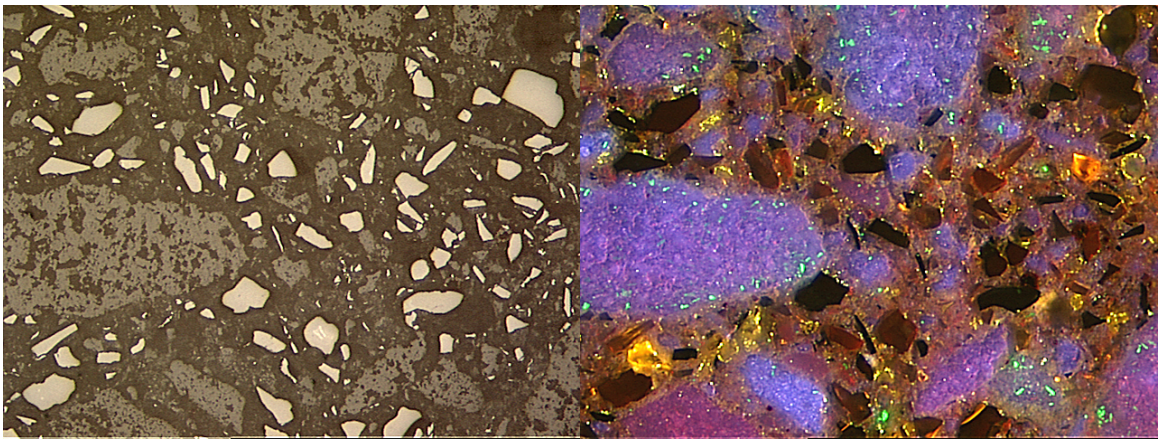

Figure 40 Sample 18 pre-test microstructure

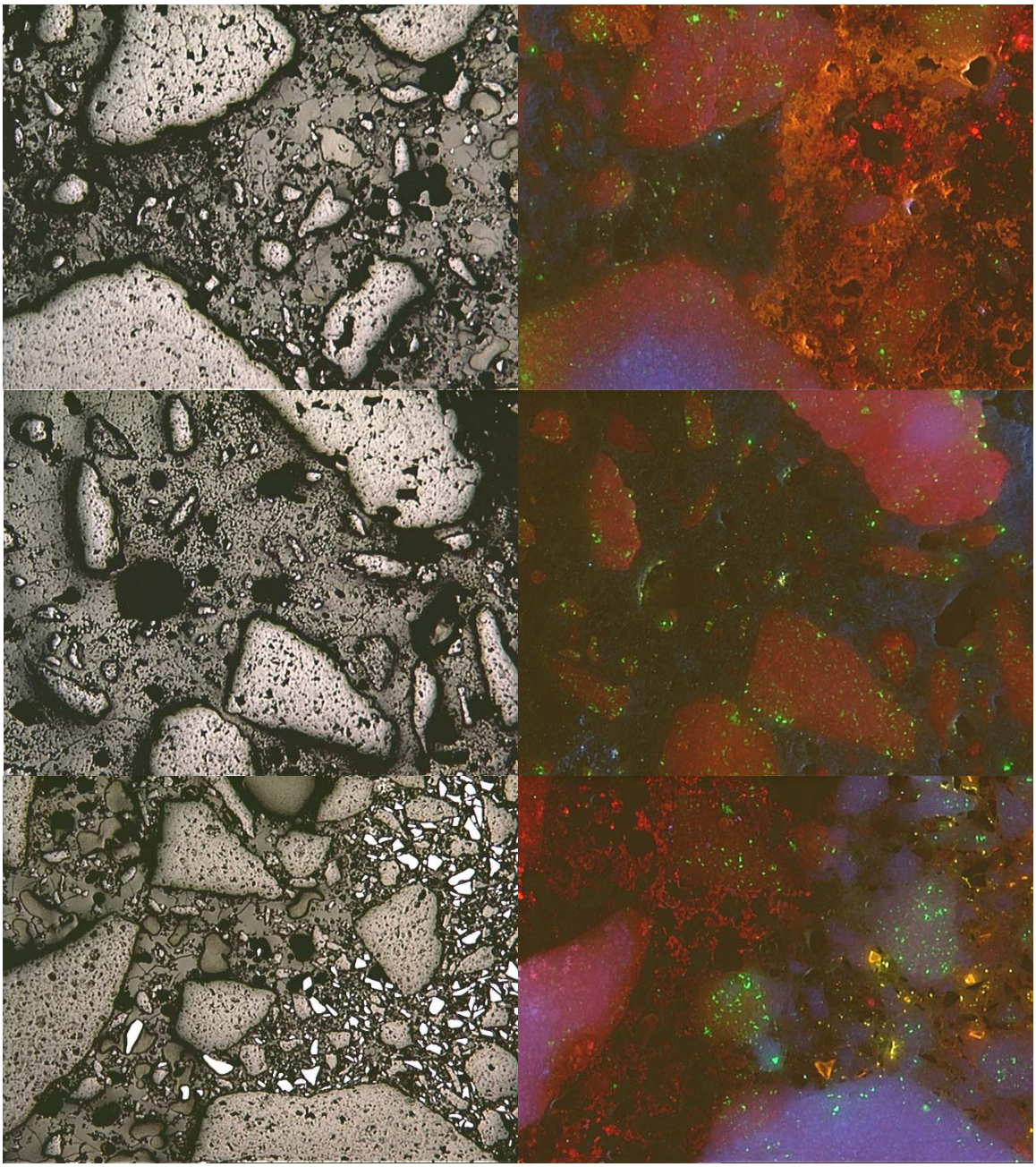

Figure 41 Sample 18 post-test microstructure (top is at reaction zone)

Sample: 22

Type: Fusion Cast

Chemistry: 92% Al2O3, 7% Na2O (data provided by manufacturer)

Density: 2.75 g/cc

Porosity: 31%

Notes: Fused cast alumina performed best in cup tests. Sample 21 has been used in black liquor smelt gasifiers and have performed well. Sample 21 exhibits chemical expansion which damages most high alumina containing products and does not seem to corrode as fast as other systems.

Figure 42 Sample 22 cup

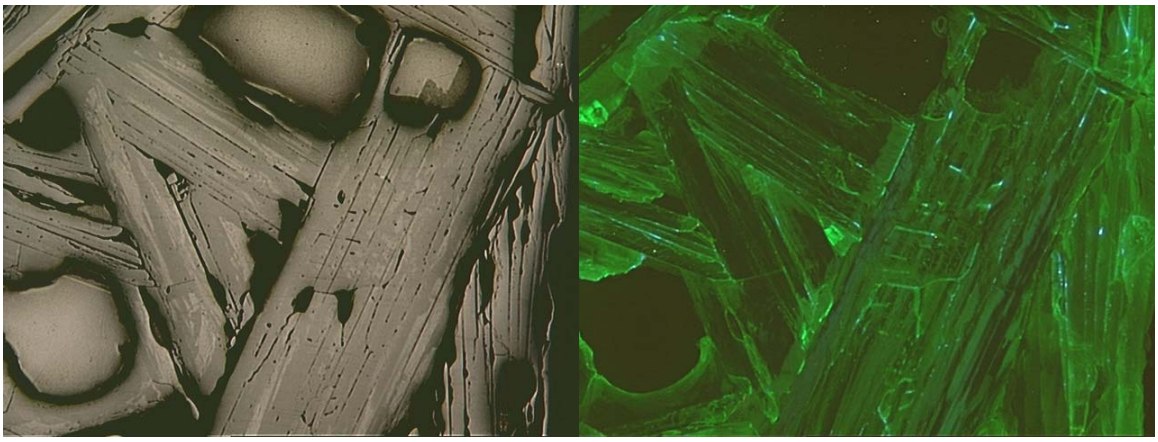

Figure 43 Sample 22 pre-test microstructure

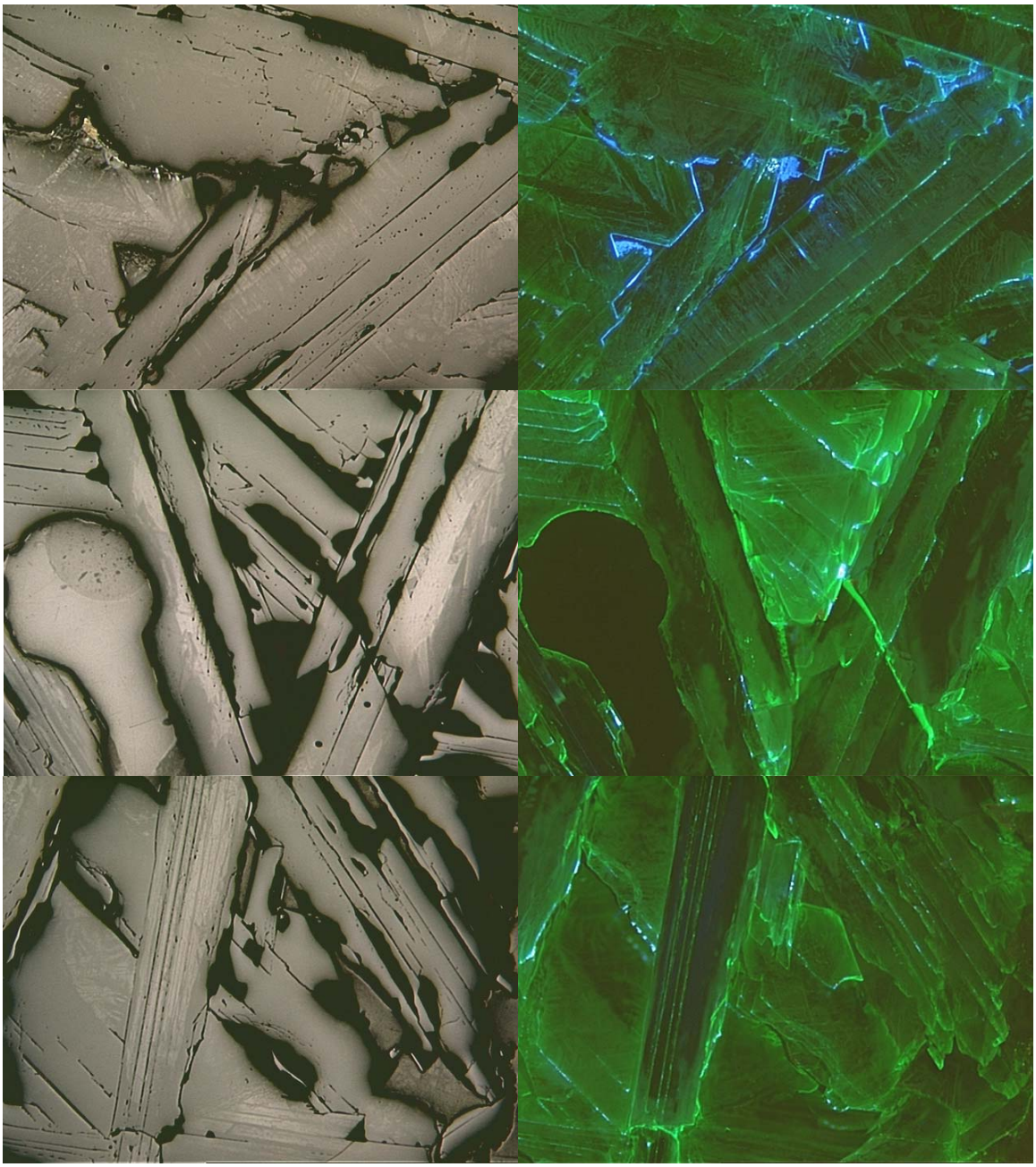

Figure 44 Sample 22 post-test microstructure (top micrographs at reaction zone) Blue intergranular material is reaction products leading to volume expansion.

The best performing materials in the cup testing were fused cast materials. Two new castables appear to be outperforming any of the previously tested materials. A fused cast magnesia or spinel should perform better than other fused cast materials. However, during shutdowns magnesia would be prone to hydration and thus problematic. Spinel would form a dense magnesia layer, as shown by sessile drop testing that would be prone to hydration and may slough off during shutdowns. Magnesia based gunning and castable materials were developed using coarse magnesia aggregate and fine spinel for the matrix. It was thought based on the work that this material would perform well as a repair or hot face material. Cup testing showed, Figure 45, that there was bloating of the material. Based on these results the manufacturer in conjunction with UMR is reevaluating the mix to improve the performance. The porosity of this material was very high and could have allowed reaction with the fine spinel in the matrix to form soda aluminate and magnesia, without forming a dense magnesia layer.

Figure 45 Bloating of magnesia castable mix.

Low open porosity and permeability appear to be important for materials although it can not be proven by the current work. Low permeability spinel and magnesia castables should be formulated and investigated. It is also show that materials that form a viscous glass smelt refractory interface layer perform well. This has not been proven in the field and may be detrimental to green liquor quality or may be rapidly removed by scouring action of the liquid with entrained solids smelt washing down the interface layer.

Currently a spinel lining is being used in New Bern, although there is no strong connection between the selection of the spinel lining and this project. It is of note that spinel is one of the materials strongly suggested by this project. Mortar, MORCOCOAT SP-P. developed was tested by Oak Ridge National Laboratory, ORNL. This mortar performed better than other mortars, and is scheduled for installation in February of 2006.

Materials were tested and modeled for the pulse combustors at Big Island. The MorcoCast AZ10 developed, tested and recommended appears to be performing adequately. It was

reported by MORCO that Big Island has ordered additional material to replace the current refractory in the remaining pulse combustors.

Refractory materials are being evaluated and modeled to be used in the pulse combustors, shown in Figure 46, that are failing at Big Island and Trenton.

Figure 46 Picture of failed pulse combustor tube sheet.

An enlargement showing the critical delamination at a depth of 5-6” into the 11” thick by 5’ diameter panel is shown in Figure 47. The delamination eventually would lead to blockage of the heat exchanger tubes and necessitates refractory replacement. Material properties of two possible replacement materials have been measured and a finite element model of the tube sheet was developed.

Figure 47 Enlargement showing critical delamination failure at 5-6" in depth and accompanying transverse cracking.

The AZ-10 material installed at Big Island failed in 2 pulse heaters due to improper installation and in 2 pulse heaters due to attack by gases generated by the surrounding Pligun LWI28 insulating castable. It is currently believed that the AZ10 is not strong enough for use in the pulse heater and that chemical attack from other refractory materials is leading to failure in the tube sheet. MORCO is redesigning the AZ10 to have higher strength and better flow characteristics. Optional materials for this installation are 90+ % alumina dense refractories. It is important that all refractory materials be compatible.

Figure 48 identifies the component layers and bricks, the brick joints and the geometry of the two-dimensional model for the BLG refractory lining problem. Region “ABCD” in Figure 48 is modeled in the study. The model is composed of two layers of refractory lining, one layer of insulation fiber and steel shell. The inner diameter of the reactor is 2.4 m. The thickness of each refractory lining is 152 mm. The thickness of fiber layer is 20 mm. The thickness of the shell is 30 mm. The interface between adjacent layers is considered to be intact initially but capable of separation and sliding. In each refractory lining, there is one-half refractory brick. The left hand side of the brick of the inner refractory lining and the right hand side of the brick of the outer refractory lining are defined to be at the centerline of the brick. The other side of the brick is defined as the brick joint. The centerline of the brick is fixed without rotation during the operation of the brick. Dry brick joints are used in the model. That is, a joint could transfer a compressive load across it and remain intact but it would open under any tensile stress so the load at the joint would be released.

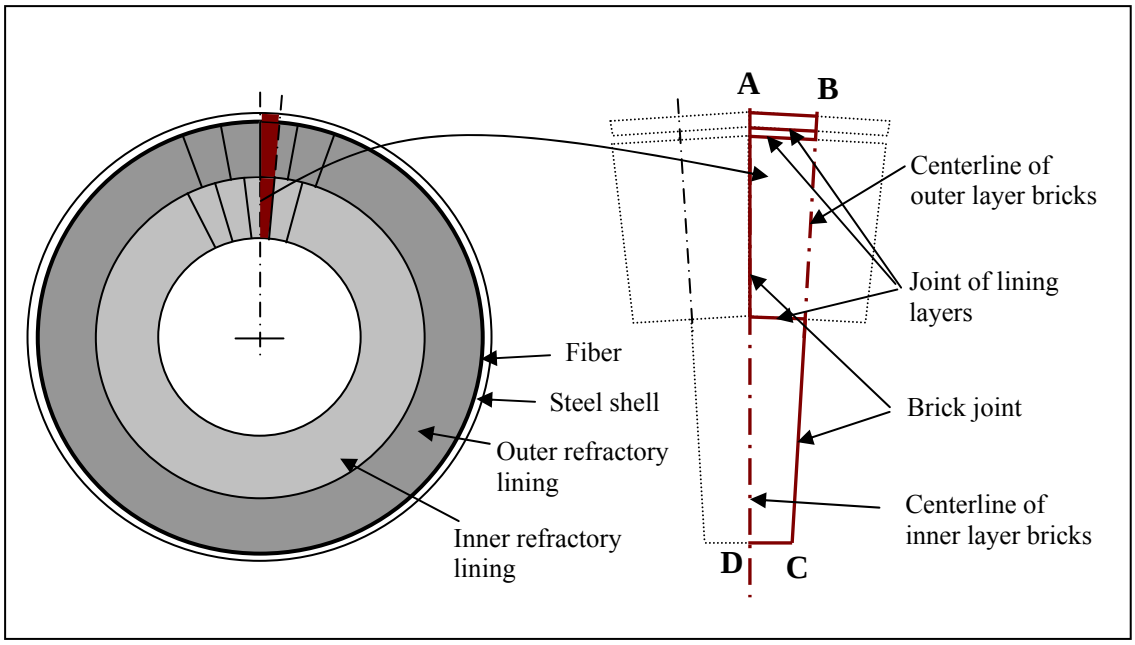

Figure 48 Idealized black liquor gasifier model.

Alumina material is selected for both the working and back-up refractory linings, a fiber layer is used as insulation, and a carbon-steel is used for the container shell. The thermal and mechanical properties of those materials are usually non-linear and temperature dependent. The refractory material is treated as an elastic-plastic material. The properties of alumina are highly temperature dependent. However, only a limited experimental data is available. Some thermal properties of the refractory are obtained with varying temperature by Hemrick's[39]. Other properties of the refractory are $E =$ 103 GPa at 23 ^{o}C and $E =$ 81 MPa at 900 ^{o}C. The Young's modulus at other temperatures will be linearly interpolated based on the above two values. The room temperature properties of the refractory are $\rho =$ 3480 kg/m^3, $\alpha =$ 8.7 x 10^{-6}/K and $\nu =$ 0.24, yield strength, $\sigma_{yield} = 200$ MPa and ultimate strength $\sigma_{ultimate} = 220$ MPa. The room temperature linear elastic-plastic properties for the carbon steel are $\rho =$ 7800 kg/m^3, $k = 55$ W/mK, $C = 500$ J/gK, $\alpha =$ 13 x 10^{-6}, $e =$ 0.8, $E =$ 210 GPa, $\nu =$ 0.3 and the yield strength, $\sigma_{yield} = 300$ MPa. A fiber material which could be compressed up to 80% in volume is used in the model. Due to the lack of data, simple temperature independent thermal and mechanical material properties for the fiber material are used; $\rho =$ 300 kg/m^3, $k =$ 0.2 W/mK, $C = 2900$ J/gK and $\alpha \approx 0$.

Gap conductance of the interface of refractory linings is given as an average value of 1000 W/m^{2}K (when the two surfaces are contacted tightly) and zero (when the gap between two contacted surfaces exceeds 100 mm) based on the work of Gmelin[40]. This value would have very little effect on the temperature, stress and strain distributions in the geometry studied. A small drop in temperature between the interfaces would be expected in the model. The same value is taken for the gap conductance of the interface between component layers due to its insignificant effect.

A coupled thermal-mechanical user interface model accounting for chemical reaction is developed and implemented into a finite element code, ABAQUS. Increments of temperature

and displacement are calculated based on equation (10). A FORTRAN language programmed user subroutine UEXPAN is developed to model the chemical expansion and implemented to interface with the main finite element code. Both the thermal expansion and chemical expansion are defined as functions of temperature and time in the subroutine. Plane stress elements CPS4T are used for all the components of the BLG system. The mesh was chosen following refinement studies in which one mesh (1307 nodes) matched a finer mesh (2765 nodes) with respect to maximum stress components to within 4%. Finer mesh of 2765 nodes and 2261 elements are employed in the finite element model. In order to better capture the stress response, a finer mesh is used in the inner surface region of the refractory linings which is exposed to the highest temperature, as shown in Figure 49. Cylindrical coordinate system is used in the model. R is referred to as radial direction and θ is referred to as tangential direction.

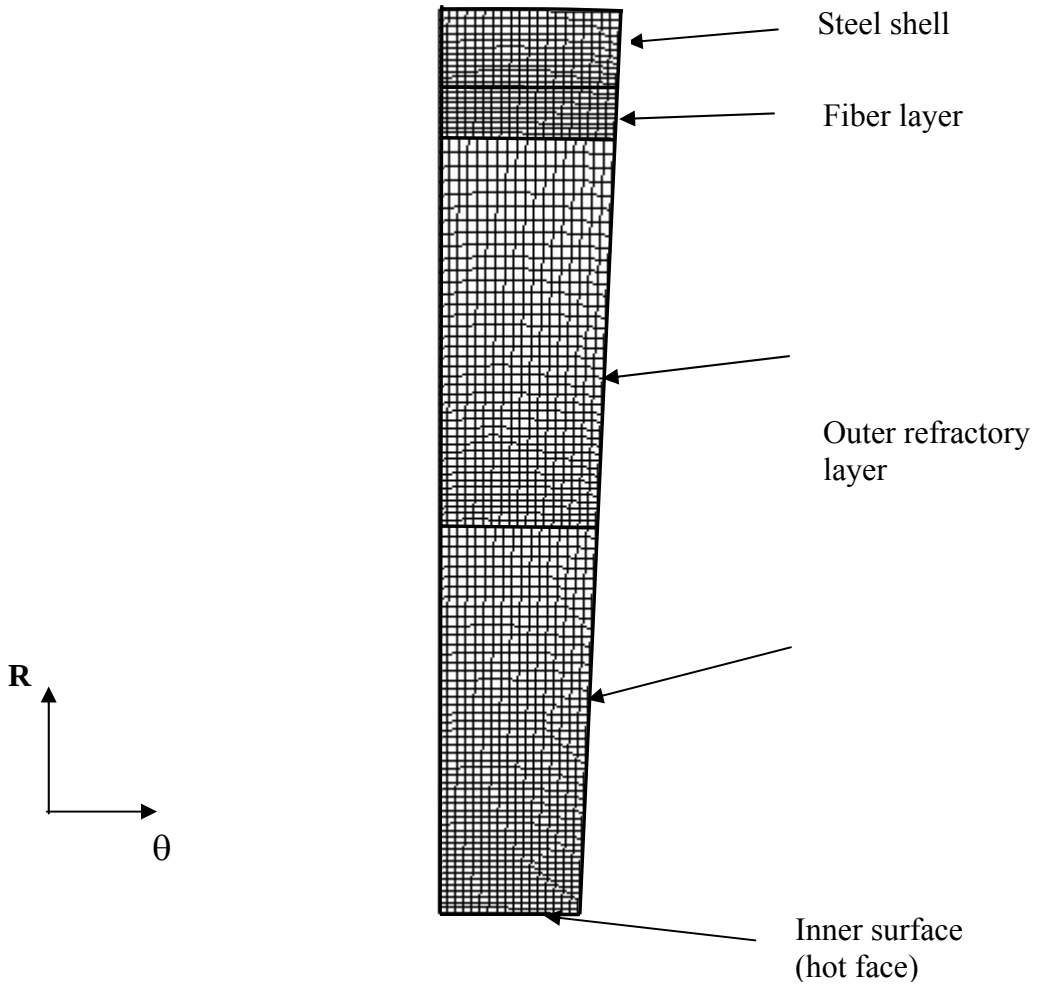

Figure 49 Illustration of assembles and meshes of the model.

The inner surface of the reactor is heated up to 950 ^{o}C at a constant heating rate of 20^{o}C per hour. The ambient temperature (surrounding the steel shell) is 23 °C in the beginning of heating and increases to 49°C at the end of heating. The value of absolute zero, $T^0 = -273$ ^{o}C and a convection coefficient, $h = 30$ W/m^2 K is used to describe the motion of the surrounding air outside the steel shell.

The chemical reaction is assumed to occur only when temperature is above 850 ^{o}C. The reaction rate changes linearly with the temperature. Chemical reaction rate at 850 ^{o}C is assumed to be 6 x 10^{-5}/h. The chemical reaction will be completed when the volume change of corroded alumina reaches 130%. It is also assumed that the chemical reaction wouldn't affect other properties of the refractory.

Temperature distribution in the refractory lining is important to the development of strain and stress in the refractory. Thermal gradient produced through the thickness of the refractory lining would cause differential strain in the refractory therefore resulting in stresses in it. Figure 50 shows the comparison of the tangential stresses in the inner refractory lining and the outer refractory lining at the same moment (time t) during the operation. It is found that the stress in the inner refractory lining is significantly larger than in the outer refractory lining. Therefore, only the thermomechanical behavior and the chemical expansion of the inner refractory lining are presented in the following studies. Moreover, because the behavior of the refractory under tension and compression is different, strain and stress components in both tangential and radial directions are analyzed.

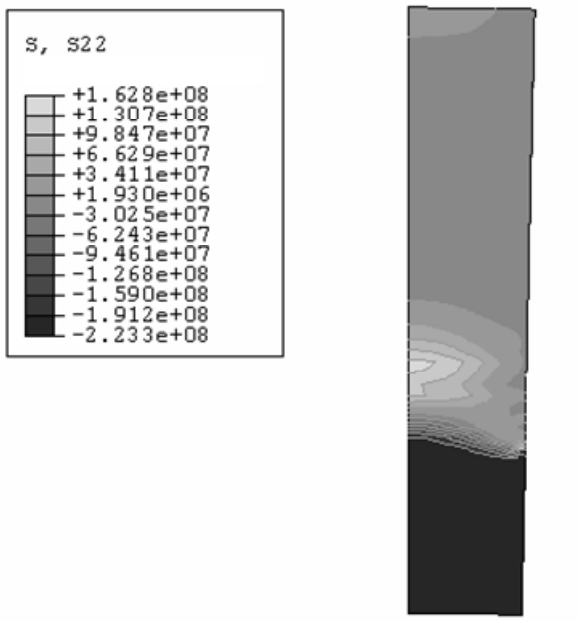

(a) Stress in inner refractory lining

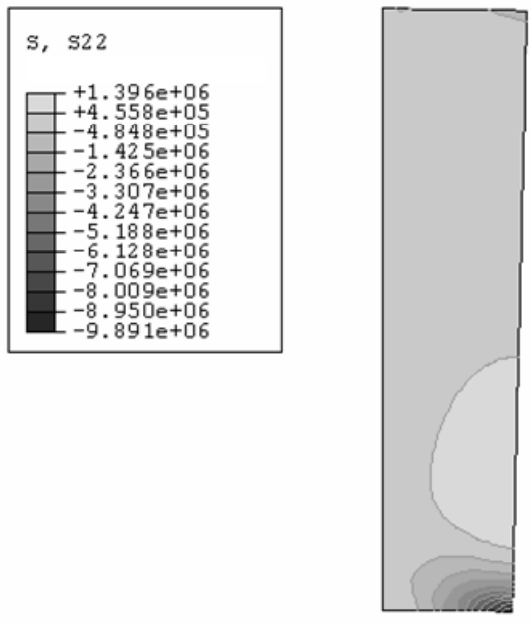

(b) Stress in outer refractory lining

Figure 50 Comparison of the tangential stresses in the inner and outer refractory linings at time t.

Figure 51 shows the tangential strain distributions in the inner refractory lining. The strains at the surface and the interior of the brick at the end of heating and after 3 months service are presented. For both time ranges, different amounts of expansion are developed through the thickness of the brick. The strains decrease approximately linearly from the hot face to the cold face at the end heating. This is caused by the thermal gradient in the refractory lining[41]. However, nonlinear strain distribution appears in the refractory brick after 3 months service. Very high tangential strains appear in the region between hot face and at a depth of about 50 mm from the hot face. The strains in the rest of the brick after 3 months are similar to the strains at the end of heating. This is because the temperature exceeds 850 ^{o}C up to the depth of about 50 mm from the hot face. This results in considerable chemical expansion in this region which is the so called reaction zone. Note that the highest tangential strain on the surface of the brick after 3 months is close to the end of the reaction zone because of the development of plastic strain in the region.

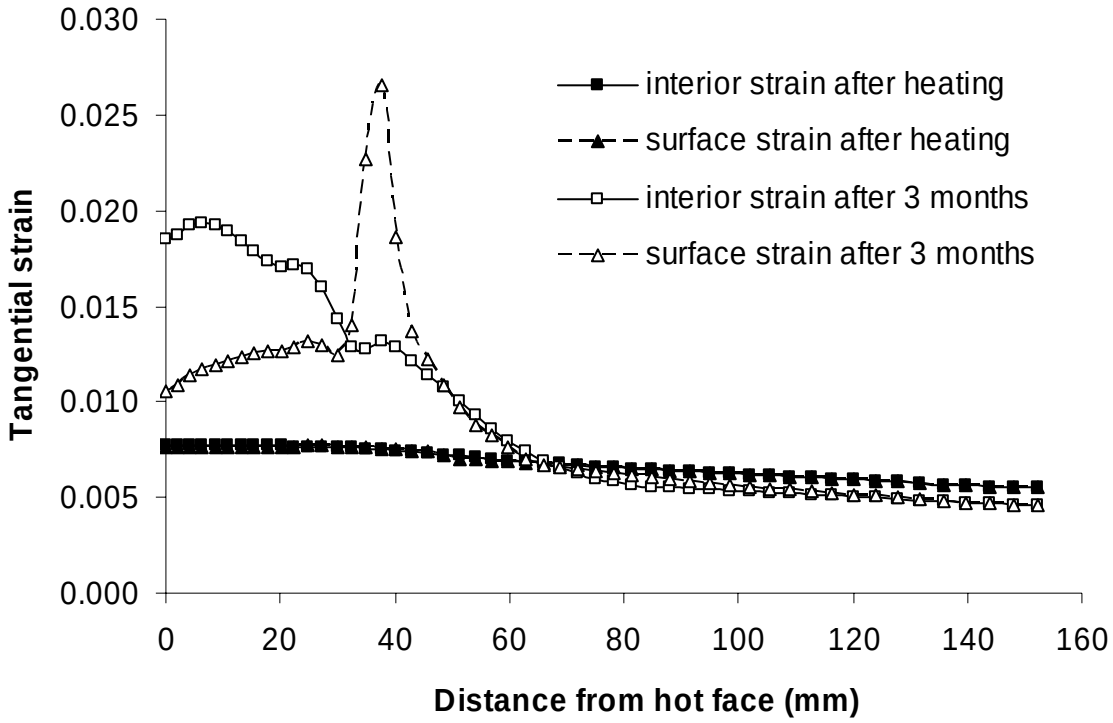

Figure 51 Tangential strain distribution in the inner refractory lining.

Figure 52 shows the radial strain distributions in the inner refractory lining. The strain distribution at the end of heating is similar to that of the tangential strain. However, extremely high radial strains, much larger than the tangential strains in the same region, are developed in the reaction zone after 3 months. Strains in the rest of the brick after 3 months are similar to the strain at the end of heating. This is due to the chemical expansion and less constraint in the radial direction than the tangential direction. As a result, a very large expansion gradient is produced at the end of reaction zone after 3 months. This differential expansion will cause significant stresses which would damage the refractory material.

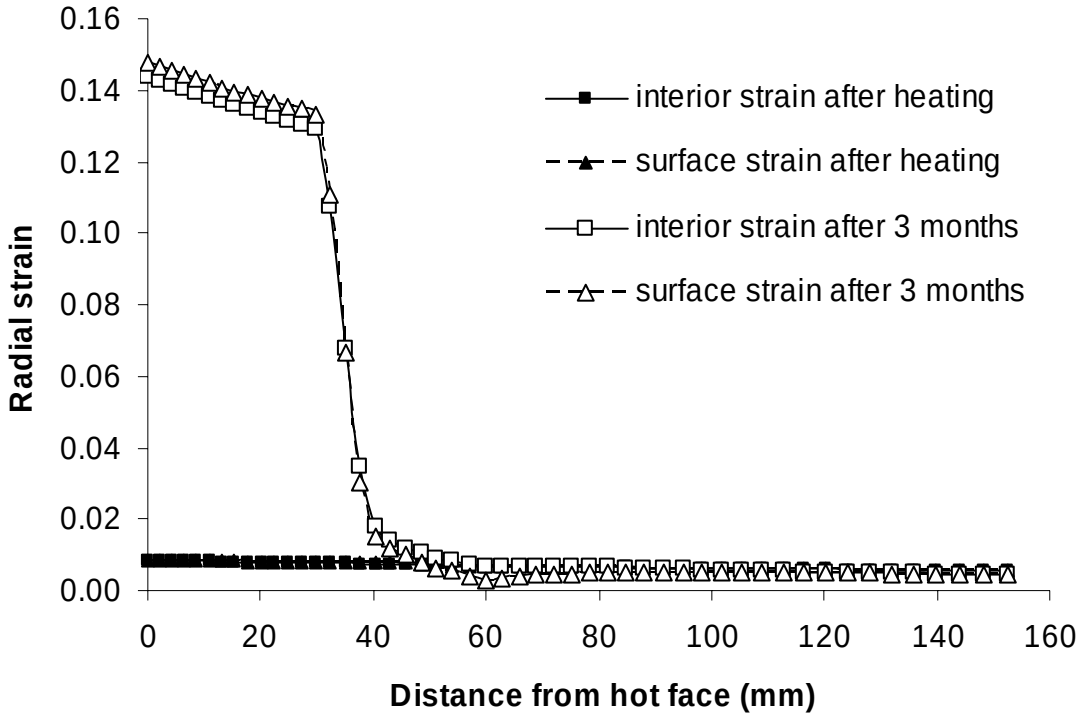

Figure 52 Radial strain distribution in the inner refractory lining.

Figure 53 shows the tangential strain history of the inner refractory lining. The minimum tangential strain is on the cold face of the refractory lining. It increases during heating due to the thermal loading, and then decreases slightly due to the compression of the fiber and the temperature drop in this region. The maximum tangential strain is at the end of the reaction zone. It increases until about 800 hours of operation at which time the fiber layer is fully compressed. During heating, due to the combined effect of thermal loading and chemical reaction, the strain increases at a much higher rate. The tangential strain history of the brick corner is also shown in Figure 53. The strain in this region begins to decrease after about 320 hours of operation due to the development of the plastic strain.

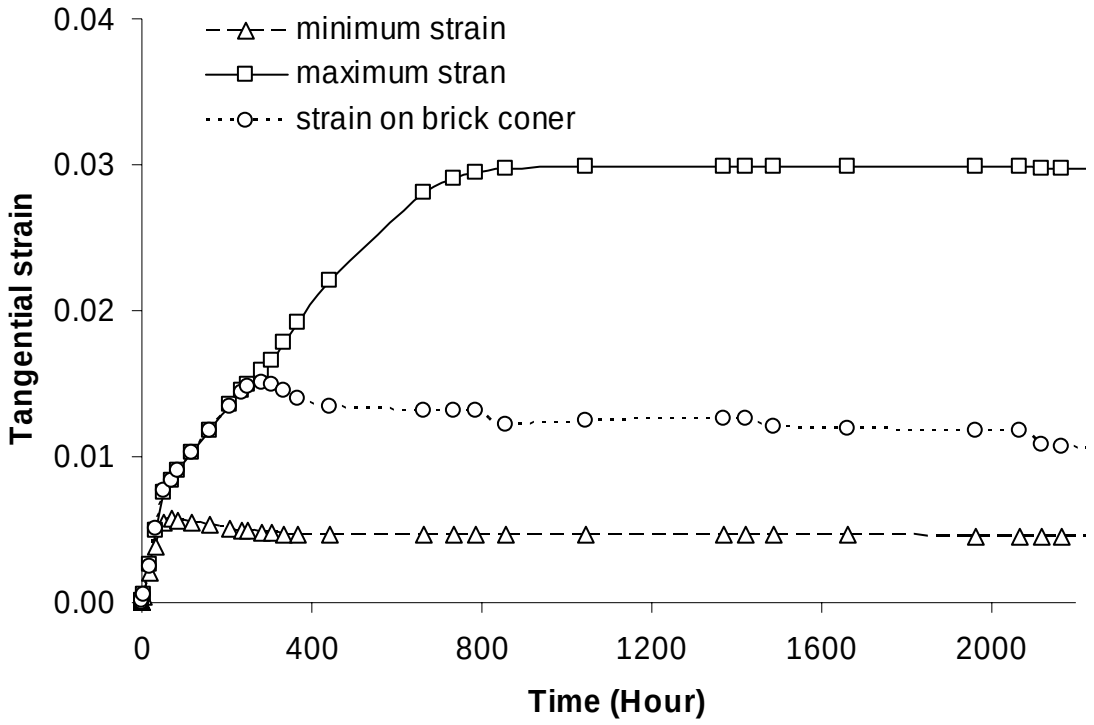

Figure 53 Tangential strain history in the inner refractory lining.

Figure 54 shows radial strain history of the inner refractory lining. The minimum radial strain is on the cold face of the lining. It increases during heating due to the thermal loading, and then decreases slightly until about 400 hours because of the temperature drop in this region due to the compression of the fiber layer during this period. The minimum radial strain reaches steady state after the full compression of the fiber. However, the pressure on the cold face increases due to the confinement from the steel shell. The mechanical strain is fairly small compared to the thermal strain. The maximum radial strain is on the hot face. It increases nearly linearly throughout the operation although the refractory lining is confined from the outside. The hot face can expand inward when spalling occurs at the corners of the brick.

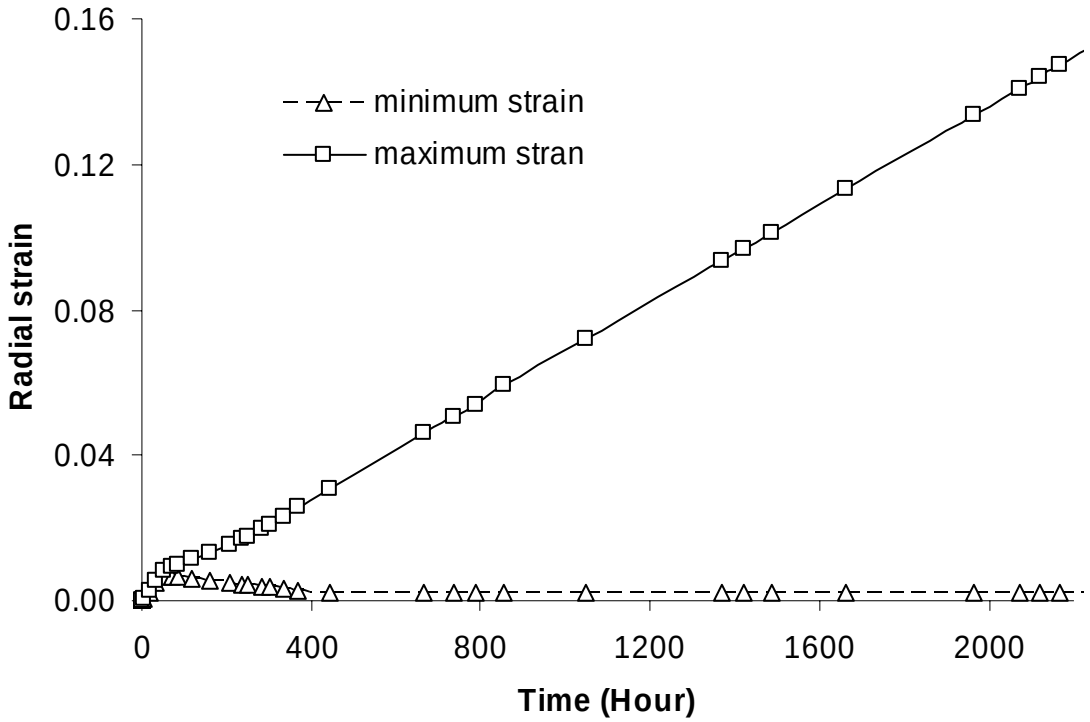

Figure 54 Radial strain history in the inner refractory lining.

The expansion of the refractory lining and the confinement from the surrounding structures induces significant stresses in the refractory lining. Figure 55 shows the tangential stress distribution in the inner refractory lining. Compressive tangential stress is developed in the high temperature region, about 40 mm deep from the hot face at the end of heating. Almost no tangential stress is developed in the rest of the brick at the end of heating. These results indicate that the brick joint opening takes place from the cold face and extend up to the region about 40 mm from hot face. Ultimate compressive tangential stress is reached in the unopened portion of the brick after 3 months, which means that spalling occurs in this region. Tangential stress on the brick surface after 3 months is very small due to the brick joint opening. Very high tensile tangential stress is developed in the interior of the brick at the end of the reaction zone after 3 months. This is caused by the considerable differential expansion in this region by the chemical reaction. As a result, crack in radial direction could possibly develop in the interior of the brick due to this high tensile tangential stress.

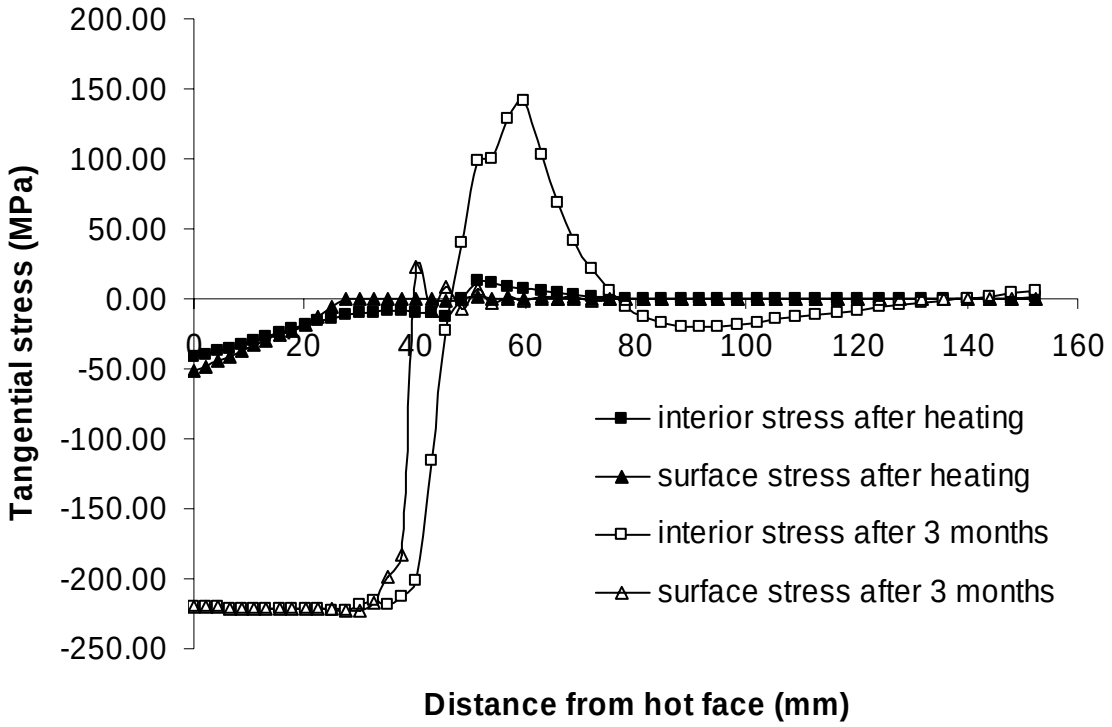

Figure 55 Tangential stress distribution in the inner refractory lining.

Figure 56 shows the radial stress distribution in the inner refractory lining. Radial stress in the inner lining brick is very small at the end heating due to expansion allowance. High tensile radial stress is developed on the surface of the brick at the tip of the brick joint opening at the end of heating. As a result, cracks parallel to the hot face would initiate at this point. Significant radial stress is developed after 3 months due to the extremely large differential expansion caused by chemical reaction. Very high tensile radial stress is developed in the interior of the brick at the end of the reaction zone. This means the slabbing crack would initiate either from the tip of brick joints opening during heating and propagate inward towards the center of the brick after heating, or starts in the interior of the brick during long term service. Very high compressive radial stress is developed on the surface of the brick after 3 months due to the high compressive tangential stress and the pressure from the second refractory lining.

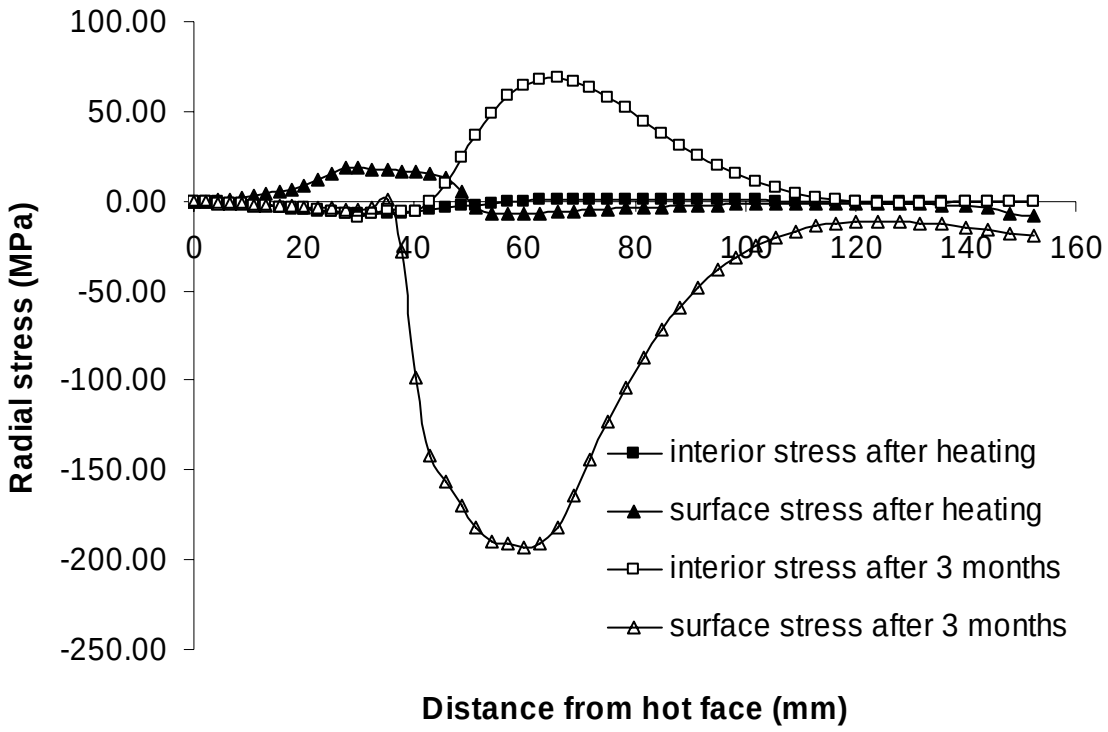

Figure 56 Radial stress distribution in the inner refractory lining.

From the foregoing stress and strain analysis, the following four failure modes of the inner refractory lining are envisioned as outlined in Figure 57:

(1) Pinch spalling at the brick corners or spalling of the entire hot face.

(2) Cracking parallel to the hot face from the interface.

(3) Cracking parallel to the hot face in the interior of the brick.

(4) Radial cracks in the interior of the brick.

The failure modes observed from the real gasifier refractory bricks relate to the thermomechanical and chemical expansion study presented above.

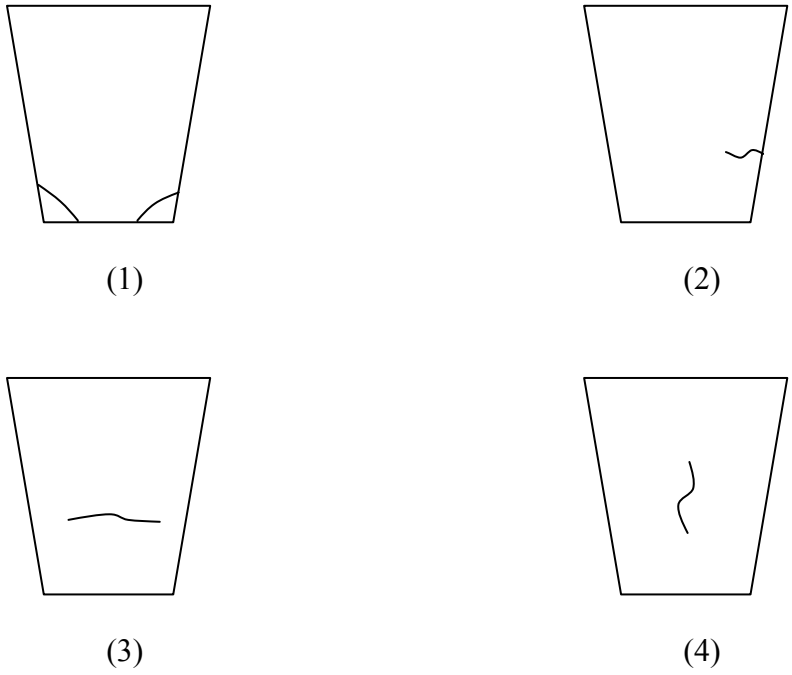

Figure 57 Possible failure modes due to the stress in the inner refractory lining. (1). Pinch spalling at the brick corners or spalling of the entire hot face. (2). Cracking parallel to the hot face from the interface. (3). Cracking parallel to the hot face in the interior of the brick. (4).Radial cracks in the interior of the brick.

Based on above results, it can also be observed that the chemical reaction of the smelt and refractory dominates the developments of strain and stress and hence the failure in the refractory lining. Better corrosion resistance will improve the performance of the refractory material in a high temperature BLG system.

The compressive and tensile damage patterns of refractory lining with 10 mm fiber layer are given in

Figure 58. Dark color means higher damage and light color means less damage.

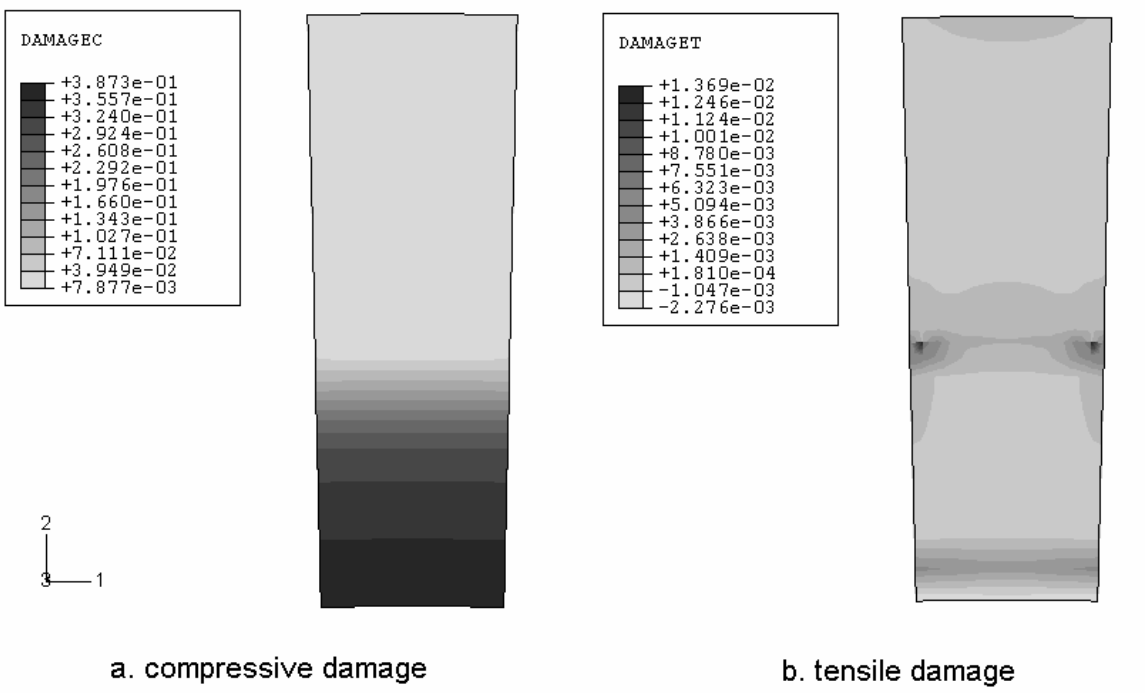

Figure 58 Damage of the refractory lining with 10 mm fiber layer after 3 months

High compressive damage occurs in the high temperature region of the inner layer refractory material. The highest compressive damage is 0.39. Tensile damages occurred near the hot face and the region about 1/3 of the total thickness of inner refractory layer from the hot face. The highest tensile damage is 0.014. The failure here does not mean fracture but rather refers to the formation of micro-cracks. As discussed before, no experimental data is yet available for the damage parameters. Therefore, the results of this study should be treated in a qualitative sense and should only be used to study the possible trends in refractory structures in real situations. A brick sample taken from a glass melting furnace, which has been exposed to similar environments as the black liquor gasifier, is shown in Figure 59 for comparison. The comparison of damage patterns predicted for BLG refractory and the observed damage pattern for glass melting furnace refractory is encouraging. From this point of view, the model presented here may be appropriate for evaluating the failure behavior of the refractory structure.

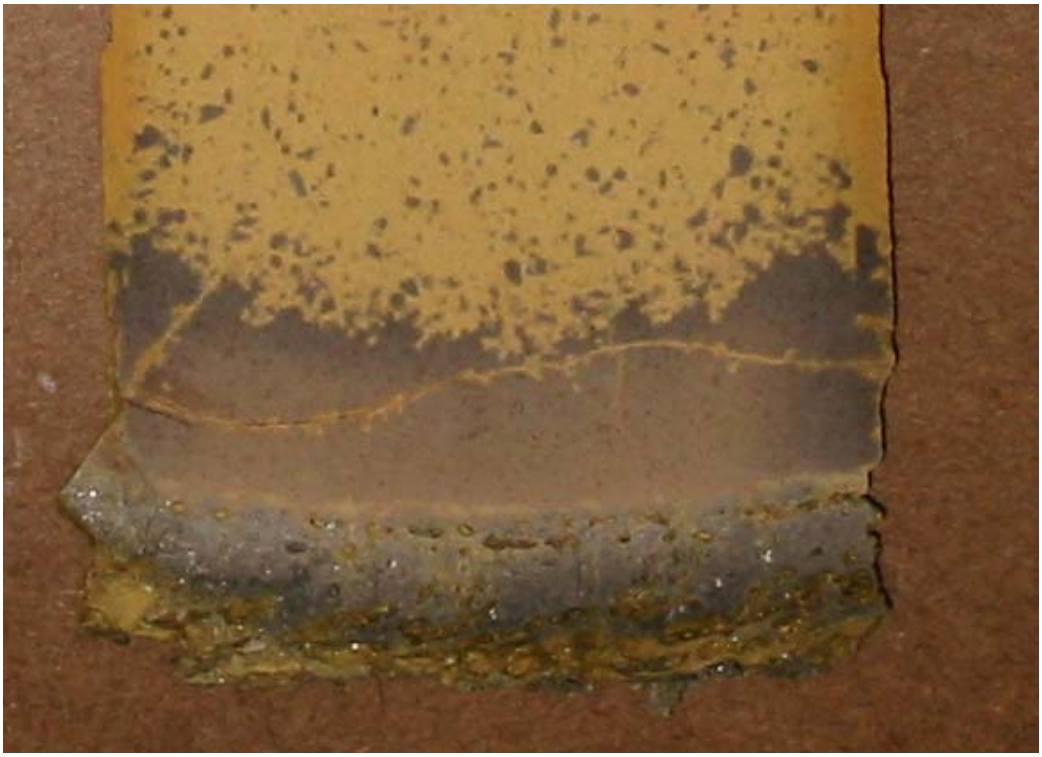

Figure 59 Damage observed in a silica brick taken from a glass melting furnace

The fiber layer plays an important role in the black liquor gasifier. It provides expansion allowance for the refractory linings and insulation for the structure. Thickness of the fiber layer affects the behavior of the refractory lining. Insufficient expansion allowance (thin fiber layer) would produce significant stresses in the refractory structure and therefore damage the refractory material. Excessive expansion allowance (thick fiber layer) would not provide enough confinement to the refractory linings, thereby resulting in an unstable lining structure. Effects of the fiber layer thickness are also studied.

The compressive and tensile damage patterns for the refractory lining with 20 mm fiber layer are given in Figure 60. The compressive damage is similar to that of the lining with 10 mm fiber layer. Only one slabbing damage pattern is found in the lining with 20 mm fiber layer. It is clear from the results that fiber thickness has little effect to the compressive damage, however, it affects the tensile damage of the refractory lining.

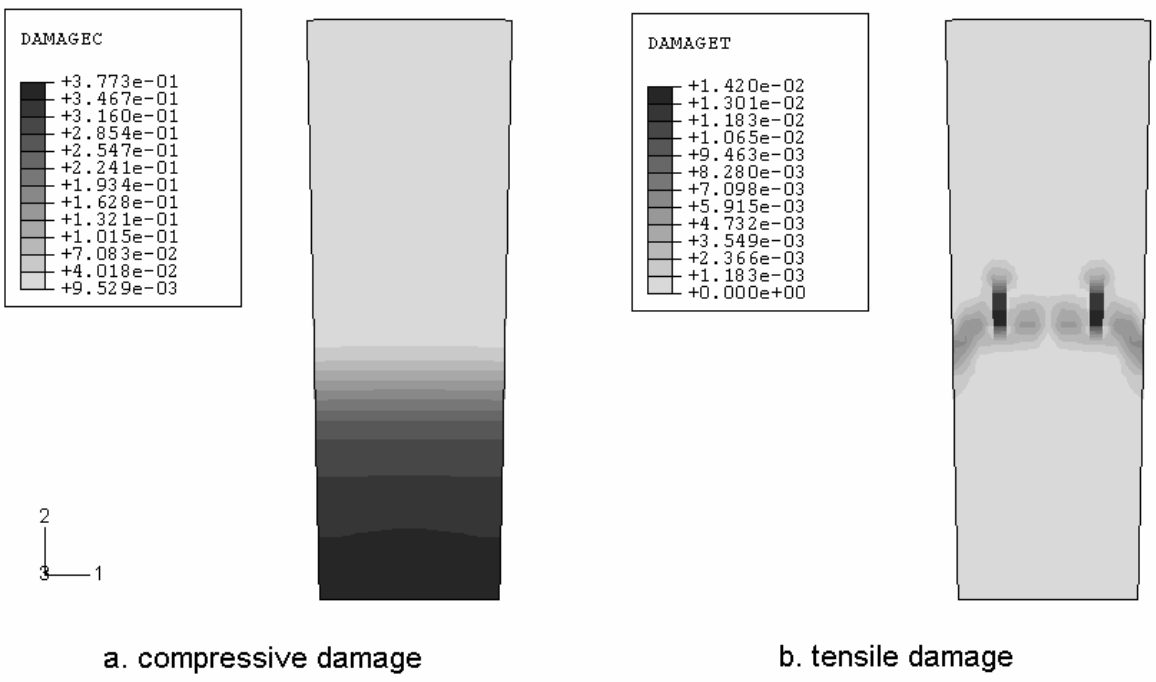

Figure 60 Damage of the refractory lining with 20 mm fiber layer after 3 months

The through thickness compressive and tensile damage for the refractory lining is given in Figure 61 and Figure 62, respectively. The compressive damages in the two linings with different fiber layer thicknesses are almost the same. The compressive damage is maximum at the hot face and decreases with a steep gradient from the refractory hot face to the region about 50 mm from hot face where the expansion is dominated by the chemical reaction. In the other word, the reactive strain causes the most damage in the refractory. The damage curve decreased with a much higher gradient after the first 25 mm from the hot face of the refractory. This may have been caused by the separation of the refractory bricks. The opening provides an increased space for the expansion of the refractory lining, thereby causing a decreased compressive stress and subsequentially reducing the damage. The through thickness tensile damage along the centerline of the inner layer brick, Figure 62 shows a layered damage occurs in the refractory lining with 10 mm fiber layer. The damages are located occur near the hot face area and at the end of reaction zone. Only one damage region is developed in the lining with 20 mm fiber layer due to larger expansion allowance. The damage is located at the end of the reaction zone

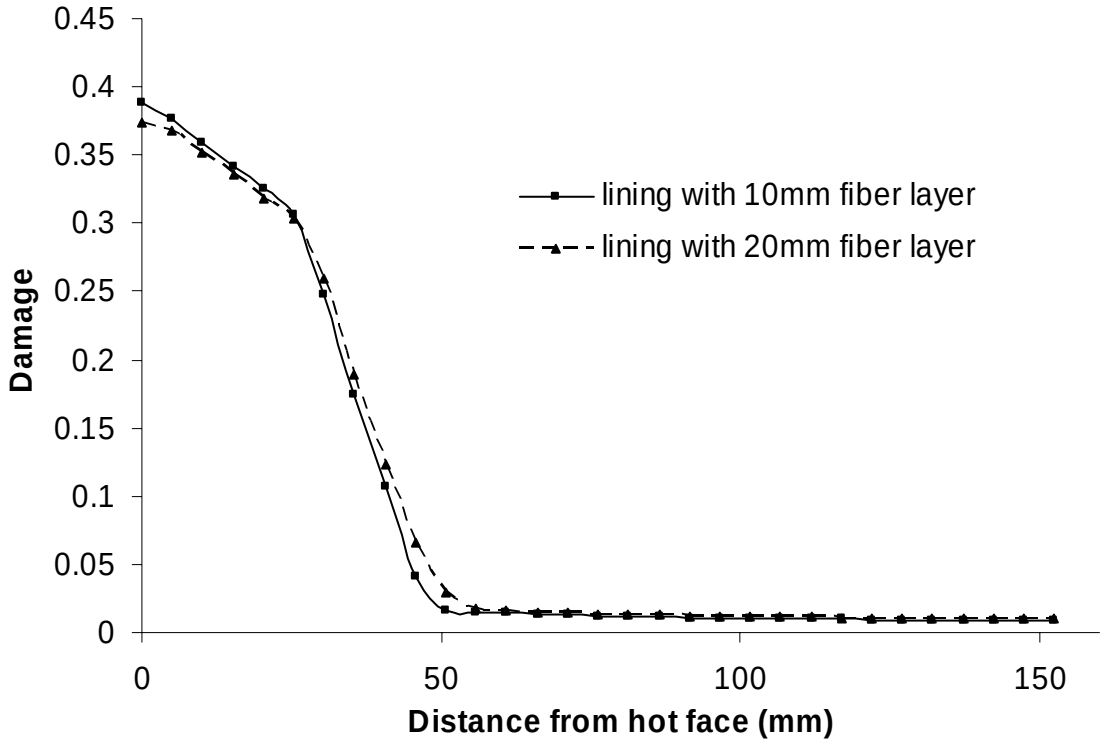

Figure 61 Through thickness compressive damage for two fiber layer thicknesses

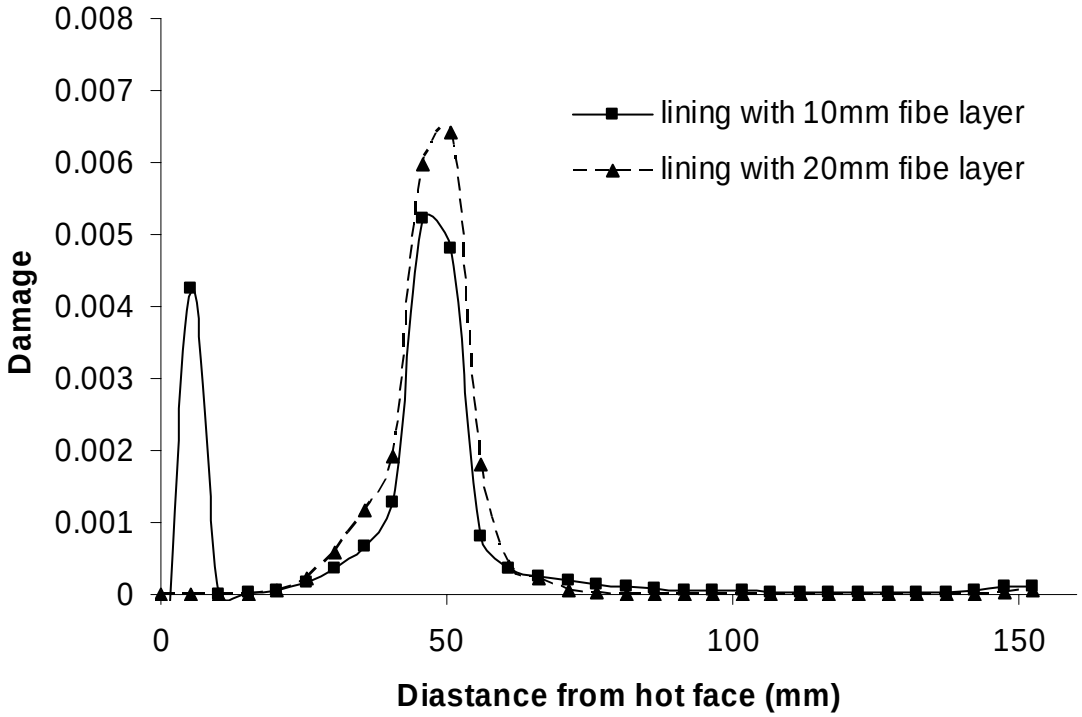

Figure 62 Through thickness tensile damage for two fiber layer thicknesses

The compressive and tensile damage histories for a 3-month time span are given in Figure 63 and Figure 64, respectively. The compressive damage shows a linear dependence on time. Since the damage was assumed to depend linearly on the chemical reaction, this result reinforces the earlier observation that the compressive damage is primarily caused by reaction strain. The compressive damage of the refractory linings with 10 mm and 20 mm fiber layers were almost the same numerically. The tensile damage-time relationship is non-linear. Most tensile damage occurs during the first 200 to 300 hours. When the fiber layer is compressed to the highest capacity of compression, the confinement from the steel shell limits the increase in the tensile deformation. A systematic experimental study is needed before one can give a phenomenological explanation of the damage process.

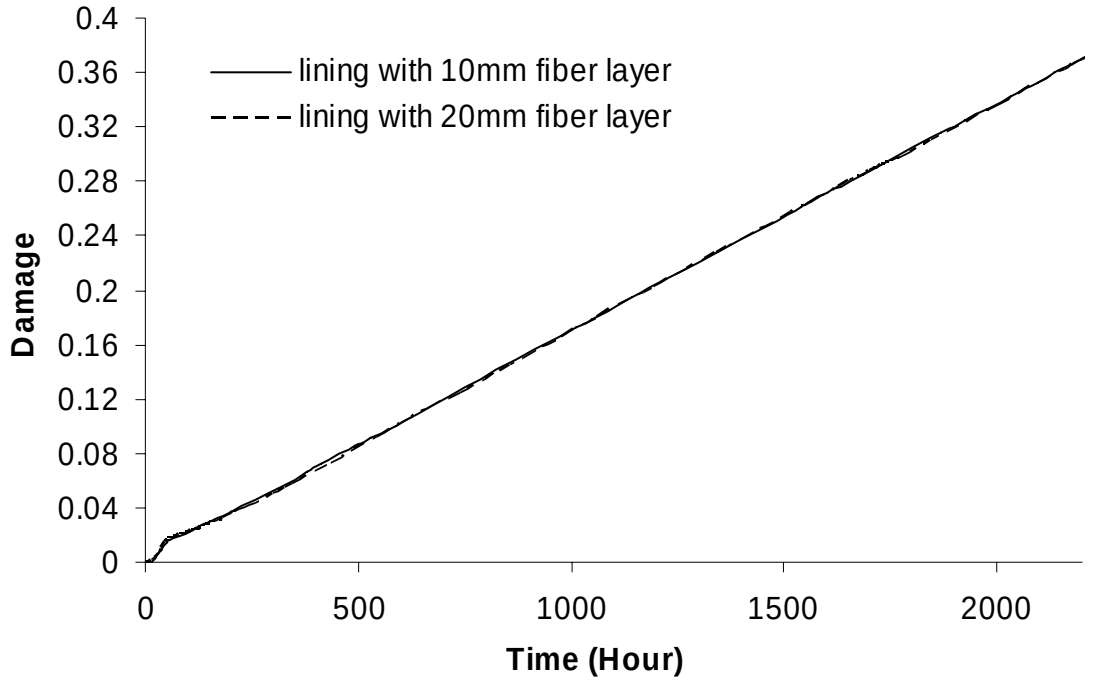

Figure 63 Compressive damage history in the refractory structure for two fiber layer

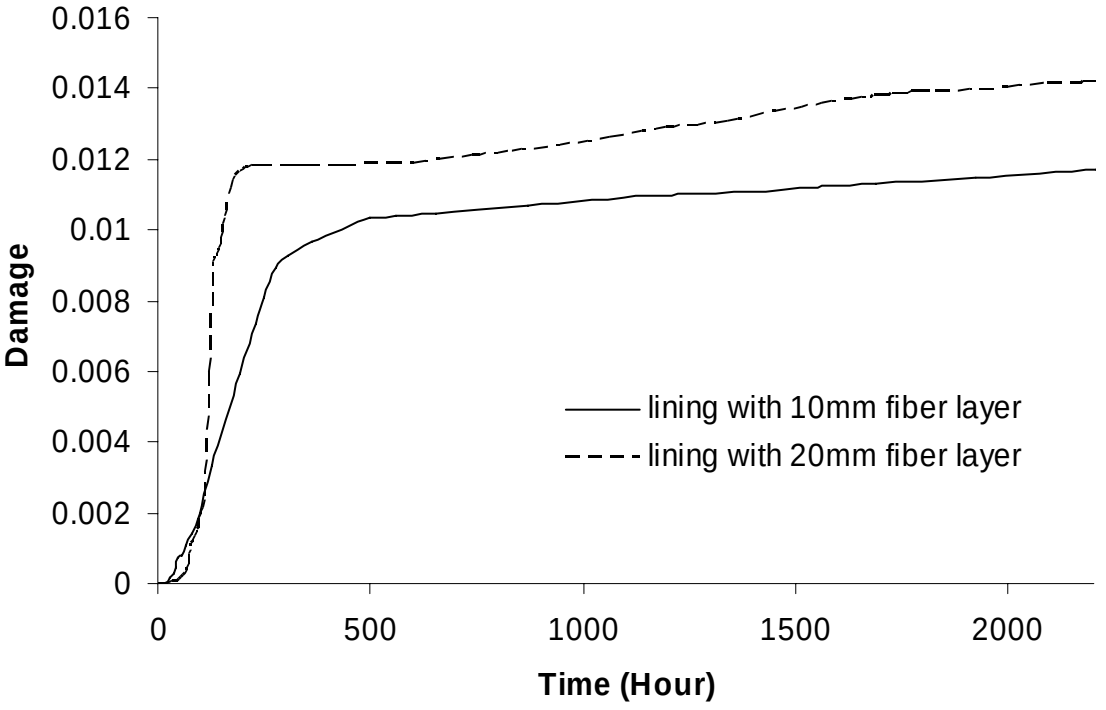

Figure 64 Tensile damage history in the refractory structure for two fiber layer thicknesses

A 2-D axisymmetric coupled temperature-displacement finite element model is used to simulate the refractory cup under thermal loading and chemical attack. Commercial finite element package ABAQUS is used for the modeling. A FORTRAN language programmed user material subroutine UMAT is developed and implemented to interface with the main ABAQUS code to simulate the constitutive and damage behavior of the refractory using the approach described earlier.

Due to the unavailability of property data for the tested material, the properties of an alumina refractory material studied by Hemrick are employed in this model. Some temperature dependent properties of the refractory are given in Table 8. Other properties of the refractory are described below. $E =$ 103 GPa at 23 ^{o}C and $E =$ 77 GPa at 1000 ^{o}C, the Young's modulus at other temperatures will be linearly interpolated based on the above two values. The following properties of the refractory are at room temperature: $\rho =$ 3480 kg/m^3, $\alpha =$ 8.7x10^{-6}/K and $\nu =$ 0.24.

Compressive and tensile strengths of alumina refractories at ambient temperature can reach about 3000 MPa and about 200 MPa, respectively. However, it is well known that the strength of refractory materials would be decreased dramatically when exposed to high temperature and chemical corrosion environments. Due to the paucity of knowledge on the strength of refractories under such environments, the threshold compressive and tensile strengths are assumed to be 50 MPa and 10 MPa in the model, respectively. The critical compressive and tensile strengths are assumed to be 300 MPa and 100 MPa as the damage criterion of the refractory material, respectively.

Table 8. Temperature dependent properties.

Temperature (^{o}C)	Thermal conductivity (W/m K)	Specific heat (J/g K)
23	9.34	778
100	9.28	916
200	8.29	1010
300	7.55	1080
400	6.75	1130
500	5.81	1170
600	4.37	1210
700	4.65	1220
800	4.76	1240
900	4.86	1250
1000	5.21	1270

The chemical reaction is taken to be linearly related to all the factors mentioned earlier due to the unavailable experimental data. Reaction is also assumed to occur only at temperatures above 800 ^{o}C. The chemical expansion rate is assumed to be 0.006/hour. The depth of the penetration is limited to maximum of 5 mm. The penetration rate is assumed to be 0.05 mm per hour.

The idealized geometry of the refractory cup used in the model is shown in Figure 65. The outer radius of the refractory cup is 57 mm, the inner radius of the cup is 19 mm, the thickness of the cup is 76 mm and the depth of hole is 38 mm.

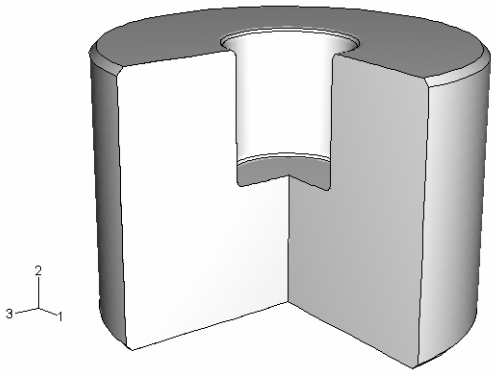

Figure 65. A cut-away view of the refractory cup used in the model.

In this section, the CDM constitutive model and finite element method described above are employed to predict the damage pattern and growth for the refractory cup in the corrosion test.

Figure 66 is a picture of the cross section of the refractory cup after the corrosion test. The refractory material reacted with the smelt. A thin layer of reaction zone is created behind the surface of the hole. The volume of the reaction zone increased. Spalling is observed on the reaction surface and cracks are observed starting from the top edge of the hole and directly behind the reaction zone.

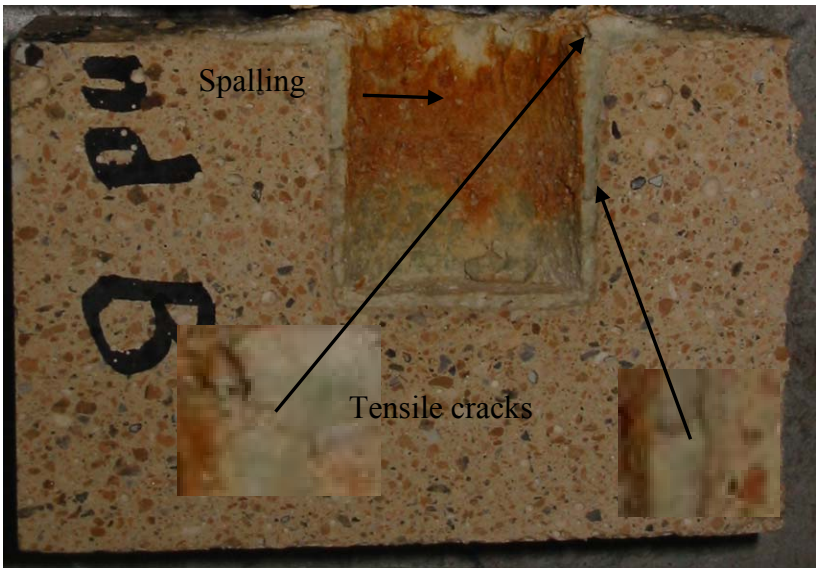

Figure 66. Cross section of the refractory cup after testing.

Figure 67 shows the reactive strain in the refractory cup after the test. The curve in the plot is the reactive strain along the dotted line in the contour pattern. The depth of the reaction zone is about 5 mm from the reaction surface. Reactive strain is the highest on the surface and reduces to zero at the end of the reaction zone. Compared with the picture in Figure 66, the results shown in Figure 67 describe the corrosion of the refractory cup very well.

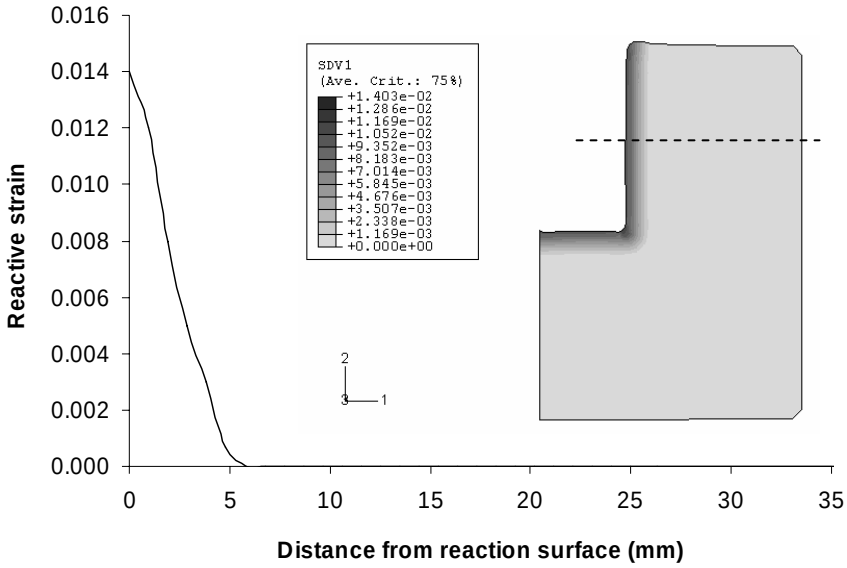

Figure 67. Reactive strain pattern and numerical result.

Figure 68 shows the predicted tensile damage in the refractory cup after the corrosion test. Highest tensile damage occurs from the top edge of the hole toward the inside of the cup and then stays in the region right behind the reaction. This result means that the tensile cracks would be developed from the top edge of the hold and behind the reaction zone. Cracks observed in the tested refractory cup shown in Figure 66 exactly lay on the predicted damaged regions. So the model could be verified based on this.

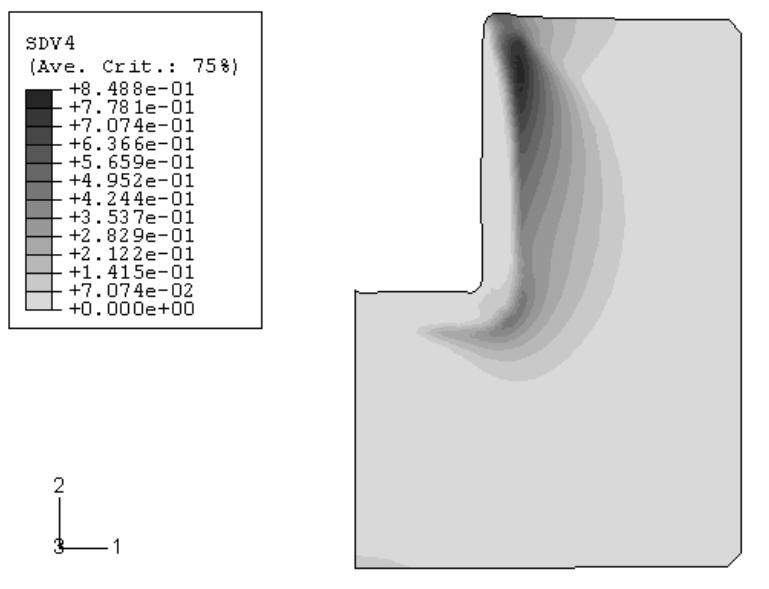

Figure 68. Predicted tensile damage pattern.

Figure 69 shows the predicted compressive damage in the refractory cup. Highest compressive damage occurs on the reaction surface, which means the spalling could occur on the surface of the hole. This phenomenon is also observed in the cup after the test, as shown in Figure 66.

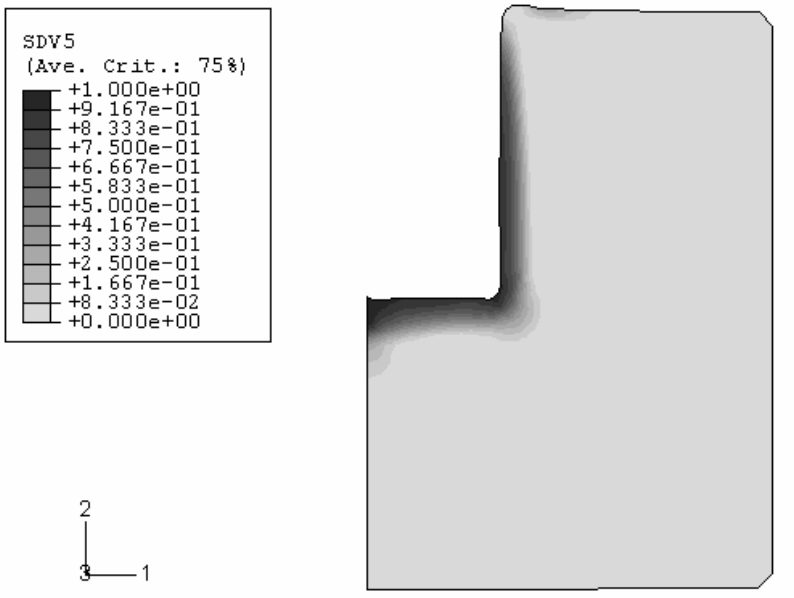

Figure 69. Predicted compressive damage pattern.

Figure 70 gives the numerical results of the damage in the cup. The curves in the plot are the damage along the dotted line in Figure 67. Compressive damage starts from the reaction surface and ends at a depth about 4 mm away from the surface. The maximum compressive damage, which is about 0.85, is on the surface. Tensile damage starts about 2.5 mm away from the reaction surface and ends about 20 mm away from the reaction surface. The

maximum tensile damage, which is about 0.7, is right behind the reaction zone. The total damage is dominated by the compressive damage in the reaction zone and by the tensile damage in the remainder of the refractory cup.

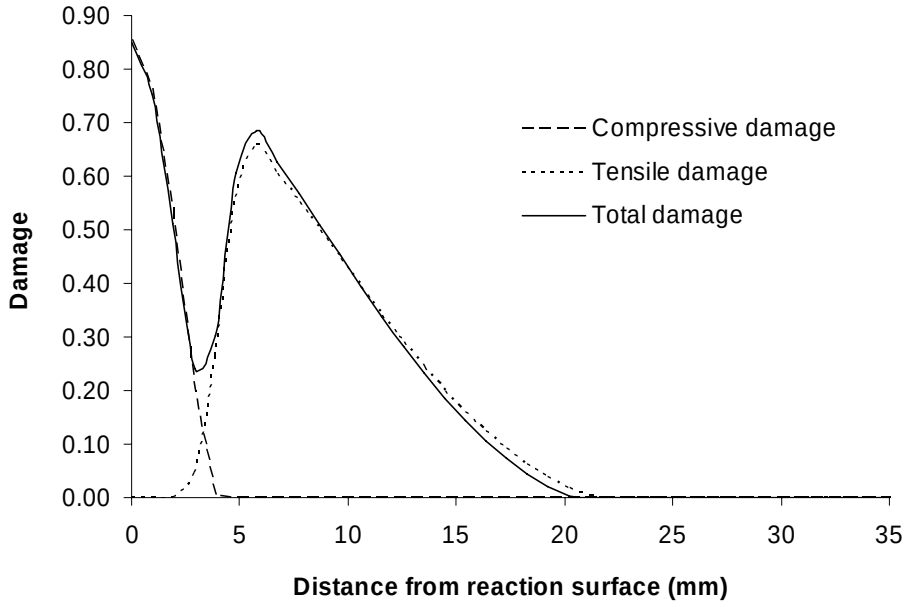

Figure 70. Through thickness damages.

Figure 71 shows the history of the maximum reactive strain. The reaction starts after about 10 hours during heating when the temperature is above 800 ^{o}C. Then the reactive strain increases linearly until the temperature is lower than 800 ^{o}C during cooling. The history of the maximum damage is shown in Figure 72. However, the growth of damage shows nonlinear behavior due to the degradation of the material stiffness. For the case studied, compressive damage starts after about 35 hours of the test and reaches steady state after about 180 hours. The tensile damage starts after the occurrence of the compressive damage. The tensile damage is always less than the compressive damage at the same moment. As a result, the maximum total damage is controlled by the maximum compressive damage.

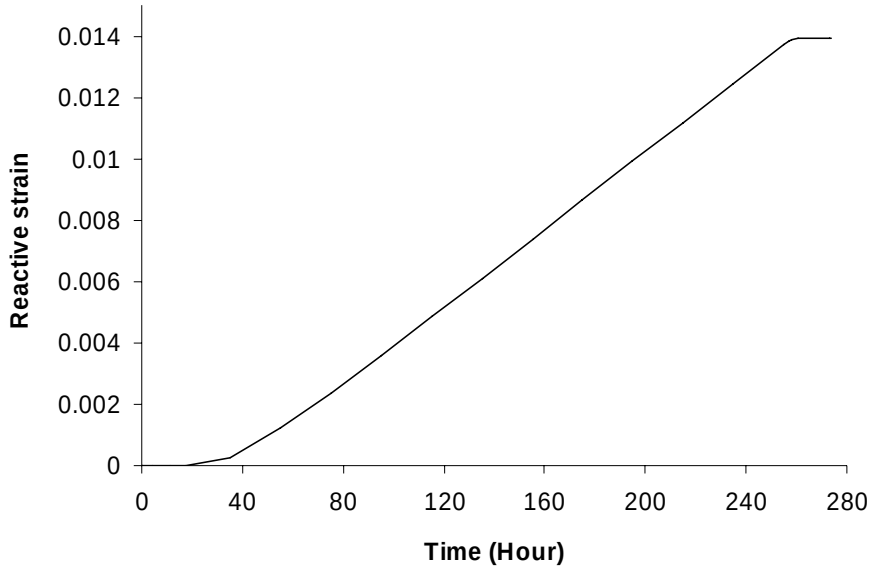

Figure 71. History of the reactive strain.

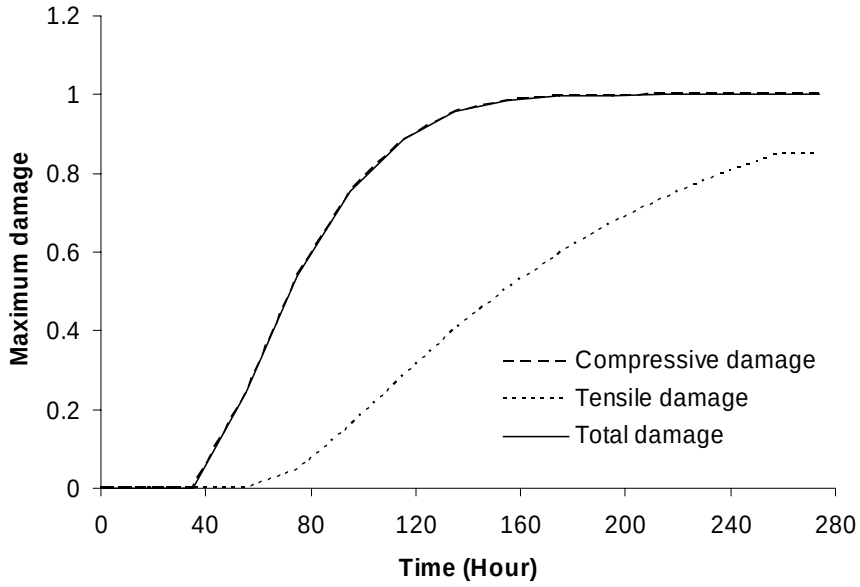

Figure 72. History of the damages.

A modeling of pulse combustor refractory tubesheet was completed. The model has been idealized based on the real combustor tubesheet, as shown in Figure 73 and Figure 74. The tubesheet is simplified into a 2-D axisymmetry problem. The radius of the tubesheet (R in the figures) is 715 mm. The thickness of the tubesheet (Z in the figures) is 280 mm. The tubesheets are held by only one hook or "v" shape anchor. The hook and anchor are attached to the steel base. The roots of the hook and "v" shape anchor are 250 mm away from the centerline of the tubesheet. There is a 1 mm gap between the tubesheet and the anchor. The tubesheet and the steel base are in contact initially and capable of separation.

A constant thermal expansion rate of 8.0 x 10^{-6}/ ^{o}C is used for the refractory material for temperatures below 1200 ^{o}C. Shrinkage of the refractory material occurs when temperature is higher than 1200 ^{o}C, a shrinking rate of 1.1 x 10^{-5} / ^{o}C is used. Emissivity of 0.8 is used for the steel.

The hot face of the tube sheet is heated up to 1370 ^{o}C in 3 days linearly. Then the temperature is hold constantly for another 7 days. The surrounding media temperature is 250 ^{o}C instantly from the beginning of heating. Convection coefficient of 568 W/m^{2} ^{o}C is used for the heat transfer between the steel base and the surrounding fluid.

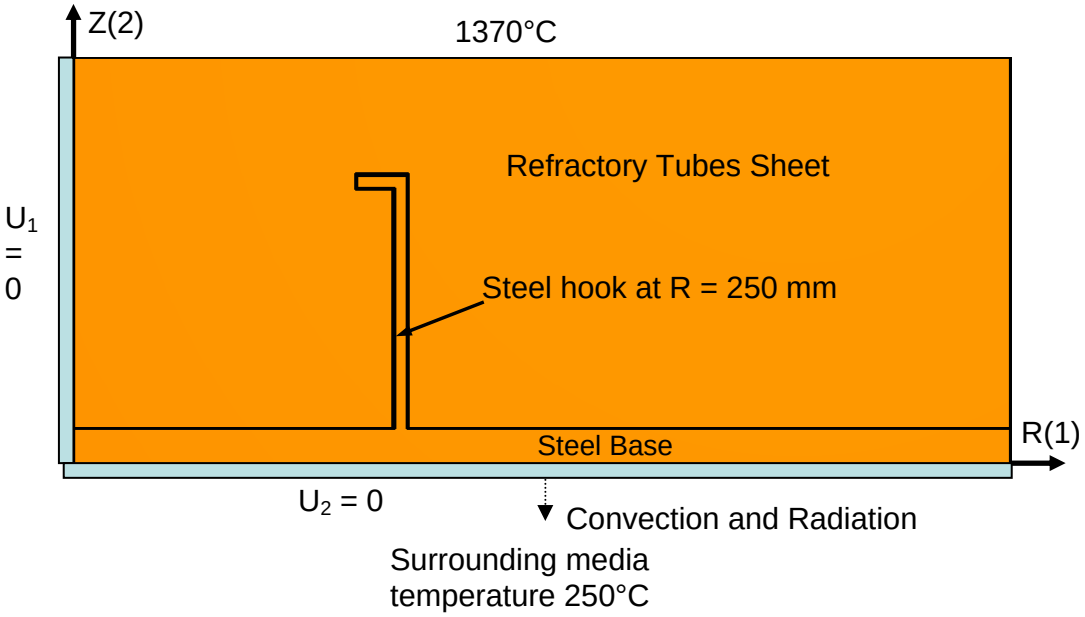

Figure 73. Idealized model of refractory tubesheet held by a hook

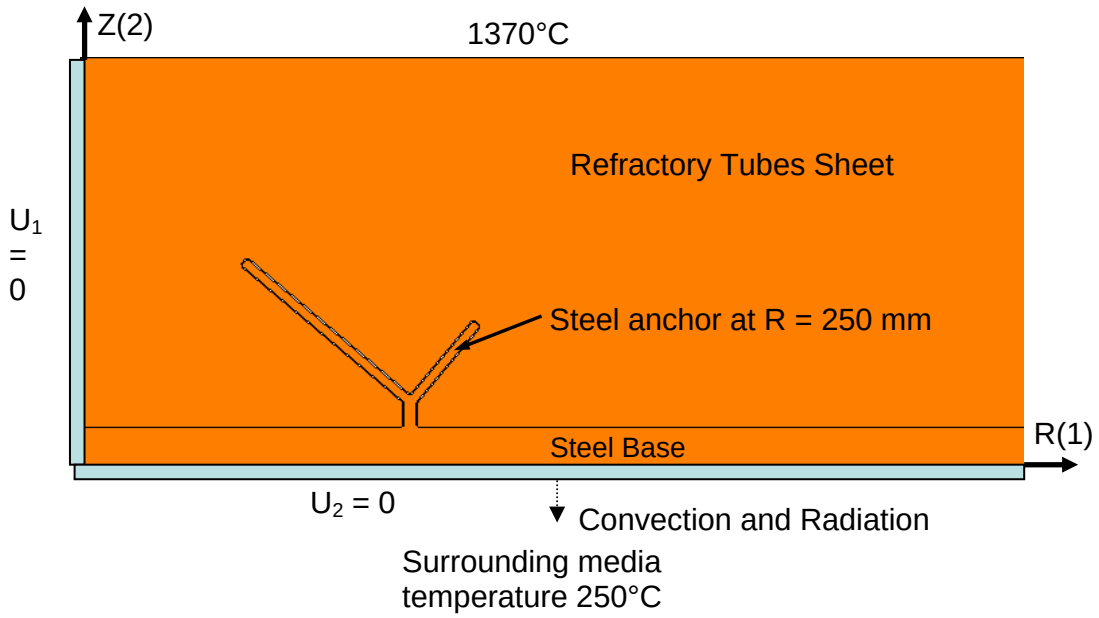

Figure 74. Idealized model of refractory tubesheet held by a "v" shape anchor

Models of the pulse combustor tube sheet were completed. It was determined that there is a minimal change in stress distribution with different anchor shapes. The wavy V anchor was the best at distributing the stress along the length of the anchor. Maximum principal stress in the refractory with hook occurs at 62.9 hours of heating when hot face temperature is 1223°C; Maximum principal stress in the refractory with anchor occurs at 66.9 hours of heating when hot face temperature is 1302°C.

Figure 75 and Figure 76 show the maximum principal stress distributions in the tubesheets during heating. The maximum stresses developed in the tubesheet held by hook occur at 62.9 hours of heating when hot face temperature is 1197 ^{o}C. The maximum stresses in the tubesheet held by "v" shape anchor occur at 66.9 hours of heating when hot face temperature is 1273 ^{o}C. Due to the stress concentration in this region, the maximum stress components in the tubesheet held by hook occur at the end of the hook hole, and the maximum stress components in the tubesheet held by "v" shape anchor occur at the end of the anchor hole of the longer leg.

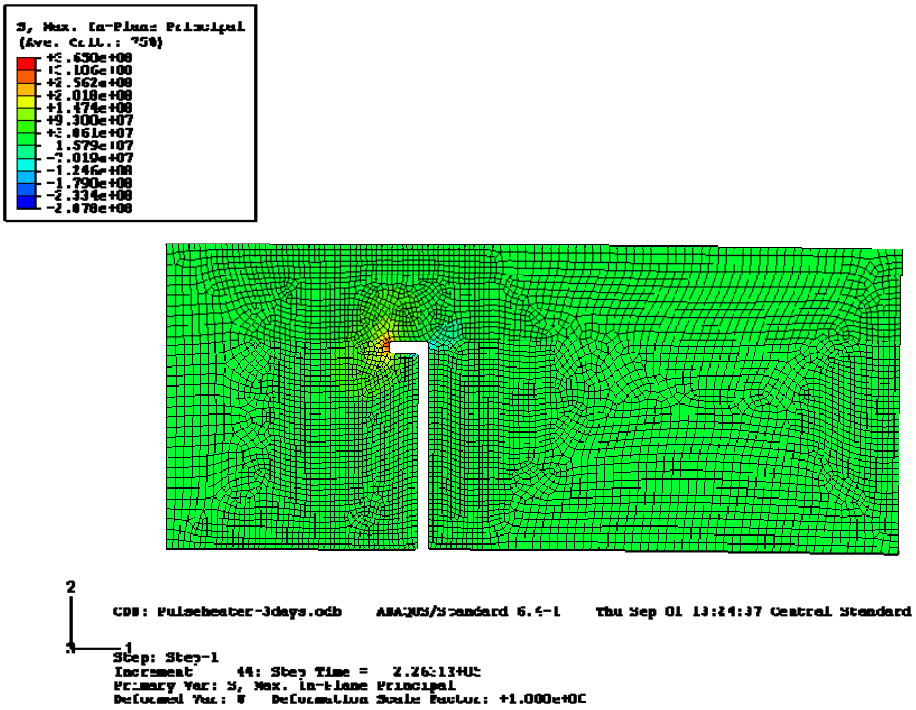

Figure 75. Maximum principal stress in the tubesheet held by hook

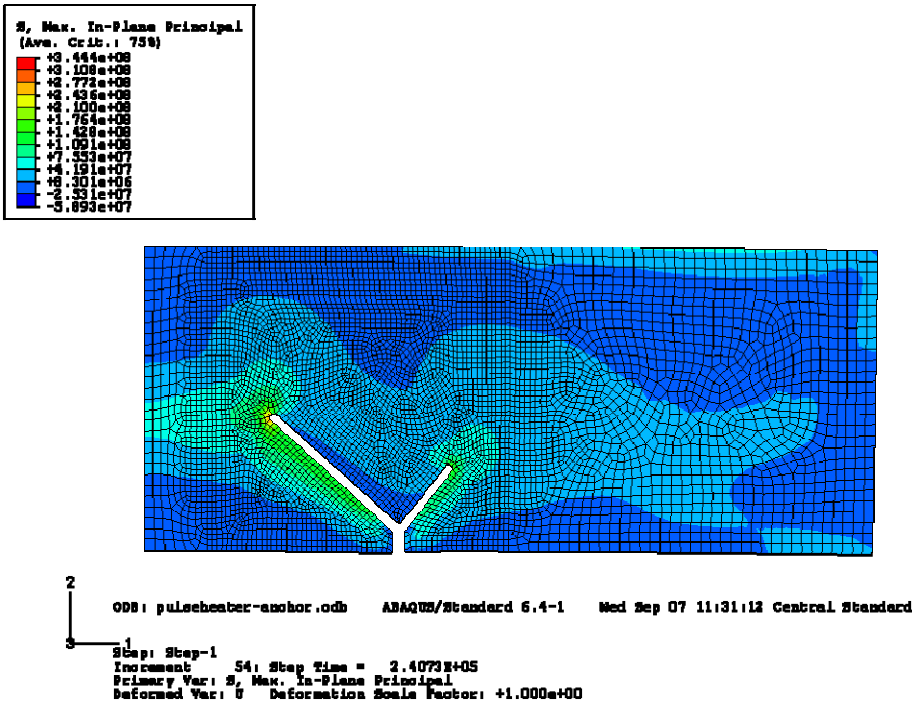

Figure 76. Maximum principal stress in the tubesheet held by “v” shape anchor

Table 9 gives the comparison of the maximum stress components in the tubesheets held by hook and “v” shape anchor. The maximum radial stress is lower in the tubesheet held by “v” shape anchor than in the tubesheet held by hook. However, the maximum axial stress is higher in the tubesheet held by “v” shape anchor than in the tubesheet held by hook. From the overall consideration, there is a little improvement on the maximum principal stress in the tubesheet by using the “v” shape anchor to hold the tubesheet.

Table 9. Comparison of the maximum stress components in the tubesheets held by hook and “v” shape anchor during heating

	Maximum principal stress (MPa)	Maximum radial stress (MPa)	Maximum axial stress (MPa)
Refractory with hook	365	200	326
Refractory with anchor	344	153	342

Stresses in the tubesheets after 10 days of operation which is the steady state of the heat transfer were also investigated. Figure 77 and Figure 78 show the maximum principal stress distribution in the tubesheets after 10 days. The maximum principal stresses in the tubesheets during the steady state occur at the end of the anchor holes also, same as that during heating. Comparing the stresses in the tubesheets during the steady state, there is no difference in the maximum principal stresses, as shown in Table 10. This result means anchor type has very little effect on the maximum stress in the tubesheet.

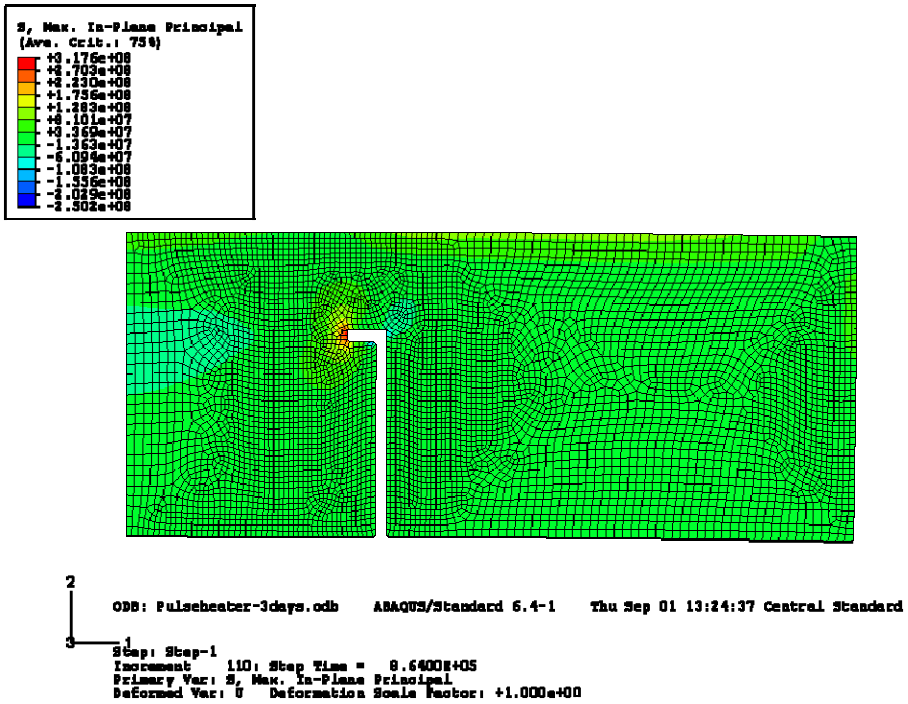

Figure 77. Principal stress in the tubesheet held by hook after 10 days

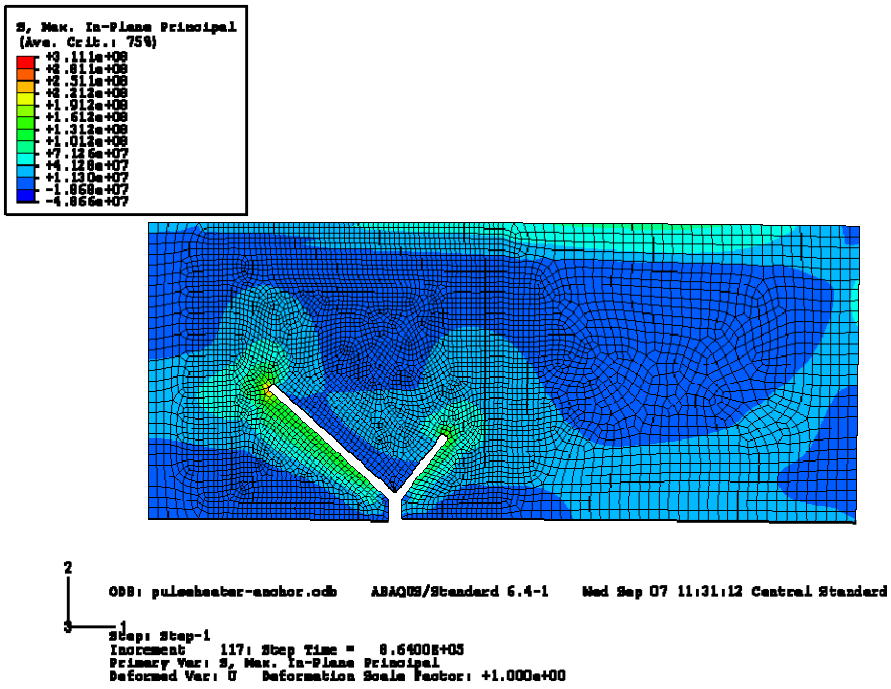

Figure 78. Principal stress in the tubesheet held by “v” shape anchor after 10 days

Table 10. Comparison of the maximum stress components in the tubesheets held by hook and "v" shape anchor during steady state

	Maximum principal stress (MPa)	Maximum radial stress (MPa)	Maximum axial stress (MPa)
Refractory with hook	318	150	308
Refractory with anchor	311	150	308

Due to the thermal expansion, the tubesheets held both by hook and by "v" anchor deform more in the center region, resulting in bow shapes after heating, as shown in Figure 79 and Figure 80. For the tubesheet held by a hook, gap between the center of the tubesheet and the steel base is 4.2 mm after heating. For the tubesheet held by a "v" anchor, gap between the center of the tubesheet and the steel base is 3.8 mm after heating. Furthermore, contact between the tubesheets and the anchors are also resulted due to the deformation. As results, significant tensile stresses have been induced at the neck of the hook and at the region where the legs are connected to the "v" anchor screw.

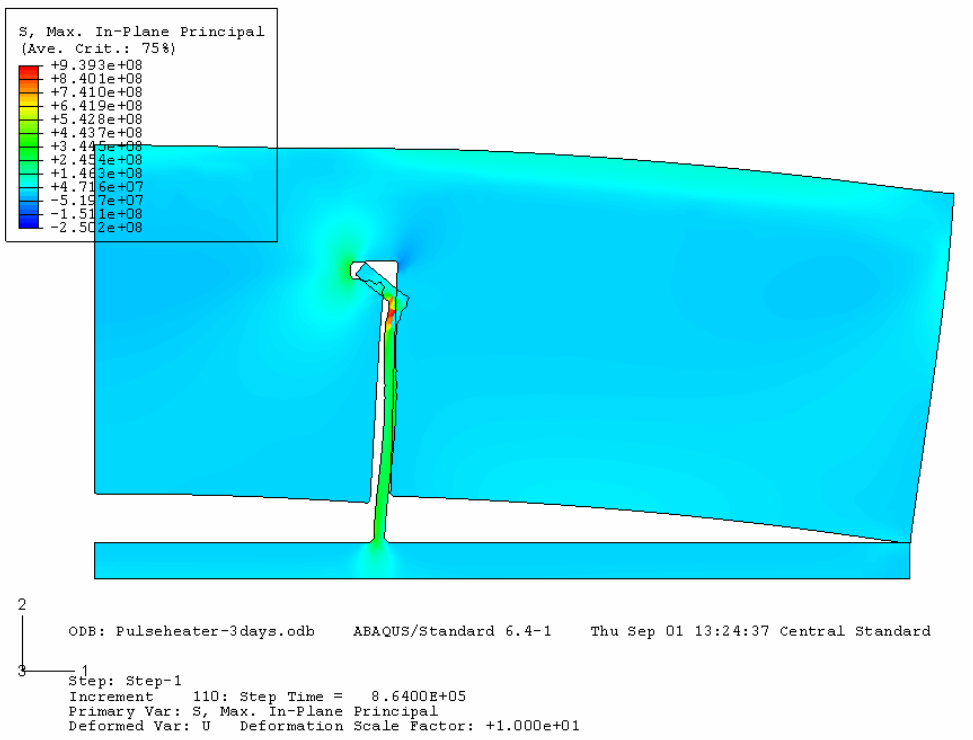

Figure 79. Deformation of the tubesheet held by a hook after heating (shape is magnified to 10 times)

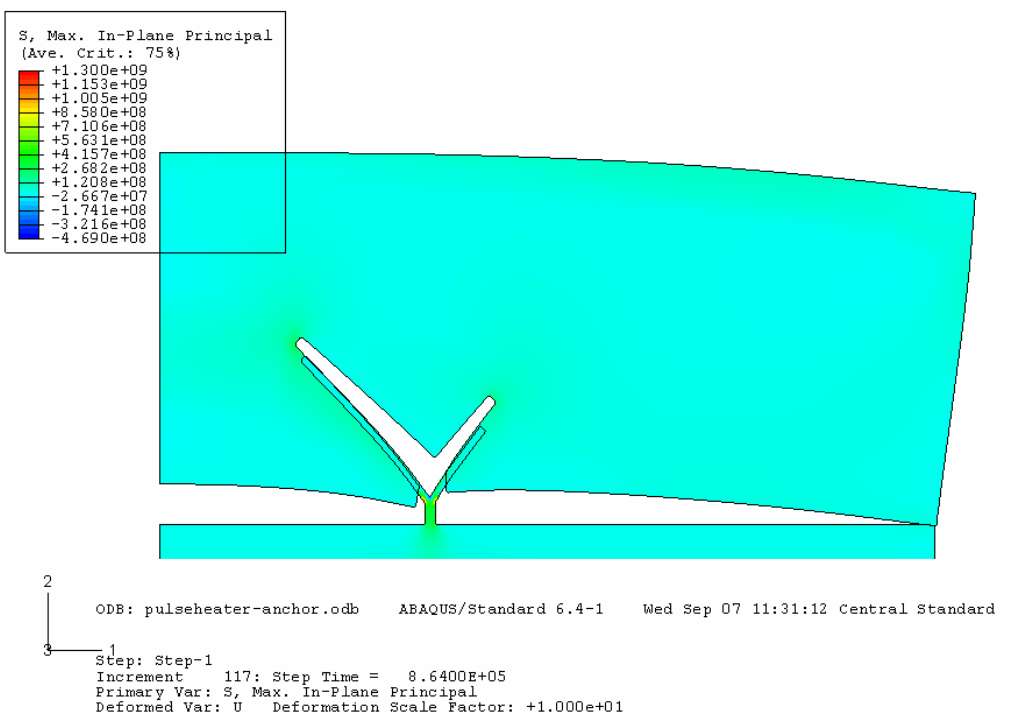

Figure 80. Deformation of the tubesheet held by a "v" shape anchor after heating (shape is magnified to 10 times)

CONCLUSION

The results of thermodynamics and experiment for the reaction of black liquor smelt with various ceramics were in agreement for some candidate materials but not for others. Reactions were correctly predicted for Al_2O_3, CeO_2, MgO, $MgAl_2O_4$, but not for $3Al_2O_3.2SiO_2$, ZrO_2, Y_2O_3, $LiAlO_2$, $BaAl_2O_4$. Failure of the thermodynamic predictions was attributed to lack of data for the reaction products produced by reaction of molten black liquor smelt with candidate materials. Sessile drop experiments were used to verify thermodynamic predictions and to determine contact angles of the molten Na_2CO_3 and K_2CO_3 on candidate materials. $MgAl_2O_4$ showed the highest contact angle with Na_2CO_3 (13.3 ± 1.2 degrees) while, the highest contact angle for K_2CO_3 (9.9 ± 1.5 degrees) was obtained with MgO. Although CeO_2 and MgO were wet by Na_2CO_3 and K_2CO_3, they did not react with either. Consequently, either CeO_2 or MgO could be used for refractories for applications requiring contact with black liquor smelt. The best choice for this application may be $MgAl_2O_4$. Although $MgAl_2O_4$ reacts with both Na_2CO_3 and K_2CO_3, a dense layer of MgO forms quickly and prevents further attack. Based on these considerations, MgO and $MgAl_2O_4$ were suggested for further investigation in the form of rotary finger corrosion tests, sessile drop studies with actual black liquor smelt, or trials in test gasifiers.

Samples provided by in-kind sponsors were tested using cup testing. The best performing materials in the cup testing were fused cast materials. Magnesia brick and castables performed well and should be further developed and moved into industrial trials. A spinel based mortar, MORCOCOAT SP-P, has been commercially prepared and is to be used in future gasifier installations.

This study presented continuum damage mechanics based analytical model for predicting the failure behavior of refractory lining black liquor gasifiers, pulse combustors and cup testing. The damage model accounts for the chemical expansion in addition to mechanical and thermal expansion. A comparison of predicted damage patterns for BLG refractory material with the observed damage pattern in the cups used indicates that this model could be used to evaluate failure behavior of refractory linings in black liquor gasifier.

A coupled thermal-mechanical model accounting for the chemical reaction was developed for refractory linings in a high temperature black liquor gasifier. This model was implemented into a commercial finite element code. The stress and strain distributions, time dependent thermomechanical behavior of the refractory lining under thermal loading and chemical attack are evaluated. The chemical reaction of the black liquor smelt and the refractory dominates the stress and strain development in the refractory lining. Four possible failure modes of the refractory lining were surmised by the stress and strain analysis. The model helps understand the failure behavior of the refractory lining in a high temperature black liquor gasifier system.

Chemical reaction and thermal expansion with improper constraints causes the most compressive damage in the refractory structure. Layered damage occurred in the refractory structure due to the tensile damage. Expansion allowance affects the damage of the refractory structure. Tensile damage could be reduced by allowing for larger expansion.

Continuum damage mechanics based analytical model is appropriate for predicting the failure behavior of refractory cup under thermal loading and chemical attack. The predicted

damage patterns predicted by the model are in qualitative agreement with those observed in practice in the cup test. The maximum compressive damage occurs on the surface of the cup where is in contact with the black liquor smelt. The maximum tensile damage occurs at the end of the reaction zone. Chemical corrosion is the dominate factor of the damage of the refractory brick.

The thermomechanical model of the pulse combustor refractory tubesheet showed that the maximum stresses in the refractory tubesheets through the operation occur slightly before the end of heating. Maximum stresses were located at the end of the anchor holes due to the stress concentration. Lower maximum principal stress is developed in the tubesheet held by "v" shape anchor. However, during the steady state, anchor type has very little effect on the stresses. The tubesheets deform into bow shapes. Contact between the tubesheet and the anchor are resulted due to the deformation and resulting in significant tensile stresses at the neck of the hook and at the region when the "v" anchor legs are connected to the screw.

No systematic experimental work has been done so far to characterize the failure behavior of refractory materials in black liquor gasifier. Experimental work is needed to validate the models presented here.

Gasifier end-users are still experiencing major refractory problems. Refractories are one of many issues still slowing use of this energy saving technology. Without continued assistance from DOE black liquor gasifiers currently in use may be shut down and future work abandoned.

BIBLIOGRAPHY

"Coal Gasification for Power Generation", http://www.dti.gov.uk/energy/developep/chevron_texaco_part2.pdf

"Gasification of Solid and Liquid Fuels for Power Generation", Technology status report to Department of Trade and Industry, 1998, http://www.dti.gov.uk/energy/coal/cfft/cct/pub/tsr008.pdf

"ABAQUS/Standard User's Manual," version 6.3, Hibbitt, Karlsson and Sorensen, Inc., 2000

"Refractories Handbook," The Technical Association of Refractories, Japan, 1998

A. Brown and W. D. Hunter, "Operating Experience at North America's First Commercial Black Liquor Gasification Plant", International Chemical Recovery Conference, 655-662, 1998

A. Weirauch Jr, J. E. Lazaroff and P. D. Ownby, "Wetting in an Electric Packaging Ceramic System: II, Wetting of Alumina by a Silicate Glass Melt under Controlled PO_2 conditions," J. Am. Ceram. Soc., **78** [11] 2923-28 (1995).

Alexander Klein, "Gasification: An Alternative Process for Energy Recovery and Disposal of Municipal Solid Wastes", Master Thesis, Columbia University, 2002,

Ayhan Demirbas, "Pyrolysis and Steam Gasification Processes of Black Liquor," Energy Conversion and Management, 43, 877-884, 2002

B. Aghamohammadi, "Large Scale Pilot Testing of the MTCI/Thermochem Black Liquor System Reformer", Proceedings of International Chemical Recovery System, Toronto, Ontario, Vol.B, pp297-301, 1995.

Barrie H. Bieler, "Corrosion of AZS, Zircon and Silica Refractories by Vapors of NaOH and of Na_2CO_3", *J. Am. Ceram. Soc. Bull*, **61**[7], 745-749, (1982).

Boisse, P.; Gasser, A.; Rousseau, J. (2002): Computations of Refractory Lining Structures Under Thermal Loadings. *Advances in Engineering Software*, Vol. 33, pp. 487-496.

Brown, C. A.; Hunter, W. D. (1998): Operating Experience at North America's First Commercial Black Liquor Gasification Plant. *International Chemical Recovery Conference*, pp. 655-662.

Brown, C. A.; Leary, R.; Gorog, J. P.; Abdullah, Z. (2004): The Chemrec Black Liquor Gasifier at New Bern – A Status Report. *2004 International Chemical Recovery Conference*, pp. 1089- 1093.

Brown, I. Landalv, "The Chemrec Black Liquor Recovery Technology – A Status Report," 2001 International Chemical Recovery Conference, Whistler, B.C., 2001

Brown, N.R. "Alkali Vapor Attack of Alumino-Silicate refractories", Proceedings of International Ceramic Conference: AUSTCERAM 88, Sydney, pp.711-715, (1988).

Buyukozturk, O.; Tseng, T. (1982): Thermomechanical Behavior of Refractory Concrete Lining. *Journal of the American Ceramic Society*, Vol. 65[6], pp. 301-307.

C. A. Brown, "Operating Experience at North America's first Commercial Black Liquor Gasification Plant", Proceedings of International Chemistry Recovery Cconference", pp655-662 (1998).

C. A. Brown, P. Smith, "Update of North America's First Commercial Black Liquor Gasification Plant" Proceedings of Engineering & Papermakers Conference; Nashville, TN, pp33-49, 1997.

C. L. Verrill, "Development and Evaluation of a Low-Temperature Gasification Process for Chemical Recovery from Kraft Black Liquor", International Chemical Recovery Conference, Tampa, Florida, pp1067-1078, 1998.

C. Wagner, "The Dissolution Rate of Sodium Chloride with Diffusion and Natural Convection as Rate-Determining Factors", J. Phys. Colloid Chem., 53, 1030-33, 1949.

Chaboche, J. L. (1988): Continuum Damage Mechanics, Part I & II. *J. Appl. Mech.*, Vol. 55, pp. 59-72.

Chen, E. (1990): Simulation of the Thermomechanical Behavior of Monolithic Refractory Lining in Coal Gasifier Environment. *Radex Rundschau*, Vol. 4, pp. 376-384.

Craig A. Brown, Ray Leary, J. Peter Gorog and Zia Abdullah, "The Chemrec Black Liquor Gasifier at New Bern – A Status Report," 2004 International Chemical Recovery Conference, 1089- 1093, 2004

Dave G. Newport, Lee N. Rockvam and Robert S. Rowbottom, "Leading Paper-Black Liquor Steam Reformer Start-up at Norampac," Presented at 2004 International Chemical Recovery Conference, Charleston, SC, June, 2004

Dickinson, J. A.; Verrill, C. L.; Kitto, J. B. (1998): Development and Evaluation of a Low-Temperature Gasification Process for Chemical Recovery from Kraft Black Liquor. *International Chemical Recovery Conference*, June 1-4.

Dominic Au, S. Cockcroft and D. Maijer, "Crack Defect Formation During Manufacture of Fused Cast Alumina Refractories," Metallurgical and Materials Transactions, **33A**, 2053-2065, 2002

E. A. Thomas, "A Study of Soda and Potash Vapor Attack on Super Structure Refractories", J. Can. Ceram. Soc, 44, 37-41 (1975).

E. Gmelin, M. Asen-Palmer, M. Reuther and R. Villar, "Thermal Boundary Resistance of Mechanical Contacts between Solids at Sub-ambient Temperatures," J. Phys. D: Appl. Phys. **32** R19-R43, 1999

E. Marotta, S. Mazzuca and J. Norley, "Thermal Joint Conductance for Graphite Materials," http://www.electronics-cooling.com

E.D. Larson, D. R. Raymond, "Commercialization Black Liquor and Biomass Gasifier/Gas Turbine Tecknology",Tappi Journal, Vol.80, No.12, pp50-57, 1997

EnSheng Chen, "Simulation of The Thermomechanical Behavior of Monolithic Refractory Lining in Coal Gasification Environment," Radex Rundschau, 4, 376-384, 1990

Eric D. Larson and Delmar R. Rqymond, "Commercializing Black Liquor and Biomass Gasifier/Gas Turbine Technology", TAPPI Journal, 50 – 57, 1997

Eric D. Larson, Stefano Consonni, and Ryan E. Katofsky, “A Cost-Benefit Assessment of Biomass Gasification Power Generation in the Pulp and Paper Industry,” Final report, Princeton Unversity, Navigant Consulting, Inc., and Dipartimento di Energetica, 2003

G. Kelleher and A. L. Kohl, "Black Liquor Gasification Technology", Presented at the 1986 Summer National Meeting, American Institute of Chemical Engineers, August 24-28, 1986

Gupta Abha, Rajan Nidhi, Mathur R.M. and Kulkarni A.G., "Development of Lignin By-Products for Industrial Applications", IPPTA Convention, 13, 49-55, 2001

H. Bieler, “Corrosion of AZS, Zircon and Silica Refractories by Vapors of NaOH and of Na_2CO_3”, J. Am. Ceram. Soc. Bull, 61[7], 745-749, (1982).

Hibbitt, Karlsson & Sorensen, INC. (2002): ABAQUS/Standard User’s Manual. Version 6.3.

Hillerborg, A.; Modeer, M.; Petersson, P. E. (1976): Analysis of Crack Formation and Crack Growth in Concrete by Means of Fracture Mechanics and Finite Elements. *Cement and Concrete Research*, Vol. 6, pp. 773-782.

http://www.ceramics.nist.gov. NIST WebSCD Database, Ceramic division, National Institute of Standards and Technology.

http://www.matweb.com. MatWeb.com, a division of Automation Creations, Inc.

J. A. Dickinson, C. L. Verrill and J. B. Kitto, “Development and Evaluation of a Low-Temperature Gasification Process for Chemical Recovery from Kraft Black Liquor,” International Chemical Recovery Conference, June 1-4, 1998

J. E. Lazaroff and P. D. Ownby, “Wetting in an Electric Packaging Ceramic System: I, Wetting of Tungsten by Glass in Controlled Oxygen Partial Pressure Atmospheres,” J. Am. Ceram. Soc., **78** [3] 539-44 (1995).

J. G. Hemrick, “Creep Behavior and Physical Characterization of Fusion-Cast Alumina Refractories”, PhD Dissertation, University of Missouri-Rolla, 2001

J. Gullichsen, H. Paulapuro, “Chemical Pulping, Paper Making Science and Technology”, Book 6B.

J. Gullichsen, H. Paulapuro, “Chemical Pulping, Paper Making Science and Technology”, Book 6B.

J. R. Keiser, R. A. Peascoe and C. R. Hubbard, ”Corrosion Issues in Black Liquor Gasifiers”, San Diego, CA, March 16–20, 2003.

J. R. LeBlanc, ”Brockway’s Lower Checker Sulfate Test”, J. Can. Ceram. Society, 52, 58-60, (1983).

J. Rawers, J. Kwong, and J. Bennett, “Characterizing Coal-gasifier Slag-refractory Interactions,” Materials at High Temperatures, 16[4] 219-222, 1999

J. Rudberg, Chemrec AB, Presentation at IEA ANNEX XV Semi-Annular Meeting, Atlanta, USA, February 11, 2003.

J. Sweeney and M. Cross, “Analyzing the Stress Response of Commercial Refractory Structures in Service at High Temperatures, II. A Thermal Stress Model for Refractory Structures,” Trans. J. Br. Ceram. Soc., 81, 47-52, 1982

James Cantrell, P.E., "Simulation of Kraft Black Liquor Gasification – A Comparative Look at Performance and Economics", Engineering/Fishing & Converting Conference & Trade Fair, 1181-1195, 2001

K. Andreev, H. Harmuth, "FEM Simulation of The Thermo-mechanical Behaviour and Failure of Refractories - A Case Study," Journal of Materials Processing Technology, 143-144[1] 72-77, 2003

K. McAlister & E. Wolfe, "A Study of the Effects of Alkali Attack on Refractories Used in Incineration", Proceedings of Incineration Conference, Albuquerque, New Mexico, pp.631-638 (1992).

K. McAlister & E. Wolfe, "A Study of the Effects of Alkali Attack on Refractories Used in Incineration", Proceedings of Incineration Conference, Albuquerque, New Mexico, pp.631-638 (1992).

K. Whitty, University of Utah, ACERC Annual Meeting, 14-15 March, 2002.

Kachanov, L. M. (1958): Rupture Time under Creep Conditions. *Izv. Acad. Nauk USSR, OTN*, Vol. 8, pp. 26-31.

Kachanov, L. M. (1986): Introduction to Continuum Damage Mechanics. Martinus Nijhoff Publishers, Dordrecht, the Netherlands.

Keijo Salmenoja, "Black-Liquor Gasification: Theoretical and Experimental Studies,", Bioresource Technology, 46, 167-171, 1993

Kelleher, E. G.; Kohl, A. L. (1986): Black Liquor Gasification Technology. *Presented at the 1986 Summer National Meeting*, American Institute of Chemical Engineers, August 24-28.

Ken Patrick, "Gasification Edges Closer to Commercial Readily with Three N.A. Mill Startups", PaperAge, 30-33, 2003

Kennedy, Christophere R, "Alkali attack on mullite refractory in the grand forks energy technology center slagging gasifier", *Journal of Materials for Energy Systems*, **3**[N-1, June] 27-31, (1981).

Kenneth T. Hood and Gunnar B. Henningsen, "Black Liquor Gasification…Evaluation of Past Experience in order to Define the Roadmap of the Future Pathway", TAPPI Fall Conference & Trade Fair, 1451-1463, 2002

Kirk J. Finchem, "Black Liquor Gasification Research Yields Recovery Options for Future", 69[11] 51-59, 1995

L. Reed, L. R. Barrett, "The Slagging of Refractories, I. The Controlling Mechanism in Refractory Corrosion", Trans. Brit. Ceram. Soc, 54, 671-676, 1955.

L. Stigsson, "Chemrec Black Liquor Gasification", International Chemical Recovery Conference, Tampa, Florida, pp663-674, 1998.

L.L. Stigsson, B. Hesseborn, "Gasification of Black Liquor", Proceedings of International Chemical Recovery System, Toronto, Ontario, ppB277-295, 1995

Lars Stigsson, "ChemrecTM Black Liquor Gasification," International Chemical Recovery Conference, 663-674, 1998

Larson, E. D.; Consonni, S.; Katofsky, R. E. (2003): A Cost-Benefit Assessment of Biomass Gasification Power Generation in the Pulp and Paper Industry. *Final report, Princeton University, Navigant Consulting, Inc., and Dipartimento di Energetica.*

LeBlanc, John R, "Brockway's Lower Checker Sulfate Test", *J. Can. Ceram. Society*, **52**, 58-60, (1983).

Lee, J.; Fenves, G. L. (1998): Plastic-Damage Model for Cyclic Loading of Concrete Structures. *Journal of Engineering Mechanics*, Vol. 124[8], pp. 892-900.

Lemaitre, J. (1985): A Continuum Damage Mechanics Model for Ductile Fracture. *J. Engrg. Mat. and Technol.*, Vol. 107[1], pp. 83-89.

Lubliner, J.; Oliver, J.; Oller, S.; Oñate, E. (1989): A Plastic-Damage Model for Concrete. *International Journal of Solids and Structures*, Vol. 25, pp. 299-329.

M. L. Millard, "The Effect of Microstructure on the Liquid Corrosion of Sodium Chloride and Aluminum Oxide", Ph.D. Dissertation, Department of Ceramic Engineering, University of Missouri-Rolla, 1982.

M. M. Akiyoshi, R. Pereira, A. P. da Silva and V. C. Pandolfelli, "Thermal Conductivity of Refractories," American Ceramic Society Bulletin, **82** [6] 29-33, 2003

M. M. Yovanovich, 'New XContact and Gap Correlations for Conforming Rough Surface," AIAA-81-1164, presented at AIAA 16th Thermophysics Conference, Palo Alto, CA., June 1981

M. P. Borom, R. H. Arendt, "Dissolution of Oxides of Y, Al, Mg, and La by Molten Fluorides", Ceramic Bulletin, 60 [11], 1169-1174, 1981.

Magnus Marklund, "Black Liquor Recovery: How Does It Work?" ETC, (Energy Technology Center, Sweden, http://www.etcpitea.se/blg/document/PBLG_or_RB.pdf

Mikael Ahlroth, Gunnar Svedberg, "Case Study on Simultaneous Gasification of Black Liquor and Biomass in a Pulp Mill," International Gas Turbine & Aeroengine Congress & Exhibition, 1998

N. McCallum, L. R. Barrett, "Some Aspects of the Corrosion of Refractories", Trans. Brit. Ceram. Soc., 51, 523-543, 1952.

N. R. Brown, "Alkali Vapor Attack of Alumino-Silicate refractories", Proceedings of International Ceramic Conference: AUSTCERAM 88, Sydney, pp.711-715, (1988).

N. Samaddar, W. D. Kingery, A. R. Cooper, "Dissolution in Ceramic Systems: II, Dissolution of Alumina, Mullite, Anorthite, and Silica in a Calcium-Aluminum-Silicate Slag", J. Am. Ceram. Soc, 47 [5] 249-254.

Oral Buyukozturk and Tsi-Ming Tseng, "Thermomechanical Behavior of Refractory Concrete Lining," Journal of the American Ceramic Society, 65[6] 301-307,1982

P. D. Ownby, Ke Wen K. Li, D. A. Weirauch Jr, "High Temperature Wetting of Sapphire by Aluminum," J. Am. Ceram. Soc., **74** [6] 1275-81 (1991).

P. Tucker from International Paper (session leader), K. Bowers, "Closing in on Black Liquor and Biomass Gasification/Combined-Cycle", http://www.tri-inc.net/A2020BLGasification.pdf.

P. Ulmegren, R. Radestrom, "On the Chemistry of Non-Process Elements in Systems with a Pressurized Black Liquor Gasifier", International Chemical Recovery Conference, Tampa, Florida, pp721-732, 1998.

Peascoe, R. A.; Keiser, J. R.; Hubbard, C. R.; Brady, M. P.; Gorog, J. P. (2001): Performance of Selected Materials in Molten Alkali Salts. *International Symposium on Corrosion in the Pulp & Paper Industry*, pp. 189-200.

R. A. McCauley, "Corrosion of Ceramics", 1994, New York, Marcel Deker.

R. A. Peascoe, J. R. Keiser, "Performance of Selected Materials in Molten Alkali Salts", 10th International Symposium on Corrosion in the Pulp and Paper Industry (10th ISCPPI); Marina Congress Center, Helsinki, Finland, pp189-200, 2001.

R. A. Peascoe, J. R. Keiser, C. R. Hubbard, J. P. Gorog, C. A. Brown and B. H. Nilsson, "Comparison of Refractory Performance in Black Liquor Gasifiers and A Smelt Test System," 2001 International Chemical Recovery Conference, Whistler, B.C., 2001

R. B. Hetnarski, "Thermal Stresses I," Elsevier Science Publications B.V., 1986

R. Cooper, Jr, W. D. Kingery, "Dissolution in Ceramic Systems: I, Molecular Diffusion, Natural Convection and Forced Studies of Sapphire Dissolution in Calcium Aluminum Silicate", J. Am. Ceram. Soc, 47 [1], 37- 43, 1964.

R. Kennedy, "Alkali attack on mullite refractory in the grand forks energy technology center slagging gasifier", Journal of Materials for Energy Systems, 3[N-1, June] 27-31, (1981).

R. Sangiorgi, "Corrosion of Ceramics by Liquid Metals", NATO ASI Ser., Ser E., Applied Sciences, Vol. 267, pp. 261-84, 1994

S. E. Feldman, W. K. Lu, "Kinetics of the Reactions between Silica and Alumino-Silicate Refractories and Molten Iron", Metallurgical Transactions, 5, 249-253, 1974.

S. L. Cockcroft, J. K. Brimacombe, D. G. Walrod and T. A. Myles, "Thermal Stress Analysis of Fused-Cast AZS Refractories during Production: Part II, Development of Thermo-elastic Stress Model," J. Am. Ceram. Soc., **77** [6] 1512-1521, 1994

S. Song, M. M. Yovanovich and F. O. Goodman, "Thermal Gap Conductance of Conforming Surface in Contact," Journal of Heat Transfer, **115**, 533-540, 1993

Saetta, A.; Scotta, R.; Vitaliani, R. (1998): Mechanical Behavior of Concrete Under Physical-Chemical Attacks. *Journal of Engineering Mechanics*, pp. 1100-1109.

Schacht, C. A. (1995): Refractory Linings. Marcel Dekker, Inc.

Shigekastu Mori et. al., "Gasification Process of Organic Wastes for Electric Power Generation by Fuel Cell", http://www.cape.canterbury.ac.nz/Apcche_Proceedings/APCChE/Data/720REV.pdf

Stigsson, L. (1998): Chemrec™ Black Liquor Gasification. *International Chemical Recovery Conference*, pp. 663-674.

StoneChem, Inc, Presentation at IEA ANNEX XV Semi-Annular Meeting, Atlanta, USA, February 11, 2003.

Suat Yilmaz, "Thermomechanical Modeling for Refractory Lining of a Steel Ladle Lifted by Crane," Steel Research, 74[8] 485-490, 2003

Taber, W. A. (2003): Refectories for Gasification. *Refectories Applications and News*, Vol. 8[4], pp. 18-22.

Tadaoki Fukui, "Corrosion of Zircon Refractories by Vapors of Sodium Compounds", *Ashi Gavasu Kenkya Hokoku*, **17**(2), 77-98 (1967).

Tadaoki, "Corrosion of Zircon Refractories by Vapors of Sodium Compounds", Ashi Gavasu Kenkya Hokoku, 17(2), 77-98 (1967).

Terry N. Adams, "Black Liquor Properties, Crystallization, and Sodium Salt Scaling in Concentrators," TAPPI 2001 Pulping Conference, 1209-1222, 2001

Thomas, Everett A, "A Study of Soda and Potash Vapor Attack on Super Structure Refractories", *J. Can. Ceram. Soc*, **44**, 37-41 (1975).

V. G. Levich, "Physicochemical Hydrodyanamics", 1962. Englewood Cliffs, NJ, USA, Prentice-Hall.

V. W. Antonetti and M. M. Yovanovich, "Thermal Contact Resistance in Microelectronic Equipment," in "Thermal Management Concepts in Microelectronic Packaging from Component to System," ISHM Technical Monograh Series 6984-003, 135-151, 1984

W. D. Kingery, H. K. Bowen, D. R. Uhlmann, "Introduction to Ceramics", Second ed. , John Wiley & Sons. New York, 1976.

W. E. Lee, S. Zhang, "Melt Corrosion of Oxide and Oxide-Carbon Refractories", A Review from Dept. of Engineering Materials, University of Sheffield, UK., 1999.

Xiaoting Liang, "Modeling of Thermomechanical, Cracking and Creep Behavior in Glasstank Crown," MS Thesis, University of Missouri-Rolla, 2003

Y. A. Cengel and R. H. Turner, "Fundamentals of Thermal-Fluid Sciences," McGraw-Hill Higher Education, 2001

Y. Chung, "Corrosion of Partially Stabilized Zirconia by Steelmaking Slags", M.S. Thesis, Department of Ceramic Engineering, University of Missouri-Rolla, 1993.

Y. Kuromitsu, H. Yoshida, "Interaction between Alumina and Binary Glasses", J. Am. Ceram. Soc, 80 [6] 1583-87, 1997.

Yamaguchi, "Reactions between Alkaline Vapors and Refractories for Glass Tank Furnaces", Proceedings of International Congress on Glass, Kyoto, Japan, pp.1-8 (1974).

REFERENCES

[1] M. Marklund, "Black Liquor Recovery: How does it work?" (ETS), http://etcpitea.se/blg/document/PBLG_or_RB.pdf.

[2] K. Whitty, University of Utah, ACERC Annual Meeting, 14-15 March, 2002.

[3] L.L. Stigsson, B. Hesseborn, "Gasification of Black Liquor", Proceedings of International Chemical Recovery System, Toronto, Ontario, ppB277-295, 1995.

[4] J. Rudberg, Chemrec AB, Presentation at IEA ANNEX XV Semi-Annular Meeting, Atlanta, USA, February 11, 2003.

[5] E.D. Larson, D. R. Raymond, "Commercialization Black Liquor and Biomass Gasifier/Gas Turbine Tecknology",Tappi Journal, Vol.80, No.12, pp50-57, 1997.

[6] C. A. Brown, P. Smith, "Update of North America's First Commercial Black Liquor Gasification Plant" Proceedings of Engineering & Papermakers Conference; Nashville, TN, pp33-49, 1997.

[7] C. L. Verrill, "Development and Evaluation of a Low-Temperature Gasification Process for Chemical Recovery from Kraft Black Liquor", International Chemical Recovery Conference, Tampa, Florida, pp1067-1078, 1998.

[8] J. R. Keiser, R. A. Peascoe and C. R. Hubbard, "Corrosion Issues in Black Liquor Gasifiers", San Diego, CA, March 16–20, 2003.

[9] P. Tucker from International Paper (session leader), K. Bowers, "Closing in on Black Liquor and Biomass Gasification/Combined-Cycle", http://www.tri-inc.net/A2020BLGasification.pdf.

[10] L. Stigsson, "Chemrec Black Liquor Gasification", International Chemical Recovery Conference, Tampa, Florida, pp663-674, 1998.

[11] B. Aghamohammadi, "Large Scale Pilot Testing of the MTCI/Thermochem Black Liquor System Reformer", Proceedings of International Chemical Recovery System, Toronto, Ontario, Vol.B, pp297-301, 1995.

[12] P. Ulmegren, R. Radestrom, "On the Chemistry of Non-Process Elements in Systems with a Pressurized Black Liquor Gasifier", International Chemical Recovery Conference, Tampa, Florida, pp721-732, 1998.

[13] StoneChem, Inc, Presentation at IEA ANNEX XV Semi-Annular Meeting, Atlanta, USA, February 11, 2003.

[14] C. A. Brown, "Operating Experience at North America's first Commercial Black Liquor Gasification Plant", Proceedings of International Chemistry Recovery Cconference", pp655-662 (1998).

[15] S. Consonni, E. Larson and N. Berglin, "Black Liquor Gasifier/Gas Turbine Cogeneration", ASME, **97**, 1-9 (1997).

[16] K. McAlister & E. Wolfe, "A Study of the Effects of Alkali Attack on Refractories Used in Incineration", Proceedings of Incineration Conference, Albuquerque, New Mexico, pp.631-638 (1992).

[17] A. Yamaguchi, "Reactions between Alkaline Vapors and Refractories for Glass Tank Furnaces", Proceedings of International Congress on Glass, Kyoto, Japan, pp.1-8 (1974).

[18] E. A. Thomas, "A Study of Soda and Potash Vapor Attack on Super Structure Refractories", J. Can. Ceram. Soc, 44, 37-41 (1975).

[19] N. R. Brown, "Alkali Vapor Attack of Alumino-Silicate refractories", Proceedings of International Ceramic Conference: AUSTCERAM 88, Sydney, pp.711-715, (1988).

[20] C. R. Kennedy, "Alkali attack on mullite refractory in the grand forks energy technology center slagging gasifier", Journal of Materials for Energy Systems, 3[N-1, June] 27-31, (1981).

[21] B. H. Bieler, "Corrosion of AZS, Zircon and Silica Refractories by Vapors of NaOH and of Na_2CO_3", J. Am. Ceram. Soc. Bull, 61[7], 745-749, (1982).

[22] J. R. LeBlanc, "Brockway's Lower Checker Sulfate Test", J. Can. Ceram. Society, 52, 58-60, (1983).

[23] R. A. Peascoe, J. R. Keiser, "Performance of Selected Materials in Molten Alkali Salts", 10th International Symposium on Corrosion in the Pulp and Paper Industry (10th ISCPPI); Marina Congress Center, Helsinki, Finland, pp189-200, 2001.

[24] F. Tadaoki, "Corrosion of Zircon Refractories by Vapors of Sodium Compounds", Ashi Gavasu Kenkya Hokoku, 17(2), 77-98 (1967).

[25] Taber, W. A. (2003): Refectories for Gasification. *Refectories Applications and News*, Vol. 8[4], pp. 18-22.

[26] Larson, E. D.; Consonni, S.; Katofsky, R. E. (2003): A Cost-Benefit Assessment of Biomass Gasification Power Generation in the Pulp and Paper Industry. *Final report, Princeton University, Navigant Consulting, Inc., and Dipartimento di Energetica.*

[27] Brown, C. A.; Hunter, W. D. (1998): Operating Experience at North America's First Commercial Black Liquor Gasification Plant. *International Chemical Recovery Conference*, pp. 655-662.

[28] Brown, C.; Landalv, I. (2001): The Chemrec Black Liquor Recovery Technology – A Status Report. *International Chemical Recovery Conference*, Whistler, B.C.

[29] Peascoe, R. A.; Keiser, J. R.; Hubbard, C. R.; Brady, M. P.; Gorog, J. P. (2001): Performance of Selected Materials in Molten Alkali Salts. *International Symposium on Corrosion in the Pulp & Paper Industry*, pp. 189-200.

[30] Brown, C. A.; Leary, R.; Gorog, J. P.; Abdullah, Z. (2004): The Chemrec Black Liquor Gasifier at New Bern – A Status Report. *2004 International Chemical Recovery Conference*, pp. 1089- 1093.

[31] A. R. Rezaie, W.G. Fahrenholtz, and W.L. Headrick, "Thermodynamics of Refractories for Black Liquor Gasification," pp. 53-62 in Ceramic Transactions Vol. 158, *Surfaces, Interfaces, and the Science of Ceramic Joining.* Edited by K. S. Weil, I. E. Reimanis, and C. A. Lewinsohn, The American Ceramic Society, Westerville, OH, 2004.

[32] A. R. Rezaie, W.L. Headrick, and W.G. Fahrenholtz, "Refractories for Black Liquor Gasification," pp. 92-103 in *Proceedings of the Tehran International Conference on Refractories*, Tehran, Iran, May 4-6, 2004.

[33] Stephen C. Carniglia and Gordon L. Barna, "*Handbook of Industrial Refractories Technology: Principles, Types, Properties, & Applications,***"** Noyes Publications, Park Ridge, N.J, 1992.

[34] C. R. Hubbard, R. A. Peascoe, and J. R. Keiser, "Pulp and Paper Plant Materials Issues Addressed by X-ray and Neutron Diffraction Methods," *Adv. X-Ray Anal,* **46** 278-284 (2003).

[35] A. Yamaguchi, "Reactions between Alkaline Vapors and Refractories for Glass Tank Furnaces"; pp.1-8 in *10th International Congress on Glass Proceedings*, Edited by M. Kunigi, M. Tashiro and N. Saga, Ceramic Society of Japan, Kyoto, Japan, 1974.

[36] J. G. Hemrick, J. R. Keiser, R. A. Peascoe, and, C. R. Hubbard, "Refractory Testing and evaluation at Oak Ridge National Laboratory for Black Liquor Gasifier Applications," *Refractories Applications and News,* **9** [6] 13-20 (2004).

[37] R. A. Peascoe, C. R. Hubbard, J. R. Keiser, P. Gorog, "Alkali Resistant Refractories," US. Pat. No. US20050037226A1, Feb. 17, 2005.

[38] R. A. Peascoe, C. R. Hubbard, J. R. Keiser, P. Gorog, "Alkali Resistant Refractories," US. Pat. No. US20050037226A1, Feb. 17, 2005.

[39] J. G. Hemrick, "Creep Behavior and Physical Characterization of Fusion-Cast Alumina Refractories," PhD Dissertation, University of Missouri-Rolla, (2001).

[40] E. Gmelin, M. Asen-Palmer, M. Reuther and R. Villar, "Thermal Boundary Resistance of Mechanical Contacts between Solids at Sub-ambient Temperatures," *J. Phys. D: Appl. Phys.*, **32**, R19-R43 (1999).

[41] X. Liang, "Analysis of Thermomechanical and Failure Behavior of Refractory Linings in a High Temperature Black Liquor Gasifier," PhD Dissertation, University of Missouri-Rolla, (2005).